VISIONS • SCIENCE • TECHNOLOGY • RESEARCH HIGHLIGHTS

Dissertation
23

A human thermal model for improved thermal comfort

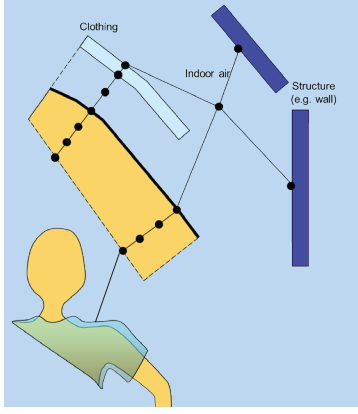

Riikka Holopainen

VTT

VTT SCIENCE 23

A human thermal model for improved thermal comfort

Riikka Holopainen

VTT

Thesis for the degree of Doctor of Science in Technology to be presented with due permission for public examination and criticism in Auditorium T2, at Aalto University, on the 14th of December, 2012 at 12 noon.

ISBN 978-951-38-7948-8 (soft back ed.)
ISSN 2242-119X (soft back ed.)

ISBN 978-951-38-7949-5 (URL: http://www.vtt.fi/publications/index.jsp)
ISSN 2242-1203 (URL: http://www.vtt.fi/publications/index.jsp)

JULKAISIJA – UTGIVARE – PUBLISHER

VTT
PL 1000 (Tekniikantie 4 A, Espoo)
02044 VTT
Puh. 020 722 111, faksi 020 722 7001

VTT
PB 1000 (Teknikvägen 4 A, Esbo)
FI-02044 VTT
Tfn +358 20 722 111, telefax +358 20 722 7001

VTT Technical Research Centre of Finland
P.O. Box 1000 (Tekniikantie 4 A, Espoo)
FI-02044 VTT, Finland
Tel. +358 20 722 111, fax + 358 20 722 7001

Smaller cover picture Pekka Tuomaala

Kopijyvä Oy, Kuopio 2012

A human thermal model for improved thermal comfort

Termisellä ihmismallilla parempaan lämpöviihtyvyyteen. **Riikka Holopainen.** Espoo 2012. VTT Science 23. 141 p.

Abstract

Energy efficient very low-energy houses, passive houses and nearly zero-energy houses have a significantly lower heating power demand than traditional buildings. Therefore, the typical design and dimensioning criteria of conventional structural and building service system concepts need to be verified to avoid problems concerning the thermal sensation and comfort of the building users.

Fanger's Predicted Mean Vote, PMV-method is traditionally used for estimating thermal sensation and comfort. The PMV method is based on a heat balance model, also referred to as a "static" or "constancy" model. While assuming that the effects of the surrounding environment are explained only by the physics of heat and mass exchanges between the body and the environment, heat balance models do not take into account the human thermoregulatory system but view the human being as a passive recipient of thermal stimuli. According to previous research results, the PMV method progressively over-estimates the mean perceived warmth of warmer environments and the coolness of cooler environments. It is therefore valid for the prediction of thermal comfort only under severely restricted conditions. To accurately estimate thermal sensation and comfort in transient conditions, the calculation method should take into account the natural tendency of people to adapt to changing conditions in their environment by means of the human thermoregulation system.

Human thermal models represent the human body from a thermokinetic point of view and they have been used for modelling the thermoregulation system. Over the last hundred years, numerous human thermal models have been developed. The utilization rate of these models has been low due to the complexities of the models and the difficult determination of calculation variables. This thesis presents the first approach, where a human thermal model is implemented in a building simulation environment: the Human Thermal Model (HTM).

HTM can be used for predicting thermal behaviour of the human body under both steady-state and transient indoor environment conditions. It is based on true anatomy and physiology of the human body. The connection with the building simulation environment enables defining the external boundary conditions such as surface temperatures and radiation heat transfer more accurately than with the previous human thermal models. The thermal sensation and thermal comfort estimation methodology presented by Zhang is integrated in HTM.

HTM tissue heat transfer, thermal sensation and thermal comfort calculation has been successfully validated under various steady-state and transient indoor environment boundary conditions comparing the simulation results to measurements made with real human beings. The simulated thermal sensations with the

HTM method showed a better correlation with measured values than the Fanger's PMV method.

The boundary conditions for a good thermal comfort were estimated by studying the effects of various internal and external parameters on human thermal sensation. According to the simulation results, the operative temperature, metabolic rate and clothing are the most dominant boundary conditions for the human thermal sensation and comfort.

As a module of the VTT House building simulation tool, HTM can be used for estimating the effects of alternative building structures, as well as building service systems, on occupants under different conditions more accurately and easily than before. This integrated method enables quantitative analysis of the significance of both external (structure insulation level, heating/cooling system) and internal (clothing, metabolism) boundary conditions on thermal sensation and comfort. The realistic thermal comfort of the user can be used as a design parameter for designing better thermal environments in new and renovated buildings. The various utilization possibilities of HTM were represented by two realistic case studies: effects of alternative energy renovation measures and heating distribution systems on thermal sensation and comfort.

Keywords human thermoregulation, building simulation

Termisellä ihmismallilla parempaan lämpöviihtyvyyteen

A human thermal model for improved thermal comfort.
Riikka Holopainen. Espoo 2012. VTT Science 23. 141 s.

Tiivistelmä

Energiatehokkaissa matalaenergia-, passiivi- ja nollaenergiataloissa on merkittävästi pienempi lämmitystehontarve kuin perinteisissä rakennuksissa. Tämän vuoksi perinteisiä rakenne- ja talotekniikkaratkaisuiden suunnittelukriteerejä on tarkistettava lämpöviihtyvyyden varmistamiseksi myös energiatehokkaissa rakennuksissa.

Lämpöviihtyvyyden laskentamenetelmänä on perinteisesti käytetty Fangerin PMV-menetelmää (Predicted Mean Vote). Ihmisen ja ympäristön väliseen lämpötaseeseen perustuva PMV-menetelmä ei huomioi ihmisen omaa lämmönsäätelymekanismia, vaan pitää ihmistä passiivisena lämpöärsykkeen vastaanottajana. Aikaisempien tutkimusten mukaan PMV-menetelmä progressiivisesti yliarvioi koettua lämpötilaa lämpimissä olosuhteissa ja aliarvioi sitä viileissä olosuhteissa. PMV-menetelmää tulisikin käyttää lämpöviihtyvyyden arviointiin vain hyvin rajallisissa olosuhteissa. Lämpöviihtyvyyden arvioimisen muuttuvissa olosuhteissa tulisi huomioida ihmisen luontainen taipumus sopeutua muuttuviin ympäristöolohin lämmönsäätelyjärjestelmän avulla.

Termisillä ihmismalleilla voidaan mallintaa ihmisen lämpöfysiologista ja -fysikaalista toimintaa ja lämmönsäätelyjärjestelmää. Sadan viime vuoden aikana on kehitetty kymmeniä erilaisia termisiä ihmismalleja. Näiden mallien hyödyntäminen käytännön sovelluksissa on ollut vähäistä mallien monimutkaisuuden vuoksi. Tässä väitöskirjassa esitetään ensimmäinen sovellus, jossa terminen ihmismalli on liitetty dynaamiseen rakennuksen energialaskentaohjelmaan: Human Thermal Model (HTM).

HTM-mallia voidaan käyttää lämpöviihtyvyyden laskentaan sekä pysyvissä että muuttuvissa olosuhteissa. Malli perustuu ihmisvartalon todelliseen anatomiaan ja fysiologiaan. Koska malli on osa dynaamista rakennuksen energialaskentaohjelmaa, ulkoiset reunaehdot – kuten ympäröivien pintojen lämpötilat ja säteily-lämmönsiirto eri pintojen välillä – voidaan kuvata tarkemmin kuin aiemmissa ihmismalleissa. HTM käyttää lämpöaistimuksen ja -viihtyvyyden laskennassa Zhangin kehittämää laskentametodia, jolla voidaan arvioidaan lämpöaistimusta ja -viihtyvyyttä myös muuttuvissa lämpöolosuhteissa.

Kudosten lämmönsiirron, lämpöaistimuksen ja lämpöviihtyvyyden laskenta erilaisilla pysyvillä ja muuttuvilla reunaehdoilla on validoitu vertaamalla simulointituloksia oikeilla ihmisillä tehtyihin mittauksiin. HTM-mallilla simuloidut lämpöaistimukset vastasivat mittaustuloksia paremmin kuin Fangerin PMV-menetelmällä lasketut.

Hyvän lämpöviihtyvyyden reunaehtoja arvioitiin simuloimalla erilaisten sisäisten ja ulkoisten muuttujien vaikutusta lämpöaistimukseen. Tulosten mukaan ope-

ratiivinen lämpötila, aktiivisuustaso ja vaatetus ovat tärkeimpiä reunaehtoja lämpöaistimukselle ja -viihtyvyydelle.

Osana rakennuksen energialaskentaohjelmaa HTM-mallilla on mahdollista vertailla aiempaa tarkemmin ja helpommin eri rakennevaihtoehtojen ja talotekniikkajärjestelmien vaikutusta käyttäjän lämpöviihtyvyyteen. Tämän laskentatavan avulla erilaisten ulkoisten (rakenteiden lämmöneristävyys, lämmitys-/jäähdytysjärjestelmä) ja sisäisten (vaatetus, aineenvaihdunta) reunaehtojen vaikutusta lämpöaistimukseen ja -viihtyvyyteen on mahdollista vertailla numeerisesti. HTM-mallin avulla rakennuksen käyttäjän todellista lämpöviihtyvyyttä voidaan pitää lähtökohtana suunniteltaessa laadukkaampia sisäolosuhteita sekä uudisrakennuksiin että korjauskohteisiin. HTM-mallin useita käyttömahdollisuuksia esiteltiin kahdella realistisella esimerkkitapauksella, joissa vertailtiin eri energiakorjaustoimenpiteiden ja lämmönjakotapojen vaikutusta lämpöaistimukseen ja -viihtyvyyteen.

Avainsanat human thermoregulation, building simulation

Preface

This dissertation is based on research work made at VTT Technical Research Centre of Finland during 2005–2012. The aim of the research was to develop and implement a human thermal model module in the VTT House building simulation environment. The members of the research team were principal scientist, Dr. Pekka Tuomaala, senior scientist Riikka Holopainen, senior scientist Kalevi Piira and programming expert Jouko Piippo. Francois Randaxhe, a visiting student from the University of Liège, Belgium was part of the research group during 2009. Dr. Pekka Tuomaala was the head of the research team and the supervisor of this thesis.

The author of this thesis was responsible for the development of the Human Thermal Model (2005–2012). The idea to develop such a model came from Dr. Pekka Tuomaala. The model creation work started from the core issues and the author of this thesis reported and validated all the model simulation results while adding new features or sub-methods to the model (such as blood circulation and thermoregulation). The author was the main responsible person for developing the model by choosing relevant sub-methods, developing and performing the validation tests with different sub-models and analysing the test results, e.g. the effect of using different skin blood flow models on the accuracy of the model in representing the thermal responses of a real human being. Moreover, it was the author who alone estimated the effects of internal and outer boundary conditions on the simulated thermal sensation, and planned and executed the utilization examples of HTM in a renovation case study and in the comparison case study of heating distribution systems.

As the author of this thesis, I want to express my deepest gratitude for my excellent supervisor Dr. Pekka Tuomaala for his continuous enthusiasm and encouragement. I am also deeply grateful to programming expert Jouko Piippo for his invaluable input and patience during the thesis work.

I am very grateful to Markku Lampinen, my supervising professor from the Aalto University Research group of Applied Thermodynamics for the interesting discussions we had during the pre-examination process and for his valuable advice concerning e.g. the thermodynamic aspects of the human thermal model. I want to express my gratitude for the pre-examiners of this thesis: Dr. Dusan Fiala, Dr. Zhang Hui and Dr. Hannu Rintamäki for their valuable advice during the pre-examination process. I am also thankful for the feedback given by research pro-

fessor Miimu Airaksinen from VTT, and Maunu Kuosa and Tuula Noponen from the Aalto University Research group of Applied Thermodynamics.

I am deeply grateful to VTT's STOR TIC members Dr. Sami Katzi and Dr. Matti Kokkala for the valuable financial and scientific backup. I also want to thank all my colleagues at VTT who have been supporting me during my research and the writing process.

I want to thank my dear parents Tuula and Seppo Tielinen for giving me a loving childhood and raising me up to believe in my skills. Besides my parents, I also want to thank my dear mother-in-law Marjatta Holopainen for helping out with the practical details in the everyday life of a family with children. Last but definitely not least I want to heartily thank my family: my dear husband Marko and my dear children Roosa and Jaakko for their love and patience during the long writing process.

The research work has been financed by the basic funding of VTT and by Tekes, the Finnish Funding Agency for Technology and Innovation through the research projects Hattivatti and Enersis.

Academic dissertation

Supervisor
Dr. Pekka Tuomaala
VTT, Technical Research Centre of Finland
Espoo, Finland

Reviewers
Dr. Hui Zhang
Center for the Built Environment
Berkeley, USA

Dr. Dusan Fiala
Universität Stuttgart, Fakultät Architektur und Stadtplanung, Institut für Baustofflehre, Bauphysik, Technischen Ausbau und Entwerfen
Stuttgart, Germany

Dr. Hannu Rintamäki
University of Oulu, Institute of Biomedicine, Department of Physiology
Finnish Institute of Occupational Health
Oulu, Finland

Opponents
Dr. Hannu Rintamäki
University of Oulu, Institute of Biomedicine, Department of Physiology
Finnish Institute of Occupational Health
Oulu, Finland

Dr. Inger Andresen
NTNU, Department of Architecture, History and Technology
Trondheim, Norway

Contents

List of symbols

NOMENCLATURE

Acronym	***Definition***
HTM	Human Thermal Model
PMV	Predicted Mean Value
PPD	Predicted Percentage of Dissatisfied

Symbol	***Unit***	***Definition***
A	m^2	area
c_p	J kg^{-1} $°C^{-1}$	specific heat capacity
C_{res}	W m^{-2}	dry respiratory heat loss per unit area
C	J K^{-1}	heat capacity
C1-C8	–	regression coefficients
D_v	m	average vessel diameter
E_{res}	W m^{-2}	latent respiratory heat loss
E_{sk}	W m^{-2}	evaporative heat loss
f_{cl}	–	clothing area factor
G	W K^{-1}	convective heat conductance
h	J kg^{-1} K^{-1}	enthalpy
h_c	W m^{-2} $°C^{-1}$	convective heat transfer coefficient
h_e	W m^{-2} kPa^{-1}	evaporative heat transfer coefficient
H	W	heating power
I_{cl}	m^2 °C W^{-1}	thermal resistance of clothing
$I_{clu,i}$	m^2 °C W^{-1}	thermal resistance of single garment
k	W m^{-1} $°C^{-1}$	thermal conductivity

L	m	distance
m	kg	mass
$\dot{m}_{art}$	kg s^{-1}	arterial blood mass flow rate
$\dot{m}_{b}$	kg s^{-1}	blood mass flow rate
$\dot{m}_{skin,basal}$	kg s^{-1}	basal skin blood mass flow rate
$\dot{m}_{skin,con}$	kg s^{-1}	constricted skin blood mass flow rate
$\dot{m}_{skin,dil}$	kg s^{-1}	dilated skin blood mass flow rate
$\dot{m}_{skin,\min}$	kg s^{-1}	minimum skin blood mass flow rate
$\dot{m}_{skin,\max}$	kg s^{-1}	maximum skin blood mass flow rate
$\dot{m}_{sw}$	kg s^{-1}	sweat rate
$\dot{m}_{vein}$	kg s^{-1}	venous blood mass flow rate
M	W	metabolic heat generation
M''	W m^{-2}	metabolic heat generation rate
M_{shiv}	W	metabolic heat generation by shivering
$M_{shiv,max}$	W	max. increase in metabolic heat generation by shivering
n	–	regression coefficient
p	–	parameter for rectal temperature after death
P_a	Pa	ambient water vapour pressure
$P_{sk,s}$	Pa	water vapour pressure at skin surface
p_a	Pa	partial water vapour pressure
q_{rad}	W	radiative heat transfer
$R_{e,cl}$	m^2 Pa W^{-1}	evaporative heat transfer resistance
R_t	m^2 °C W^{-1}	thermal resistance
$S_{overall}$	–	overall thermal sensation
So^-	–	cool overall thermal sensation
So^+	–	warm overall thermal sensation
$S_{local,i}$	–	local thermal sensation for segment *i*
t	°C	temperature
t	s	time
t_a	°C	ambient air temperature
t_{artery}	°C	artery temperature
t_{cl}	°C	surface temperature of clothing

t_{core}	°C	core temperature
$\bar{t}_r$	°C	mean radiant temperature
t_{re}	°C	rectal temperature
$t_{re,d}$	°C	rectal temperature at time of death
t_{shiver}	°C	shivering threshold
t_{sweat}	°C	sweating threshold
t_{vein}	°C	vein temperature
v_{ar}	m s^{-1}	relative air velocity
$\dot{V}_{skin.basal}$	m^3 s^{-1} kg^{-1}	basal skin blood flow rate per skin tissue mass
$\dot{V}_{skin,\max}$	m^3 s^{-1} kg^{-1}	maximum skin blood flow rate per skin tissue mass
$\dot{V}_{skin,\min}$	m^3 s^{-1} kg^{-1}	minimum skin blood flow rate per skin tissue mass
W	W m^{-2}	external work
w	–	skin wettedness
$weight_i$	–	weighting factor for segment i
Z	–	body shape parameter

Greek symbols

Symbol	***Unit***	***Definition***
ρ	kg m^{-3}	density
ρ_b	kg m^{-3}	blood density
ρ_s	kg m^{-3}	skin density

Subscripts

art	arterial
b	blood
bp	body part
s	skin
t	tissue
ven	venous

1. Introduction

1.1 General background

The housing sector and the construction industry play a significant role in global energy consumption: Buildings account for circa 40% of the total energy use in Europe (EC 2008), and for about 36% of the EU's total CO_2 emissions (IPCC 2001, COM 2008). In the northern part of the European Union, 41% of the total final energy use comes from buildings, with 30% being used in residential buildings (Itard and Meijer 2009). In most countries, energy production is extensively based on fossil fuels, so the building sector has a clear connection to environmental issues.

Environmental and economic reasons increase the pressure to design, construct and maintain more energy-efficient buildings in future, such as very low-energy houses, passive houses and nearly zero-energy houses. Improving energy-efficiency will bring unavoidable changes in structural and building service system design practices. In energy-efficient buildings, the indoor surface temperatures of better insulating envelope components will increase during heating periods. At the same time surface temperatures of (at least traditional) heating devices tend to decrease due to heating demand reduction. Dimensioning criteria of building structures and heating or cooling systems for future very low-energy buildings need to be reconsidered to ensure the proper functionality of building service systems, and increase the applicability of renewable low-exergy energy sources (i.e., low temperature heating and high temperature cooling). This new design and dimensioning criteria must also ensure the overall thermal comfort of the building user.

During the 1970's oil crisis many energy efficiency measures were made in the Finnish building sector, which resulted in occupant discomfort. The current EU 20-20–20 goals aim in diminishing drastically the energy use of the building sector. Besides a major need of energy renovation measures, also the new buildings will have significantly more insulation than before. These increased insulation levels have been reported to cause over-heating problems during the summer and thus might be leading to installing an electricity-consuming cooling system.

More research is needed to better understand the behaviour of energy-efficient buildings, and particularly the interaction between indoor air quality, comfort, ventilation and energy consumption (Wargocki et al. 2000, Seppänen et al. 1999).

There is a quantitative relationship between work performance and temperatures inside, below and above the comfort zone (Seppänen et al. 2006).
Since thermal issues seem likely to be the dominant cause of indoor environment complaints even in the future, it is important to understand the true nature of human thermal sensation and comfort.

To estimate in advance the thermal comfort of a new or renovated building, a thermal comfort calculation method is needed. The widely used Fanger's PMV method (Fanger 1970) is a heat balance model, which views the human being as a passive recipient of thermal stimuli, assuming that the effects of the surrounding environment are explained only by the physics of heat and mass exchanges between the body and the environment.

A real human being adapts into changing conditions in the surrounding environment by means of the thermoregulation system. There is a very old and simple experiment described by English philosopher John Locke in his 1690 Essay Concerning Human Understanding: *"A person places one hand in a basin of warm water and the other in a basin of cool water. After a short time, both hands are placed together in a third basin of water, which is at intermediate temperature. The hand previously in warm water feels cool and the hand previously in cool water feels warm even though they are actually at the same temperature."* In a similar way, people are probably more often exposed to spatially non-uniform and transient temperatures than to thermal environments that are uniform and stabile. We experience transient and non-uniform temperature conditions when moving between spaces – e.g., from indoors to outdoors, from sun to shade, and when occupying spaces with widely varying temperatures (Zhang 2003).

1.2 Aim and objectives

The function of the human thermoregulation system has earlier been modelled by means of human thermal models. In spite of the high number of different human thermal models, there are few approaches where a human thermal model has been integrated with a CFD tool and presumably no previous approaches, where the model has been integrated with a building simulation environment.

The aim of this thesis is developing a new multi-node Human Thermal Model (HTM) implemented in a dynamic building simulation environment. The major new scientific knowledge of the thesis is combining the human thermal modelling with a thermal sensation and comfort model inside of a building simulation program. This approach enables calculating the boundary conditions of the surrounding space (interaction and non-uniform transient heat transfer between the skin surface and the surrounding building structures) more realistically than the Fanger's PMV method and those human thermal models, which are not implemented in a building simulation program. HTM can be utilized for estimating the interaction of alternative building structures, building service systems and individual human parameters on human thermal comfort more accurately than before.

The objectives of this thesis are to present the main features of the developed new human thermal model, show its accuracy in calculation of both tissue temperatures, thermal sensation and comfort, estimate the significance of internal and external parameters on thermal sensation and finally show with two realistic case studies how the model can be effectively utilized in estimating the effects of different structures and building service systems on the thermal sensation and comfort of the building user.

Literature review presents the history of human thermal modelling, definition of thermal sensation and comfort, Fanger's PMV method, Zhang's thermal sensation and thermal comfort calculation method and the VTT House building simulation environment.

The Human Thermal Model-chapter explains the developed passive and control systems, energy equations, and adopted thermal sensation and comfort simulation methods of HTM are explained. The emphasis of the development work was in creating a thermal comfort estimation tool, which is suitable for building design purposes. As HTM is a module of a building simulation tool, whose calculation method is based on solving heat and mass transfer balance equations, the existing human thermal models could not be straight implemented in HTM. The different sub-methods (e.g. skin blood flow) were selected based on their suitability for achieving the desired accuracy for building design purposes and the selected sub-methods had to be based on physical phenomena. The model creation work started from the core issues and the model simulation results were reported and validated continuously while adding new features or sub-methods to the model (blood circulation, thermoregulation). This working method minimised possible errors and enabled a controlled development work.

Verification and validation of the Human Thermal Model presents the various steady-state and dynamical tests cases used to develop and validate the calculation of tissue temperatures, clothing, thermal sensation and comfort. The tests have also been used by other human thermal model developers.

The significance of internal and external boundary conditions on thermal sensation is studied using the HTM method. HTM results are compared with the results obtained with the Fanger's PMV method to highlight the differences between these methods.

The utilization of HTM is presented with realistic case studies: the effect of building structures and heating distribution system on occupant's thermal sensation and comfort.

2. Literature review

2.1 History of human thermal modelling

Representing the human body from a thermokinetic point of view is not a new innovation: the first attempt was made exactly one hundred years ago, in 1911, by Lefevre (Fu 1995). Lefevre considered the body as a sphere, where the core produced heat and the shell transferred the heat to the environment. The first mathematical thermal model including the body anatomy and a control function was published by Burton in 1934 (Fu 1995). The human thermal models have evolved from a one node model into multi-layered cylinders representing separate body parts connected by a circulatory blood flow. The earliest thermal models were either 1-D or quasi 2-D models. They typically possessed a very crude model of the circulatory system, which is responsible for roughly 85% of human internal heat transfer. There was also no true geometry of the human body. According to Fu (1995) the different models can be classified into four categories:

1. one node thermal models
2. two-node thermal models
3. multi-node thermal models
4. multi-element thermal models.

One node thermal models represent the human body with only a node and they do not include a thermoregulatory system. One node models are called empirical models, because they predict thermal responses to a given environmental condition based on formulas obtained from experimental conditions (Fu 1995). Two-node thermal models are lumped parameter models. They divide the body into two concentric shells, where the central core represents internal organs, bone, muscle and subcutaneous tissue and the outer shell represents the skin layer. As the temperatures of both shells are usually assumed to be uniform, the model thermally consists of two nodes.

The most well-known two-node model is Gagge's model (also called Pierce's model), which was developed in 1971 (Gagge 1971). It calculates the thermal response by means of two energy balance equations, one for the core node and one for the skin node. Gagge's model takes into account the effects of heat accumulation, physical work done, conductive and convective heat transfer by blood

flow between the core and shell, sensible and latent heat loss caused by respiration, metabolic heat generated during exercise and shivering, energy transfer corresponding to the mass shift between nodes and the heat exchange processes between the skin and its surroundings by means of convection, radiation and evaporation of moisture.

Gagge improved the model in 1986 (Gagge et al. 1986) by adding control functions for the blood flow rate, sweat rate, shivering metabolic rate and the fraction of total mass assigned to skin layer. The thermal control functions were functions of core and skin temperature signals. When the core and skin temperatures exceeded their thermoneutral values (36.8 ºC and 33.7 ºC, respectively) their signals were warm. When the temperatures were lower than the thermoneutral values, the signals were cold. The warm core signal controlled vasodilation, the warm core and skin signals controlled the sweat rate, the cold skin signal controlled vasoconstriction and the cold skin and core signals controlled the shivering metabolic rate. A cold skin signal and a warm core signal controlled the skin mass fraction (the fraction of the total mass assigned to the skin layer) and the blood flow rate between the core and the skin.

Gagge's model is simple and easy to use, but it can only be applied to situations with moderate levels of activity and uniform environmental conditions (Smith 1991). The one-dimensional Gagge's model was extended to a quasi 2-D segmented two-node model by Jones in 1992 (Jones and Ogawa 1992). In Jones's model the core was represented by a single node, but the skin layer was represented by several nodes.

Multi-node thermal models are extended from the two-node models. They contain more than two concentric shells and the energy balance equation is written to each layer separately. The first multi-node thermal model was developed by Crosbie et al. in 1963 (Crosbie et al. 1963). Crosbie's model was also the first model, which took account of the physiological thermal regulation mechanism. The body was divided into three layers of nodes: the core, the muscle layer and the skin layer. The core was the source of basal metabolism and the muscle layer was the source of increased metabolism due to increased activity or shivering. The energy balance equations were written for each layer separately. Crosbie et al. used an analogue computer to solve the equations, which was the first time a computer was used for the simulation of an entire-body physiological temperature regulation.

One of the most well-known multi-node models is Stolwijk's thermal model created during 1966–1977 (Stolwijk and Hardy 1966, Stolwijk 1971, Stolwijk 1977), which has been the starting point of many other thermal models. Stolwijk divided the human body into five cylindrical body parts representing the trunk, arms, hands, legs and feet and a spherical body part for the head. Each part was further divided into four concentring shells representing the core and muscle, fat and skin layers. The blood temperature was assumed to be uniform. The blood circulation system was calculated with one node, a kind of central blood pool located in the trunk. The central blood pool was connected to all tissue nodes by a network of blood vessels. The heat transfer between tissue nodes was assumed by

conduction and the heat transfer between the central blood node and the adjacent tissue node was assumed by convection. The only connection between body parts was through the central blood pool. The total number of nodes in Stolwijk's model was 25 (24 tissue nodes and one blood node), and the energy balance equations were written for each node. The energy balance equations included heat accumulation, blood convection, tissue conduction, metabolic generation, respiration and heat transfer to the environment by means of convection, radiation and evaporation. The thermal control was described as functions of two tissue temperature signals: one signal was a hot/cold signal as in Gagge's model, and the other signal was related to the rate of change in tissue temperatures.

Multi-element thermal models divide the body into several elements representing body parts. The energy balance equation is established for each body part along with the control equations for blood flow rate, shivering, sweating, etc. The equations are solved with finite-difference or finite-element methods (Fu 1995). Multi-element thermal models often give better results than multi-node models because they do not apply the assumption of uniform node temperatures.

An example of a multi-element model is Wissler's model, developed between 1961 and 1985, which consisted of 6 (later 15) elements connected by the vascular system (Wissler 1964, Wissler 1985). The model took into account the heat loss through the respiratory system and the countercurrent heat exchange between large arteries and large veins. The vascular system was composed of arteries, veins and capillaries and the blood temperatures of arteries and veins were assumed to be uniform. The blood circulated from the heart (in the upper part of the trunk) through arteries to the arterial pool of each element and further into the capillaries of each element. From the capillaries, the blood circulated to the venous pool of the element and back to the heart. The connection between elements was only through macrocirculation. The model also took into account transient factors by means of a transient bioheat equation. The passive system of Wissler's model was very detailed compared to previous models.

Smith (1991) developed the first 3-D transient, multi-element thermal model for the entire human body (Fu 1995). The model included detailed control functions applied to the human thermoregulatory system. The body was divided into 15 body parts, which were connected by the central macrocirculation and superficial veins, an improvement compared to Wissler's model. The blood flow in circular vessels was 1-D steady-state Newtonian flow. Smith's model had a nearly periodic nature of respiration through inhaling and exhaling, the air velocity in respiratory tracks was calculated as a function of the volumetric oxygen consumption rate. Smith was probably first to calculate the sensible and latent respiratory heat losses. Thermal control equations were developed for the variation of skin blood vessel radii during vasomotor response, the sweat rate and the shivering metabolic rate as functions of the core and mean skin temperatures. The heat transfer equations are solved simultaneously by the finite-element method with a simple element (grid) mesh. The blood circulatory system and the respiratory tract are simulated as 1-D elements with a length of 0.01 cm.

Smith's model is based on a more realistic representation of the human body than previous models. Because of 3-D calculation, it is also applicable to situations with large temperature gradients or highly non-uniformal thermal conditions. The limitation of the model is that the fat and skin layers are modelled as one layer. This affects the heat convection to the skin surface carried by blood flow and the entire-body thermal response. As result simulation results obtained during cold or exercise conditions are not accurate (Wissler 1988). Other limitations are neglecting the blood perfusion incurred in the capillary beds and assuming no moisture accumulation on the skin surface.

Fu (1995) developed the first model for the clothed human on the basis of Smith's model. The finite-element method used by Fu enables a fine nodal spacing and employment of detailed thermoregulatory mechanisms. The model introduces new solutions for blood perfusion, fibre absorption of clothing, fabric interstice effect, radiation in the clothing, and moisture evaporation and accumulation in the skin and clothing.

The passive system of the IESD Fiala model (Fiala 1999) is a multi-segmental multi-layered representation of the human body with spatial subdivisions. The passive model consists of 15 spherical or cylindrical body elements: head, face, neck, shoulders, arms, hands, thorax, abdomen, legs, and feet. There are seven different tissue materials: brain, lung, bone, muscle, viscera, fat, and skin. The skin is modelled as two layers: the inner and the outer skin layer. Metabolic heat is generated and blood is perfused in the inner skin layer. The outer skin layer simulates the vapour barrier for moisture diffusion through the skin. Body elements are divided into three sectors: anterior, posterior, and inferior. Anterior and posterior segments permit the treatment of lateral environmental asymmetries. Inferior segments represent body sides, which are ''hidden'' by other body parts and therefore have reduced radiant heat exchange with the environment. The blood circulatory system consists of three main components: the central blood pool, counter current heat exchanges, and pathways to individual tissue nodes. Blood flows from the central pool through major arteries to body elements. Along the way, the blood is cooled by heat lost to the counter current bloodstreams in the adjacent veins. The arterial blood exchanges heat by convection in the capillary beds. The venous blood collects in the major veins and is rewarmed by heat from the adjacent arteries as it flows back to the central blood pool. It mixes with blood from other elements to produce the new central blood pool temperature. In the blood perfusion calculation, it is assumed (Fick's first principle) that heat is exchanged with the tissue in the capillary bed and no heat storage occurs in the bloodstream. Calculations are performed using the finite-difference method and the Crank-Nicholson approach was adopted for derivatives with time.

The active system of the Fiala model (Fiala 2001) was developed by means of regression analysis using measured responses (whole-body metabolism, evaporative weight/heat loss, body core temperature) obtained from air exposures to cold stress, cold, moderate, warm and hot stress conditions, and exercise intensities between 0.8–10 MET. The model has been verified and validated using independent experiments, and the results revealed good agreement with measured

data for regulatory responses, mean and local skin temperatures, and internal temperatures for the whole spectrum of boundary conditions considered.

Marken Lichtenbelt et al. (2004) have used Fiala's model to predict the average human physiological responses. The results showed discrepancies in measured responses of individuals exposed to comfortable and mild cold environmental conditions. The effect was largest on the exposed body elements, because of the largest variation in temperature on these parts. The source or error was the energy metabolism calculation. Using the actual, measured metabolism during the test improved the accuracy of the calculation on a group level but the deviations on an individual level still remained large. Fiala's active system is based on a regression model. Marken Lichtenbelt et al. suggest using a model with a more physiological background: integration of physiological based control-mechanisms in the model.

One of the most sophisticated multi-segment multi-node bioheat models is the Berkeley Comfort Model of Huizenga et al. (Huizenga 2001), which is based on the Stolwijk model. The improved blood flow model includes a counter flow heat exchange and perfusion from vessels to tissues. A clothing node has been added to the model for calculation of heat and moisture capacitances. The model also calculates the heat transfer by conduction to surfaces in contact with the body. There is a better estimation of the convection and radiation heat transfer coefficients, an explicit radiation heat transfer calculation using angle factors and the addition of a radiation heat flux model. It can simulate an arbitrary number of human body segments. Each of these segments consists of four body layers (core, muscle, fat, and skin tissues) and the clothing layer. A blood flow model (including counter flow heat exchange in the limbs, and modified blood perfusion from vessels to tissue), a clothing node to model both heat and moisture capacitance, heat transfer by conduction to surfaces in contact with the body, improved convection and radiation transfer coefficients, explicit radiation heat transfer calculation using angle factors, and radiation heat flux model (e.g., sunlight striking the body) are also included.

The Berkeley Comfort Model includes a user interface with the ability to create a room with windows and place the occupant anywhere in the room, and a library of HVAC systems. The room model can import climate data from EnergyPlus and calculate heat transfer between the occupant and the environment by convection, conduction, and radiation. The model can generate graphic results of, for example, skin temperature distributions, equivalent homogenous temperatures, and overall comfort indices.

The NREL Human Thermal Physiological Model, a three-dimensional transient finite element model, contains a detailed simulation of human internal thermal physiological systems and thermoregulatory responses (Rugh et al. 2004). The thermoregulation system is based on the analysis of a large amount of independent experimental data. The model consists of a human tissue system and a thermoregulatory system. The thermoregulatory system controls physiological responses, such as vasomotor control, sweating, and shivering. The human tissue system represents the human body, including the physiological and thermal prop-

erties of the tissues. The overall model consists of approximately 40,000 nodes and elements. Because the model is very detailed, a fairly complete picture of temperature distributions can be obtained.

Another highly sophisticated mathematical multi-segmented human thermal model was developed by Salloum et al (2007) for predicting nude human thermal and regulatory responses. The passive model segments the body into 15 cylindrical segments. Each body segment is divided into four nodes of core, skin, artery blood, and vein blood. In any body element, the blood exiting the arteries and flowing into the capillaries is divided into blood flowing in the core (exchanges heat by perfusion in the core) and blood flowing into the skin layer (exchanges heat by perfusion in the skin). The model calculates the blood circulation flow rates based on exact physiological data, and real dimensioning and anatomic positions of the arteries in the body.

Foda and Siren (2011) have modified the Gagge model (1986) based on their measurements of local skin temperature. The modification was based on manipulating the local core set points, using a modified calculation procedure for the convective heat transfer coefficients, and adjusting the heat transfer term from core to skin using common blood temperature along with local core temperatures. The new model is called the MS-Pierce-model. Foda et al. (2011) have tested the MS-Pierce model (Foda and Siren 2011), Fiala model (Fiala 1999, 2001) and the Berkeley Comfort Model (Huizenga 2001) against measured skin temperatures and Munir's dynamical test case (Munir et al 2009). The MS-Pierce-model had the best predictability of skin temperatures in the steady-state and dynamical calculation. The maximum deviation in Munir's dynamical test case of the MS-Pierce-model was close to 2 K.

Many different human thermal models have been created in recent years. However, only a few scientific articles about the utilization of the models in situations concerning everyday life can be found. In some approaches, a human thermal model has been connected with a CFD program to simulate the thermal comfort inside a vehicle cabin (Alahmer et al. 2011), but there are few, if any, approaches connected with building simulation programs.

2.2 Definition of thermal sensation and thermal comfort

As the human body continuously generates heat from about 75 W during sleep to 1 000 W during hard exercise, the excess heat must be transferred to the environment by means of radiation, convection, conduction and evaporation in a carefully controlled manner. The internal organs of a human being must maintain a fairly constant temperature for comfort, around 37.0 ± 0.5 °C. The maximum deviation of the core temperature is about 2 °C from its normal level (Fu 1995). The aim of the human thermoregulatory system is to keep the core temperature constant (Hensel 1981).

The core temperature is controlled by the thermoregulatory system consisting of thermoreceptors and hypothalamus. The thermoreceptors are located in differ-

ent parts of the body sending signals about the local temperature level and its change to the hypothalamus. Each type of thermoreceptor is activated within a specific range of temperature. When a thermoreceptor is subjected to an abrupt change in temperature, it is first strongly stimulated. This effect is called "overshoot" (Zhang 2003). The strong stimulation phase is short and the stimulation decreases asymptotically until it reaches a steady response rate. The magnitude of the stimulus depends on the stimulus area as well as on the stimulated body part (Hensel 1981). The hypothalamus reacts to the signals by means of thermoregulatory functions by either inhibiting or enhancing heat production and heat loss. The possible responses include the increase of the skin blood flow rate (*vasodilation*), decrease of the skin blood flow rate (*vasoconstriction*), sweating and shivering. Skin is the principal organ for dissipating heat: the human body dissipates approximately 85% of its heat loss through the skin under normal environmental conditions (Zhang 2003).

Thermal sensation is the sense of temperature, reflecting the response of thermoreceptors. As thermal sensation is related to how people "feel", it is not possible to define it in physical or psychological terms (Hensen 1991). According to Hensel (1981) the thermosensivity of the skin is different in different body parts. Therefore the thermal sensation and thermal comfort calculation should also take into account body part-specific thermal sensation, especially in spaces with uneven surface temperature distribution caused for example by windows or radiators.

Thermal comfort describes the synthesized feeling about the body's thermal state. Hensen (1991) defines thermal comfort as "*a state in which there are no driving impulses to correct the environment by behaviour*" (Hensen 1991). The definition by ASHRAE is "*the condition of mind in which satisfaction is expressed with the thermal environment*" (ASHRAE 2004). Thermal comfort is strongly related to the thermal balance of the body, which itself is influenced by environmental and personal parameters (Hensen 1991):

- Environmental parameters: air temperature, mean radiant temperature, relative air velocity, relative humidity
- Personal parameters: activity level or metabolic rate, thermal resistance of clothing.

2.3 Fanger's PMV method

Several methods are used for the estimation of thermal sensation and comfort. The widely used international standards ISO 7730 (2005) and ASHRAE 55 (2004) use Fanger's PMV (Predicted Mean Vote) method (Fanger 1970). Fanger's PMV method, developed in 1970, is based on a heat balance model, also referred to as a "static" or "constancy" model. While assuming that the effects of the surrounding environment are explained only by the physics of heat and mass exchanges between the body and the environment, heat balance models view the human being as a passive recipient of thermal stimuli.

The PMV method combines four physical variables (air temperature, air velocity, mean radiant temperature, and relative humidity), and two personal variables (clothing insulation and activity level) into an index that can be used to predict the average thermal sensation of a large group of people in a space. The PMV-index predicts the mean response of a large group of people according to the ASHRAE thermal sensation scale (ASHRAE 1993) presented in Table 1.

Table 1. ASHRAE thermal sensation scale (ASHRAE 1993).

Index	thermal sensation
3	hot
2	warm
1	slightly warm
0	neutral
-1	slightly cool
-2	cool
-3	cold

The PMV index is based on the heat balance of the human body: in thermal balance the internal heat production in the body is equal to the loss of heat to the environment. For the development of the PMV index the physiological response of the thermoregulatory system has been related statistically to thermal sensation votes collected from more than 1,300 subjects. (ISO 2005). The PMV index is calculated with the equation (Fanger 1970).

$$PMV = \left(0.303\,\mathrm{e}^{-0.036M} + 0.028\right)\left\{\begin{array}{l}\left(M'' - W\right) - 3.05\cdot 10^{-3}\cdot\left[5773 - 6.99\left(M'' - W\right) - p_a\right] \\ - 0.42\cdot\left[\left(M'' - W\right) - 58.15\right] - 1.7\cdot 10^{-5} M''\left(5867 - p_a\right) \\ - 0.0014 M''\left(34 - t_a\right) - 3.96\cdot 10^{-8} f_{cl} \\ \cdot\left[\left(t_{cl} + 273\right)^4 - \left(\bar{t}_r + 273\right)^4\right] - f_{cl} h_c \left(t_{cl} - t_a\right)\end{array}\right\} \quad (1)$$

where M'' is the metabolic heat generation rate, W is the external work (equal to zero for most activities), p_a is the partial water vapour pressure, f_{cl} is the clothing area factor (ratio of clothed/nude surface area), t_a is the ambient air temperature, $\bar{t}_r$ is the mean radiant temperature, h_c is the convective heat transfer coefficient and t_{cl} is the surface temperature of clothing. The clothing area factor f_{cl} is calculated as (Fanger 1970)

$$f_{cl} = \begin{cases} 1.00 + 1.29 I_{cl} \text{ for } I_{cl} \le 0.078\ \mathrm{m^2\,^oC/W} \\ 1.05 + 0.645 I_{cl} \text{ for } I_{cl} > 0.078\ \mathrm{m^2\,^oC/W} \end{cases} \quad (2)$$

where I_{cl} is the thermal resistance of clothing. The convective heat transfer coefficient h_c is (Fanger 1970)

$$h_c = \begin{cases} 2.38(t_{cl} - t_a)^{0.25} \text{ for } 2.38(t_{cl} - t_a)^{0.25} > 12.1\sqrt{v_{ar}} \\ 12.1\sqrt{v_{ar}} \text{ for } 2.38(t_{cl} - t_a)^{0.25} < 12.1\sqrt{v_{ar}} \end{cases} \quad (3)$$

where v_{ar} is the relative air velocity (relative to the human body). The surface temperature of clothing, t_{cl}, is calculated as (Fanger 1970)

$$t_{cl} = 35.7 - 0.028(M'' - W) - I_{cl}\left\{ \begin{array}{l} 3.96 \cdot 10^{-8} f_{cl} \cdot \left[(t_{cl} + 273)^4 - (\bar{t}_r + 273)^4 \right] \\ + f_{cl} h_c (t_{cl} - t_a) \end{array} \right\} \quad (4)$$

The Predicted Percentage of Dissatisfied (PPD)-index is a quantitative measure of the thermal comfort of a group of people in a particular thermal environment. Fanger (1970) related PPD to PMV as follows:

$$\text{PPD} = 100 - 95e^{-\left(0.03353\,\text{PMV}^4 + 0.2179\,\text{PMV}^2\right)} \quad (5)$$

The PMV equation (Eq. 1) rests on steady state heat transfer theory and this state never precisely occurs in daily life, which is better described as a state of dynamical thermal equilibrium (Humphreys and Nicol 2002). Fanger's thermal model is therefore applicable only to homogenous, steady-state and uniform thermal environments close to thermal neutrality.

International standard ISO 7730 (ISO 2005) is widely used for the evaluation of conditions for thermal comfort. The standard presents a method for predicting the thermal sensation and the degree of discomfort (thermal dissatisfaction) of people exposed to moderate thermal environments and specifies acceptable thermal environmental conditions for comfort. It enables the analytical determination and interpretation of thermal comfort using a calculation of PMV (predicted mean vote) and PPD (predicted percentage of dissatisfied) and local thermal comfort, giving the environmental conditions considered acceptable for general thermal comfort as well as those representing local discomfort.

According to the ISO 7730 standard, PMV is derived for steady state conditions, but it can be applied with good approximation during minor fluctuations of one or more of the variables, provided that time-weighted averages of the variables during the previous 1 hour period are applied. It is also recommended that the PMV index is used only for

- PMV values between -2 and +2
- metabolic heat generation rate M'' values between 46 W/m^2 and 232 W/m^2 (0.8 met and 4 met)
- thermal resistance of clothing I_{cl} between 0 m^2°C/W and 0.310 m^2°C/W (0 clo and 2 clo)
- ambient air temperature t_a between 10 °C and 30 °C
- mean radiant temperature $\bar{t}_r$ between 10 °C and 40 °C
- relative air velocity v_{ar} between 0 m/s and 1 m/s.

deDear (1998) has created a database of over 20,000 individual comfort votes with corresponding measurements of the thermal environment for ASHRAE. The database describes the environments of approximately 160 (mainly office) buildings, which are centrally air-conditioned, mixed mode or naturally ventilated. deDear and Brager have used the database to examine the behaviour of PMV. They found that PMV overestimates the subjective warmth sensations of people in warm naturally ventilated buildings.

Humphreys and Nicol (2000) have shown that PMV is less closely correlated with the comfort votes than with the air temperature or globe temperature. Humphreys (2000) has also shown that the discrepancy between PMV and the mean comfort vote is related to the mean temperature of the accommodation. In (Humphreys and Nicol 2002) the validity of ISO-PMV for predicting comfort votes in everyday thermal environments is examined. This comprehensive exploration shows for example that

- PMV overestimates the warmth sensation at room temperatures above about 27 °C and at higher temperatures the bias becomes severe
- PMV underestimates the cooling effect of increased air movement
- with increased activity corresponding to 1.8 met, PMV overestimates the sensation of warmth by one scale unit
- PMV overestimates the warmth of people in heavier clothing (over 1.2 clo).

The overall conclusion of (Humphreys and Nicol 2002) is that PMV is valid for everyday prediction of the comfort vote only under severely restricted conditions. PMV progressively overestimates the mean perceived warmth of warmer environments and the coolness of cooler environments. The overestimation of perceived warmth can lead to the provision of unnecessary cooling. Using PMV at the design stage might therefore, for example, misleadingly indicate that a building would need a cooling system to maintain comfortable indoor conditions in summer.

2.4 Zhang's thermal sensation and thermal comfort model

Zhang (2003) has developed a thermal sensation model to predict local and overall sensations, and local and overall comfort in non-uniform transient thermal environments. The local thermal sensation is represented by a logistic function of local skin temperature. The overall thermal sensation and comfort are calculated as a function of the local skin temperatures and the core temperature, and their change over time (Figure 1).

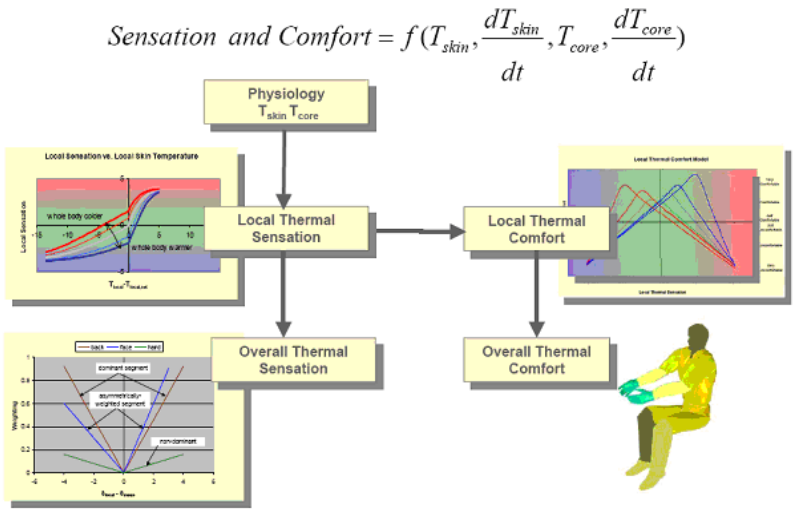

Figure 1. Calculation of thermal sensation and thermal comfort according to Zhang.

According to Fiala (2003) the relationship between the skin temperature and thermal sensation is linear in the region where the mean skin temperature is between 3 °C below and 1 °C above its set point. The set point is defined as the local skin temperature when the thermal sensation of that body part feels neutral (local thermal sensation index = 0). Zhang (2003) proposes that the local thermal sensation S_{local} is a logistic function of local skin temperature, presented as the difference between the local skin temperature and its set point:

$$S_{local} = 4\left(\frac{2}{1+e^{-C1\left(t_{skin,local}-t_{skin,local,set}\right)-K1\left[\left(t_{skin,local}-\ddot{t}_{skin}\right)-\left(t_{skin,local,set}-\ddot{t}_{set}\right)\right]}}-1\right), \quad (6)$$
$$+C2_i\frac{dt_{skin,local}}{dt}+C3_i\frac{dt_{core}}{dt}$$

where $t_{skin,local}$ is the local skin temperature, $t_{skin,local,set}$ is the local skin set point temperature, $\ddot{t}_{skin}$ is the mean whole-body skin temperature and $\ddot{t}_{set}$ is the mean whole-body skin set point temperature. Terms K1, C1, C2 and C3 are body-part specific regression coefficients.

The logistic function shows a linear relationship between the skin temperature and thermal sensation when the skin temperature is near its set point, but levels off when the skin temperature differs from the set point. When the local skin temperature differs from the local skin temperature set point, the sensation reaches the sensation scale limits between +4 and -4 (Table 2). The indexes from +3 to -3 are identical with the ASHRAE thermal sensation scale (Table 1).

In the first term on the right-hand side of Eq. 6 the multiplier 4 defines the sensation range from very cold (-4) to very hot (+4) and the first exponent $C1\left(t_{skin,local} - t_{skin,local,set}\right)$ controls the slope of the function. Besides local skin temperature, the local thermal sensation is also influenced by the overall thermal state. According to measurements by Zhang (Zhang 2003) a body part with the same local skin temperature feels relatively warmer when the rest of the body is colder, and colder when the rest of the body is warmer. The second exponent $K1\left[\left(t_{skin,local} - \ddot{t}_{skin}\right) - \left(t_{skin,local,set} - \ddot{t}_{set}\right)\right]$ represents the modifying effect of whole-body thermal status on local sensation. In the modification term, the difference between local and overall sensation is represented by the difference between local and mean skin temperatures. When the difference between local and mean skin temperatures equals the difference of their set points, the contribution from whole-body thermal sensation is zero.

Table 2. Thermal Sensation index scale (Zhang 2003).

Index	Thermal sensation
4	very hot
3	hot
2	warm
1	slightly warm
0	neutral
-1	slightly cool
-2	cool
-3	cold
-4	very cold

The measurements by Zhang (2003) showed that the relationship between sensation and skin temperature is much steeper on the warm side than on the cold side. Therefore, the regression coefficients C1 are also different when the local skin temperature is colder or warmer than the local skin set point temperature. Table 3 shows the body part-specific regression coefficients C1 and K1. A large value for C1 indicates a large cooling or heating sensation for a small decrease/increase in the skin temperature.

Table 3. Body-part specific regression coefficients C1 and K1 for the static part of the local thermal sensation calculation (Zhang 2003).

	C1 ($t_{skin,local} < t_{skin,local,set}$)	C1 ($t_{skin,local} \geq t_{skin,local,set}$)	K1
Face	0.15	0.70	0.10
Head	0.38	1.32	0.18
Neck	0.40	1.25	0.15
Chest	0.35	0.60	0.10
Back	0.30	0.70	0.10
Pelvis	0.20	0.40	0.15
Upper arm	0.29	0.40	0.10
Lower arm	0.30	0.70	0.10
Hand	0.20	0.45	0.15
Thigh	0.20	0.29	0.11
Lower leg	0.29	0.40	0.10
Foot	0.25	0.26	0.15

When the derivatives of skin and core temperatures (second and third term on the right-hand side of the equation) are zero, the model predicts thermal sensation in a steady state condition. The thermal sensation calculation method by Zhang includes a dynamic portion to predict local sensation in transient conditions. The dynamical portion is separated into two parts for positive and negative derivatives of skin temperature. A positive derivative means local heating and a negative derivative means local cooling. People's overall response to cooling is much stronger than their response to heating, which is also confirmed by measurements by Zhang. The regression coefficients C2 are therefore provided separately for positive and negative derivatives of skin temperature. The core temperature responds to local cooling of most influential body parts (face, chest, back and pelvis) with an immediate increase. This is reflected in the negative coefficient C3. Table 4 lists the body part-specific regression coefficients C2 and C3.

Table 4. Body-part specific regression coefficients C2 and C3 for the dynamical part of the local thermal sensation calculation (Zhang 2003).

	C2 (local cooling)	C2 (local heating)	C3
Face	37	105	-2289
Head	543	90	0
Neck	173	217	0
Chest	39	136	-2135
Back	88	192	-4054
Pelvis	75	137	-5053
Upper arm	156	167	0
Lower arm	144	125	0
Hand	19	46	0
Thigh	151	263	0
Lower leg	206	212	0
Foot	109	162	0

The overall thermal sensation $S_{overall}$ is a weighted average of all the local sensations:

$$S_{overall} = \frac{\sum \left(weight_i S_{local,i} \right)}{\sum \left(weight_i \right)} \tag{7}$$

where $S_{local,i}$ represents the local sensation for segment i, and $weight_i$ is the weighting factor for that segment (Table 5). The weighting factors are based on measurement results from three types of conditions: uniform/stable environments (32 tests), step change transients between two different uniform environments (5 tests), and heating/cooling of local body parts under cool/warm ambient environments (242 tests).

Table 5. Thermal Sensation weighting factors (Zhang 2003).

Body part	Weighting factor
Head	0.07
Chest	0.35
Lower arm	0.14
Hand	0.05
Thigh	0.19
Lower leg	0.13
Foot	0.07
Sum	**1.0**

The local thermal comfort function by Zhang is a piecewise linear function of local and overall thermal sensations:

$$TC_{local} = \left[\frac{-4-\left(C6+C71\left|So^{-}\right|+C72\left|So^{+}\right|\right)}{\left|\left(-4+C31\left|So^{-}\right|+C32\left|So^{+}\right|+C8\right)^{n}} - \frac{-4-\left(C6+C71\left|So^{-}\right|+C72\left|So^{+}\right|\right)}{\left|\left(4+C31\left|So^{-}\right|+C32\left|So^{+}\right|+C8\right)^{n}} \right. \\ \left. \frac{}{e^{15\left(SI+C31\left|So^{-}\right|+C32\left|So^{+}\right|+C8\right)}+1} + \frac{-4-\left(C6+C71\left|So^{-}\right|+C72\left|So^{+}\right|\right)}{\left|\left(4+C31\left|So^{-}\right|+C32\left|So^{+}\right|+C8\right)^{n}} \right] \\ \left|\left(S_{local}+C31\left|So^{-}\right|+C32\left|So^{+}\right|+C8\right)^{n}+C6+C71\left|So^{-}\right|+C72\left|So^{+}\right|\right| \quad (8),$$

where C31, C32, C6, C71, C72, C8 and *n* are body part-specific regression coefficients (Table 6), So^{-} is the overall thermal sensation (if So < 0) and So^{+} is the warm overall thermal sensation (if So > 0).

The thermal comfort scale is between +4 and -4, where +4 is very comfortable, +2 is comfortable, +0 is just comfortable, -0 is just uncomfortable, -2 is uncomfortable and -4 is very uncomfortable (Table 7). The overall comfort is the average of the two minimum local comfort votes unless the following criteria are met:

i. the second lowest local comfort vote is > -2.5
ii. the subject has some control over his/her thermal environment or the thermal conditions are transient,

then the overall comfort is calculated as the average of two minimum votes and the maximum comfort vote. When the Zhang method is used for predicting the thermal sensation and comfort of a given space, the inputs of the Zhang method, human core temperature and body part-specific skin temperatures, can be simulated by means of a human thermal model.

Table 6. Body-part specific regression coefficients for local thermal comfort calculation (Zhang 2003).

	C31	C32	C6	C71	C72	C8	*n*
Face	-0.11	0.11	2.02	0	0.4	0.41	1.5
Head	0	1.39	1.27	0.28	0.4	0.5	2
Neck	0	0	1.96	0	0	-0.19	1
Chest	-1.15	0	1.88	0.92	0	0	1.5
Back	-0.5	0.59	2.22	0.74	0	0	1
Pelvis	-1	0.38	2.7	0.83	-0.64	-0.75	1
Upper arm	-0.43	0	2.2	0	0	-0.33	1
Lower arm	-1.64	0.34	2.38	1.18	0.28	-0.41	1
Hand	-0.8	0.8	1.99	0.48	0.48	0	1
Thigh	0	0	1.98	0	0	0	1
Lower leg	-1	1.5	1.27	0.4	1.22	0.36	1.5
Foot	-2.31	0.21	1.62	0.5	0.3	-0.25	2

Table 7. Thermal Comfort index (Zhang 2003).

Index	Thermal comfort
4	very comfortable
2	comfortable
+0	just comfortable
-0	just uncomfortable
-2	uncomfortable
-4	very uncomfortable

2.5 VTT House building simulation environment

The non-commercial building simulation environment VTT House (Tuomaala 2002) simulates air infiltration, ventilation and heat transfer processes. The simulation program is designed for simulation experts, because use of the program requires good knowledge of the simulated case, the target of the simulation and the principles of the nodal network creation. VTT House simultaneously calculates both heat transfer and fluid flow processes. The calculation is based on

i) a free nodal approach with discrete definition of mass balance, momentum, and heat balance equations

ii) true modelling of thermal conduction, convection, and radiation

iii) SIMPLE Algorithm and

iv) a sparse matrix solver (Preconditioned Conjugate Gradient Method).

The nodal network consists of node capacitances and inter-nodal conductances or heat sources/sinks (e.g., net radiative heat gain components). The transient node temperatures are solved using the finite difference heat balance method (Tuomaala et al. 2002).

Thermal conduction, convection, and radiation are included in the calculation, and transient phenomena are modelled allowing transient and asymmetrical simulation results. Calculation of radiative heat transfer is based on estimating view factors between individual surfaces and solving the net radiation matrix by an improved progressive refinement method (Tuomaala and Piira 2000). VTT House building simulation tool includes several options for simulating convective heat transfer. Convective heat transfer coefficient values can either be given as constant input data or updated (based on equations for different geometries and dimensionless numbers presented in scientific literature) during simulations, whichever is appropriate for each simulation case (Tuomaala et al. 2002).

The modelling starts by drawing the test case using an IFC-based CAD-program., e.g. ArchiCAD. The CAD-drawing is saved as an IFC (Industrial Foundation Classes) standard format. The simulation project is started by creating

the objects of the building component according to the IFC-file. The project is stored as an xml-file format. Additional components (radiators, fireplaces, etc.) can be added to the simulated spaces as xmc-files (Figure 2).

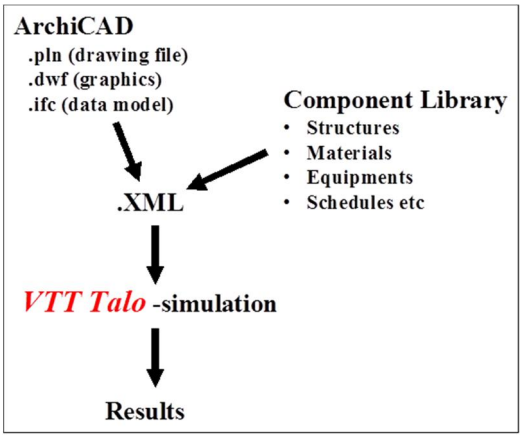

Figure 2. Data management of the VTT Talo simulation application.

When a new building is created from a IFC file, the rooms are treated as separate spaces. The indoor air of one room/space is considered to be fully mixed (represented by one heat node). The spaces are separated by enclosure elements: walls, windows, doors, roofs, floors or base floors. VTT Talo – component library contains various structures, materials, equipments, and schedules for the input data definition. A test routine can be used for a quick test environment of the thermal behaviour of the space, and for the control of the space heat loads from the devices, humans, etc. The heat load size, utilizing factor, moisture load, emissions and timetable can be defined separately. The sensitivity of the thermal calculation is defined by the maximum and minimum sizes of the enclosure elements. Holes or ducts attached to the enclosure elements represent the air passages through the structure.

The simulation results can be examined by three ways: an output file, line diagrams and 3D-file. The chosen simulation results are saved to an output file, which can be opened e.g. in Excel-program. Some of the simulation results can also be examined during the simulation by various line diagrams: node temperatures, heating and cooling powers and energies by the PID-controllers, air and fluid mass or volume flows, realized time steps, etc.

Printing files are stored in the VTT Talo directory during the calculation. The files can be used for the 3D representation of surface temperatures, air flows, etc. The starting point of the printing and the printing interval can be defined. Altogether 48 printing files are created. The temperatures of the building elements can be illustrated by means of a colour scale. Figure 3 shows simulated surface tem-

perature gradients of a cross-section of a fireplace. The blue colour on the edges indicates the low surface temperatures of the fireplace wall structure, whereas the red colour inside the fireplace shows the high temperatures of the furnace.

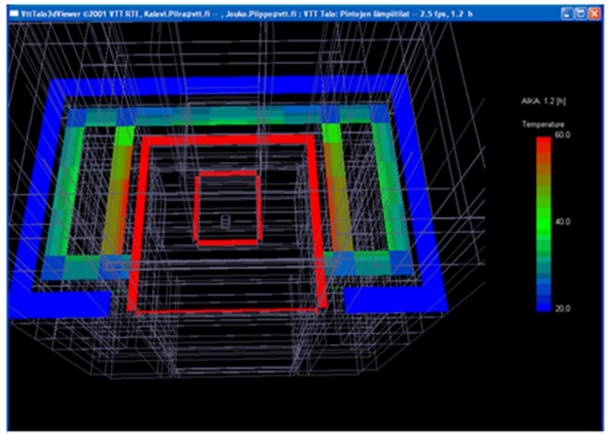

Figure 3. Example of the VTT Talo simulation of a fireplace, 3D-output.

VTT Talo simulation tool has mainly been used for the simulation of building heating energy demand and building service systems, e.g. floor heating systems, thermal functionality of fireplaces and very low-energy building concepts in different climatic conditions and with different end-user profiles.

3. Human Thermal Model

3.1 Interaction with the surrounding space

A bio-heat model of the human thermal system ought to be both sufficiently detailed to give valid thermal data from all necessary locations of the body, and at the same time be flexible enough to be easily modified for different types of applications. Therefore the new Human Thermal Model (HTM) was developed in this study as a new module for the non-commercial building simulation environment VTT House (Tuomaala 2002).

HTM models both the physical interactions between the human body and the surrounding space, and the physiological behaviour of the human body itself.
The finite-difference method with free description of the calculation network describes both the human body and the surrounding space by a thermal nodal network. The number of nodes and the accuracy of the calculation can be adjusted to the simulated situation. The current number of nodes in HTM is around 3,200 nodes, consisting of 1,600 fluid (blood) nodes and 1,600 heat nodes.

The current version of HTM uses constant body part-specific heat transfer coefficient values, defined by a set of laboratory measurements by deDear (DeDear et al. 1997) in an ambient temperature of 20 °C (Table 8). The convective heat transfer from skin or clothing results from an airstream, which perturbs the insulating boundary layer of air clinging to the surface of the body. Generally, the faster the flow of air around the body, the thinner the boundary layer of air on the body's surface, and hence the lower the thermal insulation afforded the subject. The process of convection from a heated surface such as human skin or clothing can be further classified into three distinct modes: natural convection, where the air movement is driven purely by thermally induced buoyancy and generally confined to low ambient air speeds; forced convection at speeds generally higher than 1.5 m/s, and a region of mixed-mode convection prevailing at air speeds between these two limits (ASHRAE 1993). The constant body part-specific heat transfer coefficients of HTM are used for both natural and forced convection conditions.

Table 8. Natural (air velocity v < 0.10 m s-1) and forced convection heat transfer coefficients (h_c) for a nude thermal manikin standing and seated (deDear et al. 1997).

Body part	$h_{c\_natural}$, **W/m²K**		$h_{c\_forced} = B \cdot v^n$ **W/ m²K**			
	Standing	Seated	Standing		Seated	
			B	*n*	*B*	*n*
Head	3.6	3.7	3.2	0.97	4.9	0.73
Chest	3.0	3.0	7.5	0.66	9.1	0.59
Back	2.9	2.6	7.7	0.63	8.9	0.63
Pelvis	3.4	2.8	8.8	0.59	8.2	0.65
Upper arm	2.9	3.4	10.0	0.62	11.4	0.64
Forearm	3.7	3.8	12.6	0.54	11.8	0.62
Hand	4.1	4.5	14.4	0.56	13.4	0.60
Thigh	4.1	3.7	10.1	0.52	8.9	0.60
Lower leg	4.1	4.0	12.9	0.50	13.2	0.57
Foot	5.1	4.2	12.0	0.50	12.9	0.54
Whole body	**3.4**	**3.3**	**10.4**	**0.56**	**10.1**	**0.61**

The Human Thermal Model Description (HTMD) language enables an easy adjustment of parameters for tissue temperature and thermal sensation calculation. The human geometry is represented with surfaces, which enables the reliable calculation of radiation heat transfer and a possible integration with a Computational Fluid Dynamics (CFD) tool.

The new Human Thermal Model consists of

- a passive system, which includes the body tissues, internal organs, circulatory and respiratory systems
- a control system, which initiates and controls the physiological responses of the body and
- a thermal sensation and thermal comfort calculation system.

These systems are explained in chapters 3.2, 3.3 and 3.5. Chapter 3.4 presents the energy governing equations.

3.2 Passive system

3.2.1 Tissue distribution

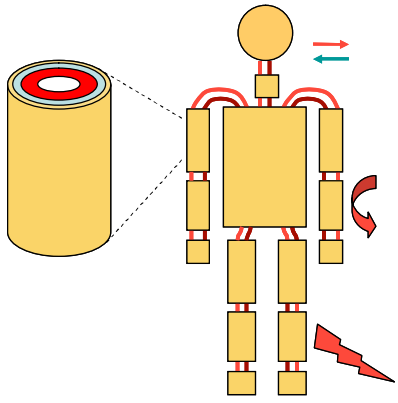

Figure 4. HTM body part composition.

The new Human Thermal Model (HTM) divides the human body into 16 body parts (Figure 4), each being further sub-divided typically in four realistic tissue layers (bone, muscle, fat, and skin) by concentric cylinders. The only exception is the head, which is approximated by concentric spheres. The basic idea is to model the body parts mimicking the true anatomy as a single bone-core surrounded by muscle, fat, and skin layers. Further divisions are then made in four or five directions (head) until each body part is composed of small tissue elements, as shown in Figure 4. The total radii and lengths of the cylinders representing the body parts and the sphere representing the head are listed in Table 9.

Table 9. HTM Body part dimensions.

Body part	Radius, m	Length, m
Head	0.094	0.188
Neck	0.057	0.083
Chest/back	0.146	0.297
Pelvis	0.161	0.297
Right or left upper arm	0.049	0.300
Right or left forearm	0.040	0.250
Right or left hand	0.030	0.180
Right or left thigh	0.063	0.400
Right or left lower leg	0.042	0.390
Right or left foot	0.036	0.241
Total height of HTM	**1.727**	

The tissue mass distribution of HTM was based on Smith (1991), and it is presented in Table 10. The tissue layers of HTM are connected to adjacent body parts by a blood circulation system, which has been used for physiological thermoregulation of the whole body. The thermal properties of the different tissues (Table 11) are based on the values used by Smith (1991) and Fiala (1999).

Table 10. HTM Tissue mass distribution (kg) according to Smith 1991.

Body part	**Tissue type**							
	Brain	Viscera	Lung	Bone	Muscle	Fat	Skin	Blood
Head	1.39			1.77	0.45	0.28	0.19	
Neck				0.23	0.58	0.07	0.03	
Chest/back		3.28	3.04	2.26	4.15	4.18	0.64	
Torso		8.34		2.73	8.34	5.21	0.64	
Upper arm				0.47	1.58	0.24	0.18	
Thigh				1.48	2.54	1.13	0.34	
Forearm				0.27	0.88	0.13	0.10	
Lower leg				0.67	1.15	0.52	0.16	
Hand				0.16	0.14	0.15	0.09	
Foot				0.41	0.21	0.35	0.13	
Total body (78.2 kg)	**1.4**	**11.6**	**3.0**	**13.3**	**26.5**	**14.8**	**3.5**	**4.1**

Table 11. Thermal properties of tissues according to Smith 1991 and Fiala 1999.

Tissue	**Thermal conductivity, W/mK**	**Density, kg/m^3**	**Specific heat capacity, J/kgK**
Brain	0.528	1 050	3 690
Abdomen	0.547	1 050	3 690
Lung	0.281	550	3 710
Bone (legs, arms, hands and feet)	2.28	1 700	1 590
Bone (head)	1.16	1 500	1 590
Bone (neck. abdomen)	0.581	1 300	1 590
Muscle	0.419	1 050	3 770
Fat	0.161	850	2 510
Skin	0.209	1 000	3 770
Blood	0.492	1 069	3 650

3.2.2 Metabolic heat generation

The metabolic heat is generated in the brain, abdomen, lungs, muscles, fat and skin. The metabolic heat generation rate M'' (W/m^2) of the body is expressed by dividing the total metabolic heat generation (W) with the body surface area (m^2). The metabolic heat generation rate is also expressed with the unit MET, where 1 MET = 58.2 W/m^2. The total basal heat generation of HTM (85.6 W) divided by the HTM body surface area (1.74 m^2) gives 49.2 W/m^2 or 0.85 Met as the metabolic heat generation rate of HTM at rest. The basal metabolic heat generation rates of all tissue types and the total heat generation of each tissue type at rest are presented in Table 12.

Table 12. Metabolic heat generation per tissue mass (Smith 1991) and total heat generation by tissue type at rest.

Body part	Basal metabolic heat generation, W/kg	Basal metabolic heat generation of total tissue mass, W
Brain	12.69	17.8
Viscera	3.83	44.4
Lung	0.67	2.0
Muscle	0.67	17.8
Fat	0.004	0.1
Skin	1.01	3.5
Total metabolic heat generation at rest, W		85.6

Table 13. Metabolic heat generation rates of different activities (ISO 7730) and the corresponding metabolic heat generation rates of the HTM muscle tissue.

Activity	Metabolic heat generation rate, W/m^2	Metabolic heat generation rate, met	Metabolic heat generation of the muscle tissue, W/ kg
Reclining	46	0.8	0.67
Seated, relaxed	58	1.0	1.38
Sedentary activity (office, dwelling, school, laboratory)	70	1.2	2.02
Standing, light activity (shopping, laboratory, light industry)	93	1.6	3.55
Standing, medium activity (shop assistant, domestic work, machine work)	116	2.0	5.07

The metabolic heat generation rate of HTM has been adjusted to different activity levels by changing the basal metabolic heat generation rate of the muscle tissue. Table 13 shows the metabolic rates of different activities defined in ISO 7730 (ISO 2005) and the corresponding metabolic heat generation rates of the HTM muscle tissue.

3.2.3 Respiration

HTM estimates the total respiratory heat loss according to the equation by ASHRAE (1993):

$$C_{res} + E_{res} = 0.0014\, M'' \,(34\ °C - t_a)\ m^2/°C + 0.0173\, M'' \,(5.87\ Pa - P_a)\ m^2/Pa, \quad (9)$$

where C_{res} is dry respiratory heat loss, E_{res} is latent respiratory heat loss, M'' is metabolic heat generation rate, t_a is ambient air temperature, and P_a is vapour pressure at ambient air temperature. The heat losses are introduced directly and uniformly to the lung tissue layer located in the chest section. The periodic nature and detailed heat transfer of respiration is neglected in this version of HTM.

3.2.4 Clothing

The relevant clothing material characteristics for heat transport are insulation, water vapour resistance and moisture absorption (Lotens 1993). The major insulating effect of clothing is based on the still air layers between the skin and the different clothing layers, which reduce conduction losses to the environment. Clothing resists convective losses by preventing convection currents from forming next to the body and by providing a barrier against air currents in the environment. Clothing also reduces radiant heat loss by serving as a thermal radiation barrier and evaporative heat loss by restricting the evaporation of sweat produced by the body. The insulation effect of an individual garment is dependent on the material properties of the garment, the looseness or tightness of fit, the body surface area covered by the garment and the increased surface area for heat loss (McGullough and Jones 1984).

The recommended method for measuring clothing insulation is a constant temperature method of measuring thermal resistance by using an electrically heated manikin in an environmental chamber. The manikin is heated internally to simulate the human skin temperature distribution. The amount of power required to keep the average skin at the proper level (e.g. 33 °C) is recorded. The power level varies in proportion to the amount of insulation provided by the garment being tested worn by the manikin. The total thermal resistance of an article of clothing plus the surface air layer is calculated as

$$R_t = \frac{A(t_s - t_a)}{H}, \quad (10)$$

where R_t is the total thermal resistance of the article of clothing plus the surface air layer, A the area of the manikin's surface, t_s the temperature at the manikin's surface, t_a the ambient air temperature and H the power required to heat the manikin (Huang 2006). As the use of the manikin method is time-consuming, the insulating values are generally estimated using tables developed from clothing insulation studies, such as the IER Clothing and fabric data base presented in McGullough and Jones (1984). The extensively used unit for clothing insulation is clo, where 1 clo approximately represents the insulation effect 0.155 m^2K/W of a warm business suit (Huang 2006). The clothing insulation value $I_{clu,i}$ of each garment (in clo) is obtained from the table and the total insulation of the clothing ensemble I_{cl} is determined according to ISO 7730 (ISO 2005) using the summation formula:

$$I_{cl} = \sum_i I_{clu,i} \tag{11}$$

In HTM the effect of clothing was taken into account by adding the clothing layer as one extra material layer above the skin layer. The clothing layer has a constant thickness of 1 mm, therefore the calculated body part-specific thermal and evaporative heat conductances of the clothing have been modified for this thickness for each body part separately (Figure 5).

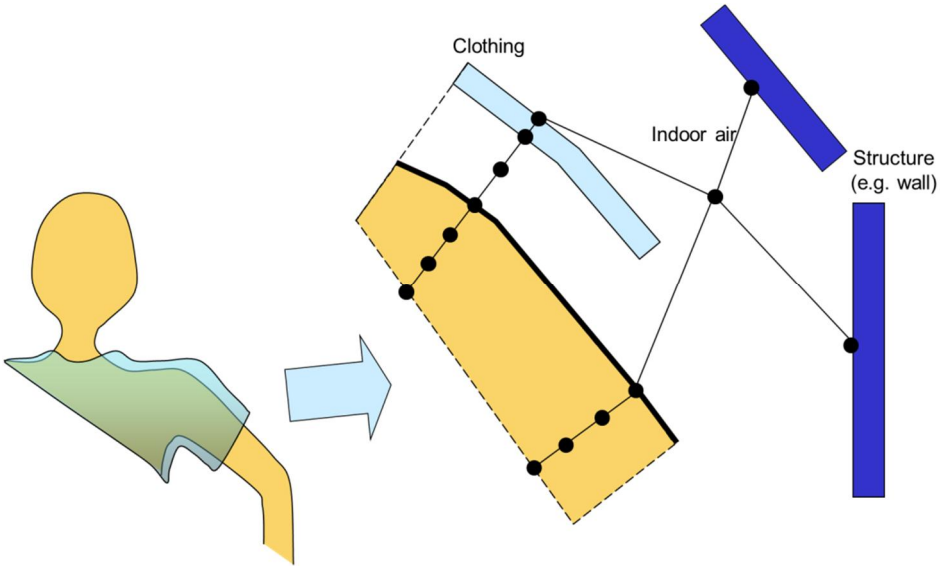

Figure 5. HTM clothing calculation.

The thermal (dry and evaporative heat transfer) resistance caused by clothing on each body part is evaluated by calculating the overall thermal resistance between skin surface and indoor air. The overall thermal resistance is calculated by adding

together the individual resistances of each garment including the resistance of the air layer between two layers. For the dry heat transfer the resistance of the air layer is 0.043 m^2K/W and for the evaporative heat transfer 0.0042 m^2kPa/W. The air layer resistances have been obtained from Fu (1995). The clothing insulation parameters by McGullough and Jones 1984 are used as the individual resistances of different garments. The moisture accumulation of the clothing layer was neglected in the current version of HTM.

HTM uses same convective heat transfer factors by deDear (Table 24) for the calculation of convective heat transfer between the ambient air and the naked skin or the clothing layer. These factors have been obtained with a naked thermal manikin and using them with a clothed model actually causes some error in the convective heat transfer calculation.

3.2.5 Basal blood circulation

The human circulatory system is an intricate network of blood vessels which transport blood to and from the body tissues. The blood circulation system of HTM is based on the main principles of the real human circulatory system. The blood circulation system consists of systemic and pulmonary circulation. In the systemic circulation the blood flows from the left ventricle of the heart through large arteries to the individual body parts where it is circulated around each three-dimensional tissue element. From the arterioles, it empties into the venules and begins its return through increasingly larger veins back to the right atrium of the heart. In pulmonary circulation the blood flows from the right ventricle of the heart to lungs and returns to the left atrium of the heart. After the systemic and pulmonary circulations the venous blood flows are mixed in the heart section to constitute a new arterial blood temperature.

The systemic circulation of HTM is further divided into macrocirculation consisting of large vessels and arteries and microcirculation consisting of the capillary bed. The systemic circulation blood flow entering a body part is therefore divided into two parts: the capillary blood flow to the different tissues of the body part representing microcirculation and the blood flow through the body part into the following body part representing macrocirculation.

Macrocirculation of HTM

Avolio (1980) has proposed a model multi-branched model of the human arterial system with 128 segments including central vessels and major peripheral arteries. To adapt Avolio's model to HTM these 128 segments were sorted by body parts and segments participating in the main blood transfer were selected for HTM. The selected numbers of arteries and vessels per body part represent the amounts of Avolio's model. The body part-specific inner diameters of arteries and vessels were calculated to constitute the same heat exchange surface as the real macrocirculation system. The body part-specific amounts and areas of arteries and vessels

are presented in Table 14. The length of one artery or vessel is the length of the body part (Table 9). The total surface area of all vessels and arteries is 0.242 m^2.

The arteries and vessels are located in the muscle tissue. The convective heat transfer conductance G_{art} between the blood flow inside an artery and the muscle tissue is calculated as

$$G_{art} = A_{s,art} \cdot h_b , \tag{12}$$

where $A_{s,art}$ is the inner surface area of an artery (Table 14) and h_b is the convective heat transfer coefficient of blood. The minor conductive resistance of the vein wall to the heat transfer has not been taken into account in this approach. The convective heat transfer coefficient of blood h_b, 984 W/m^2K, was estimated as

$$h_b = \frac{Nu \cdot k_b}{D_v} \tag{13}$$

where Nu is the Nusselt number, equal to 4 (Shitzer and Eberhart 1985), k_b is the blood thermal conductivity equal to 0.492 W/mK (Table 11) and D_v is the average vessel diameter 0.002 m. The convective heat transfer conductance G_{ven} between the blood flow inside a vessel and the muscle tissue is calculated accordingly

$$G_{ven} = A_{s,ven} \cdot h_b , \tag{14}$$

where $A_{s,ven}$ is the inner surface area of a vessel (Table 14).

Table 14. Arteries and vessels per body part.

Body part	Number of arteries	Number of vessels	Inner diameter of one artery/vessel, m	Inner surface area of one artery/vessel, m^2	Total surface area of all arteries and vessels in the body part, m^2
Neck	4	4	0.00587	0.00153	0.01224
Chest	4	4	0.00697	0.00651	0.05204
Back	4	4	0.00697	0.00651	0.05204
Pelvis	2	2	0.00835	0.00779	0.03116
Upper arm	1	1	0.00405	0.00382	0.00764
Lower arm	2	2	0.00335	0.00263	0.01053
Upper leg	1	1	0.00493	0.00619	0.01239
Lower leg	3	3	0.00227	0.00278	0.01666

Microcirculation of HTM

The transport of thermal energy by the blood flow in the microcircular system is more important to heat transfer throughout the tissue than the transport of thermal energy in the macrocirculation. The blood-tissue interface area varies tremendously through the circulation system: the approximate total cross section area of arteries in the body is 20 cm^2 while the total cross section area of capillaries is 4500 cm^2. Therefore, the capillary blood flow is the main factor in the exchange of mass and energy between the blood and surrounding tissue (Fu 1995).

The energy exchange between microcirculation and tissue is further dependent upon the tissue and blood temperature distribution and the thermophysical properties of the tissue. Detailed description of the local distribution of blood perfusion to energy exchange is an intricate task. Thus, a modeling compromise is required in order to facilitate the analysis of the important effect of microcirculation on the tissue energy balance. An approach commonly employed for this compromise, which accounts for the heat transfer behaviour between microvasculature and tissue collectively, is based on the application of energy conservation: the amount of heat taken up by tissue (or control volume) per unit time is proportional to the difference between the arterial temperature and the tissue temperature. The microcirculation heat transfer calculation assumes a thermal equilibrium between the exiting blood and the surrounding tissue. In other words, the blood leaves the tissue at the tissue temperature. This assumption is based on the very slow blood flow in the capillary bed, and it is also used by Fu (1995).

The blood flow in other tissues than the skin tissue is constant; the control system of the skin blood flow is presented in Ch. 3.3.1. Table 15 shows the basal blood flow rates in brain, viscera, lung, muscle and fat tissues according to Smith (1991).

Table 15. Basal blood flow rate per tissue mass (Smith 1991).

Body part	Basal blood flow rate, 10^{-6} m^3/ kg s
Brain	9.65
Viscera	4.12
Lung	0.45
Muscle	0.517
Fat	0.0043

3.3 Control system

As explained in Chapter 2.2 the human core temperature is controlled by the thermoregulatory system consisting of thermoreceptors and hypothalamus. The

thermoreceptors, located in different parts of the body, send signals about the local temperature level and its change to the hypothalamus. The hypothalamus reacts to the signals by means of thermoregulatory functions by either inhibiting or enhancing heat production and heat loss through increasing (*vasodilation*) or decreasing (*vasoconstriction*) the skin blood flow rate, sweating and shivering.

3.3.1 Skin blood flow

The skin blood flow is controlled by the mechanisms of *vasodilation* and *vasoconstriction* that result in a higher or lower skin blood flow, respectively. The correlations depend on the mean skin temperature and on the core temperature.

According to Smith (1991), a state of thermoneutrality exists when the core and mean skin temperatures are 36.8°C and 33.7°C, respectively. As the core temperature rises above its neutral value, vasodilation occurs and cardial output increases dramatically. Nearly 100% of this increase goes to the skin tissue. A state of maximum vasodilation is achieved when the core temperature reaches 37.2 °C. At this state, the total skin blood flow rate may be as much as seven times its basal value. Between core temperatures of 36.8 °C and 37.2 °C, the skin blood flow follows the core temperature linearly. As mean skin temperature falls below its neutral value 33.7 °C, vasoconstriction occurs. Skin blood flow and cardiac output decrease accordingly. At a state of maximum vasoconstriction when mean skin temperature falls to 10.7 °C, the total skin blood flow rate may be as low as one eighth of its basal value (Smith 1991). Between skin temperatures of 33.7 °C and 10.7 °C the skin blood flow varies linearly with the skin temperature.

The skin perfusion blood flow rate is evaluated from the thermal control equations which determine the thermal interaction between the skin and the core by blood perfusion. The vasomotor control equations are formulated based on the basal skin blood mass flow rate $\dot{m}_{skin,basal}$, maximum skin blood mass flow rate $\dot{m}_{skin,\max}$, and minimum skin blood mass flow rate $\dot{m}_{skin,\min}$ according to Salloum et al. (2007):

$$\dot{m}_{skin} = \frac{\dot{m}_{skin,dil} \cdot \dot{m}_{skin,con}}{\dot{m}_{skin,basal}} \qquad \dot{m}_{skin} = \frac{\dot{m}_{skin,dil} \cdot \dot{m}_{skin,con}}{\dot{m}_{skin,basal}} \tag{15}$$

$$\dot{m}_{skin,dil} = \begin{cases} \dot{m}_{skin,basal} & \text{for } t_{core} \le 36.8°\text{C} \\ \dfrac{(t_{core} - 36.8)}{(37.2 - 36.8)} \left(\dot{m}_{skin,\max} - \dot{m}_{skin,basal} \right) + \dot{m}_{skin,basal} & \\ & \text{for } 36.8°\text{C} \le t_{core} \le 37.2°\text{C} \\ \dot{m}_{skin,\max} & \text{for } t_{core} \ge 37.2°\text{C} \end{cases} \tag{16}$$

$$\dot{m}_{skin,con} = \begin{cases} \dot{m}_{skin,\min} & \text{for } t_{skin} \le 27.8°C \\ \dfrac{(t_{skin} - 27.8)}{(33.7 - 27.8)}\left(\dot{m}_{skin,basal} - \dot{m}_{skin,\min}\right) + \dot{m}_{skin,\min} & \\ & \text{for } 27.8°C \le t_{skin} \le 33.7°C \\ \dot{m}_{skin,basal} & \text{for } t_{skin} \ge 33.7°C \end{cases} \quad (17)$$

where $\dot{m}_{skin,con}$ is the constricted skin blood mass flow rate and $\dot{m}_{skin,dil}$ is the dilated skin blood mass flow rate. The relationships between $\dot{m}_{skin,basal}$ and $\dot{m}_{skin,\max}$, and $\dot{m}_{skin,basal}$ and $\dot{m}_{skin,\min}$ (Table 16) are based on the Smith's model (Smith 1991).

Stolwijk (Munir et al. 2009), Smith (Smith 1991) and Fiala (Fiala 1999) have suggested different basal skin blood flow models, which differ noticeably from each other. These alternative body part-specific skin blood flow rates were tested with a dynamical temperature step change test by Munir et al. (2009), explained in Chapter 4.1.3. The simulated skin temperatures using Fiala's skin blood flow had the best correlation with the measured values. Therefore the Fiala model was selected to be used as the skin blood flow rate model of HTM. The skin blood flow and total blood flow rates of HTM, with the $\dot{m}_{skin,basal}$, $\dot{m}_{skin,\max}$, and $\dot{m}_{skin,\min}$ values according to the Fiala model, are given in Table 17. The zero values do not mean that there is no blood flow in the body part, but that the heat transfer of the skin blood flow is very small when the minimum blood flow is in use. The total basal blood flow rate of HTM is 4.7 litres per minute.

Table 16. Multiplier factors for the calculation of maximum and minimum skin blood flows from basal skin blood flow (Smith 1991).

Body part	$\dot{m}_{skin,\max} / \dot{m}_{skin,basal}$	$\dot{m}_{skin,\min} / \dot{m}_{skin,basal}$
Head	2.45	0.79
Neck	7.81	0
Torso (chest, back, pelvis)	9.66	0
Upper arms	9.14	0
Thighs	8.55	0
Forearms	10.93	0
Lower legs	12.68	0
Hands	4.00	0.56
Feet	5.65	0.32

Table 17. Basal and vasomotor blood flow rates of body parts, skin blood flow according to the Fiala model (Smith 1991, Munir 2009).

Body part	Skin blood flow rate per skin tissue mass, 10^{-9} m^3/s kg			Total blood flow rate, 10^{-9} m^3/s		
	$\dot{V}_{skin,basal}$	$\dot{V}_{skin,\min}$	$\dot{V}_{skin,\max}$	Basal	Max. constrict	Max. dilate
Head	6 709	5 295	11 079	14 978	14 713	16 798
Neck	2 912	0	2 539	391	301	1 006
Chest, back, pelvis	876	0	37 483	54 536	53 458	63 870
Upper arm	542	0	6 455	915	817	1 714
Thigh	503	0	10 573	1 488	1 317	2 785
Forearm	542	0	4 306	511	456	1 054
Lower leg	516	0	7 186	659	581	1 579
Hand	2 252	1 267	5 995	282	191	906
Foot	725	234	3 729	204	142	631
Total body				**78 025**	**75 478**	**99 011**

3.3.2 Sweating and shivering

If the vasodilation response is not sufficient to keep the core temperature from rising further, the core temperature will reach a level, referred to here as the sweating threshold, where sweating begins. Beyond this threshold, the sweat rate increases linearly with increasing core temperature. Skin temperature affects sweating in two ways (Smith 1991):

(i) the higher the skin temperature, the lower the sweating threshold. No sweating occurs, however, for core temperatures less than or equal to 36.85°C no matter how high the skin temperature may be. However, for core temperatures higher than or equal to 37.1°C sweating always occurs regardless of skin temperature.

(ii) falling skin temperature inhibits the rate of sweat production.

The sweating threshold, t_{sweat}, is approximated as a function of mean skin temperature, t_{skin}. (Smith 1991)

$$t_{sweat} = \begin{cases} 42.084°\text{C} - 0.15833 t_{skin} \text{ for } t_{skin} < 33.0°\text{C} \\ 36.85°\text{C} \quad \text{for } t_{skin} \geq 33.0°\text{C} \end{cases} \tag{18}$$

If, for a given skin temperature, the core temperature exceeds either the sweating threshold or 37.1 °C, then sweating occurs. The sweat rate $\dot{m}_{sw}$ approximated by an equation from Smith (1991) is expressed in SI units as:

$$\dot{m}_{sw} = \frac{45.8°\mathrm{C} + 739.4\left(t_{core} - t_{sweat}\right)}{3.6 \cdot 10^{6} °\mathrm{C}\, s/kg} \text{ for } t_{core} > t_{sweat} \tag{19}$$

The maximum sweating rate is 696 g/h (Smith 1991) representing a skin wettedness of 1.0. When no sweating occurs, the skin wettedness is 0.06. Between the sweating rates 0 g/h and 696 g/h (0.000193 kg/s) skin wettedness w increases linearly from 0.06 to 1.0:

$$w = 0.06 + \frac{1 - 0.06}{0.000193 kg/s} \dot{m}_{sw} \tag{20}$$

The total evaporative heat loss E_{sk} from the skin (ASHRAE 1993) is

$$E_{sk} = \frac{w\left(P_{sk,s} - P_a\right)}{\left[R_{e,cl} + \frac{1}{f_{cl} h_e}\right]}, \tag{21}$$

where w is skin wettedness (having values between 0.06 and 1.0), $P_{sk,s}$ is water vapour pressure at skin (normally assumed to be that of saturated water vapour at skin temperature), P_a is the ambient water vapour pressure, $R_{e,cl}$ is the evaporative heat transfer resistance of the clothing layer, f_{cl} is the clothing area factor (the surface of the clothed body divided by the area of the nude body), and h_e is the evaporative heat transfer coefficient

If vasoconstriction is not able to keep heat in the body, the metabolic thermoregulatory function takes place and the body will start shivering in order to heat the body. The point at which shivering begins, the shivering threshold, is dependent on the core temperature and estimated by the equation (Smith 1991)

$$t_{shiver} = \begin{cases} 35.5°\mathrm{C} \quad \text{for } t_{core} \le 35.8°\mathrm{C} \\ -1.0222 \cdot 10^{4} °\mathrm{C} + 570.97 t_{core} \; - 7.9455 t_{core}^{2} \frac{1}{°\mathrm{C}} \text{ for } 35.8°\mathrm{C} \le t_{core} \le 37.1°\mathrm{C} \end{cases} \tag{22}$$

If the mean skin temperature is less than the shivering threshold for a given core temperature, shivering occurs. The maximum increase in metabolic heat generation caused by shivering, $M_{shiv,\max}$, occurs at a mean skin temperature of 20 °C. It is a function of core temperature (Smith 1991), expressed in SI units as

$$M_{shiv,\max} = \frac{-1.1861 \cdot 10^{9} W + 6.552 \cdot 10^{7} t_{core} \frac{W}{°C} - 9.0418 \cdot 10^{5} t_{core}^{2} \frac{W}{°C^{2}}}{3600} \quad (23)$$

for $t_{core} < 37.1\,°C$

The maximum increase in metabolic heat generation is 236 W in a core temperature of 36.25 °C. In HTM, the maximum shivering power per muscle tissue (W/kg) is distributed over the body parts according to Table 18. The distribution is originally based on coefficients by Fiala (2001), and it has been modified according to the muscle mass distribution of HTM. The actual shivering metabolic heat generation depending on the skin temperature and shivering threshold temperature is calculated using the following equation by Smith (1991)

$$M_{shiv} = M_{shiv,\max}\left[1.0 - \left(\frac{t_{skin} - 20.0}{t_{shiver} - 20.0}\right)^{2}\right] \text{ for } \left(40°C - t_{shiver}\right) \le t_{skin} \le t_{shiver} \quad (24)$$

Table 18. Maximum shivering power distribution over HTM body parts adopted from Fiala (1999) and modified according to the muscle mass distribution of HTM.

Body part	Weighting factor	Max shivering power, W/kg muscle	Max shivering power, W
Head	0.002	1.5	0.5
Face	0.008	23	2.1
Neck	0.010	4.5	2.6
Back	0.234	21	64
Chest	0.257	68	71
Pelvis	0.364	12	100
Upper arms	0.025	2.2	6.8
Lower arms	0.025	3.9	6.8
Hands	0.000	0	0
Thighs	0.044	2.4	12
Lower legs	0.032	3.9	8.9
Feet	0.000	0	0
Sum	**1.000**		**275**

3.4 Energy governing equations

3.4.1 Exemplary heat balance equation for a body part

The following examination was written to clarify the heat transfer mechanisms on a body part level. In this examination the boundary of the heat balance is a body part.

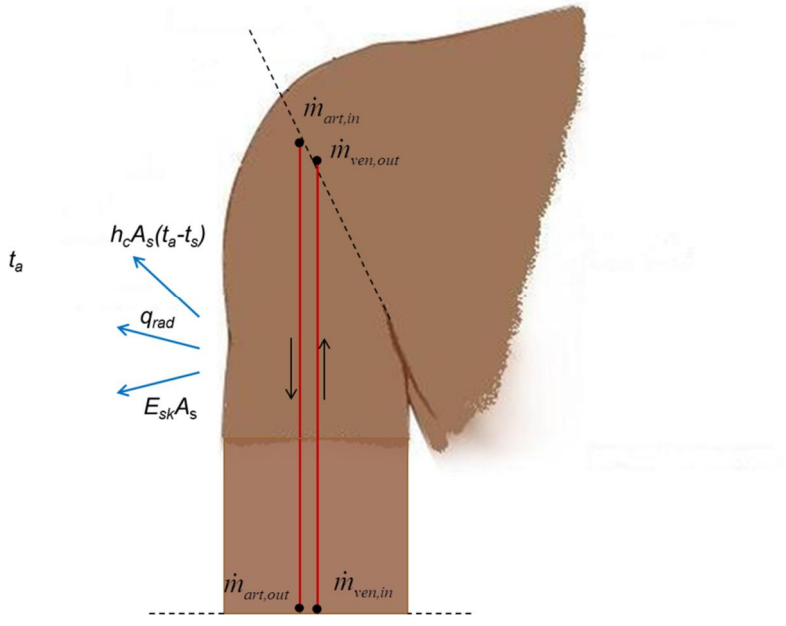

Figure 6. A simplified illustration showing parameters for the body part-specific heat balance equation. The exemplary artery and vessel are marked with red lines.

The heat balance equation for the overall heat transfer on a body-part level is

$$\begin{aligned} m_{bp} c_{p,bp} \frac{\partial t_{bp}}{\partial t} &= \left(\dot{m}_{art,in} h_{art,in} - \dot{m}_{art,out} h_{art,out}\right) \\ &+ \left(\dot{m}_{ven,in} h_{ven,in} - \dot{m}_{ven,out} h_{ven,out}\right) + m_{bp} M_{bp} - h_c A_{bp} \left(t_{bp,s} - t_a\right), \\ &- q_{rad} - E_{sk} A_{bp} \end{aligned} \tag{25}$$

where m_{bp} is the mass of the body part, $c_{p,bp}$ is the mean specific heat capacity of the body part, t_{bp} is the mean body part temperature, t is time, $\dot{m}_{art,in}$ is the incoming arterial blood flow, $h_{art,in}$ is the enthalpy of the incoming arterial blood flow, $\dot{m}_{art,out}$ is the arterial blood flow leaving the body part, $h_{art,out}$ is the enthalpy of the incoming arterial blood flow, $\dot{m}_{ven,in}$ is the incoming venous blood flow, $h_{ven,in}$ is the enthalpy of the incoming venous blood flow, $\dot{m}_{ven,out}$ is the incoming venous blood flow leaving the body part, $h_{ven,out}$ is the enthalpy of the venous blood flow leaving the body part, M_{bp} is the metabolic heat generation rate of the body part, h_c is the body part-specific convective heat transfer factor between the skin and the ambient air (Table 8), A_{bp} is the total skin surface area of the body part, t_{bp} is the mean skin surface temperature of the body part, t_a is the temperature of the ambient air, q_{rad} is the radiative heat transfer from the skin surface to the surrounding surfaces and E_{sk} is the evaporative heat transfer from the skin surface to the ambient air, calculated with Eq. 21.

Utilizing the overall expression for enthalpy

$$h = h(t) - h(t_0) = c_p t - c_p t_0 , \tag{26}$$

where t_0 is the reference point temperature, the heat balance equation can be written as

$$\begin{aligned} m_{bp} c_{p,bp} \frac{\partial t_{bp}}{\partial t} &= \left(\dot{m}_{art,in} c_{p,b} t_{art,in} - \dot{m}_{art,in} c_{p,b} t_0\right) - \\ &\left(\dot{m}_{art,out} c_{p,b} t_{art,out} - \dot{m}_{art,out} c_{p,b} t_0\right) + \left(\dot{m}_{ven,in} c_{p,b} t_{ven,in} - \dot{m}_{ven,in} c_{p,b} t_0\right), \\ &- \left(\dot{m}_{ven,out} c_{p,b} t_{ven,in} - \dot{m}_{ven,out} c_{p,b} t_0\right) + m_{bp} M_{bp} - h_c A_{bp} \left(t_{bp} - t_a\right) \\ &- q_{rad} - E_{sk} A_{bp} \end{aligned} \tag{27}$$

where $c_{p,b}$ is the specific heat capacity of the blood, $t_{art,in}$ is the incoming arterial blood temperature, $t_{art,out}$ is the arterial blood temperature leaving the body part,

$t_{ven,in}$ is the incoming venous blood temperature and $t_{ven,out}$ is the venous blood temperature leaving the body part. The blood flows in opposite directions of the body part are equal to each other, in other words the incoming arterial blood flow $\dot{m}_{art,in}$ equals the leaving venous blood flow $\dot{m}_{ven,out}$ and the leaving arterial blood flow $\dot{m}_{art,out}$ equals the incoming venous blood flow $\dot{m}_{ven,in}$. Therefore the heat balance equation can be shortened into

$$\begin{aligned} m_{bp} c_{p,bp} \frac{\partial t_{bp}}{\partial t} &= \left(\dot{m}_{art,in} c_{p,b} t_{art,in} - \dot{m}_{art,out} c_{p,b} t_{art,out} \right) \\ &+ \left(\dot{m}_{ven,in} c_{p,b} t_{ven,in} - \dot{m}_{ven,out} c_{p,b} t_{ven,out} \right) + m_{bp} M_{bp} \\ &- h_c A_{bp} \left(t_{bp} - t_a \right) - q_{rad} - E_{sk} A_{bp} \end{aligned} \quad . \tag{28}$$

3.4.2 Nodal heat balance equations

This chapter presents how the nodal heat balance equations for a skin surface node and a tissue node have been derived using the heat balance Eq. 28. The nodal calculation network of HTM represents different body part tissue sections (skin, fat, muscle, bone and internal organs), blood vessels, and segments of the respiratory track. Energy, momentum, and mass balance equations of the network, incorporating the environmental conditions, can then be solved for the unknown variable of interest, e.g., variations of the skin temperatures around the body.

The incoming arterial blood flow $\dot{m}_{art,in}$ is divided inside of the body part into the capillary blood flow to all different tissue nodes of the body part (microcirculation) and the blood flow through the body part (macrocirculation). Thus the mass balance of the arterial blood flow is

$$\dot{m}_{art,in} = \sum \dot{m}_{b,t} + \dot{m}_{art,out} \, , \tag{29}$$

where $\sum \dot{m}_{b,t}$ is the sum of the capillary blood flows to all tissue nodes inside of the body part. The basal, constricted and dilated values for capillary skin blood flow are presented in Table 17 and the basal capillary blood flow values for other tissues in Table 15. The venous blood flow leaving the body part consists from the macrocirculation blood flow through the body part and microcirculation blood flow from all different tissue nodes of the body part. The mass balance of the venous blood flow is correspondingly

$$\dot{m}_{vein,out} = \dot{m}_{vein,in} + \sum \dot{m}_{b,t} \, . \tag{30}$$

Substituting $\dot{m}_{art,out}$ and $\dot{m}_{vein,out}$ of the heat balance Eq. 28 with Eqs. 29 and 30 the heat balance of the body part can be written as

$$m_{bp}c_{p,bp}\frac{\partial t_{bp}}{\partial t} = \left(t_{art,in} - t_{art,out}\right)c_{p,b}\dot{m}_{art,out} + \left(t_{ven,in} - t_{ven,out}\right)\dot{m}_{ven,in}c_{p,b} + \sum \dot{m}_{b,t}c_{p,b}t_{art,in} - \sum \dot{m}_{b,t}c_{p,b}t_{vein,in} + m_{bp}M_{bp} - h_c A_{bp}\left(t_{bp} - t_a\right) - q_{rad} - E_{sk}A_{bp} \quad (31)$$

where the two first terms on the left hand side represent the macrocirculation blood flow and the third and fourth terms represent the microcirculation blood flow. The two first terms can also be approximated using the convective heat conductances G_{art} and G_{ven} of the macrocirculation heat transfer between the tissue and an artery or vessel

$$\left(t_{art,in} - t_{art,out}\right)c_{p,b}\dot{m}_{art,out} + \left(t_{ven,in} - t_{ven,out}\right)\dot{m}_{ven,in}c_{p,b} = G_{art}\left(t_{art,out} - t_{bp}\right) + G_{ven}\left(t_{ven,out} - t_{bp}\right) \quad , \quad (32)$$

where the arterial and venous outlet temperatures have been used instead of the mean temperatures of the artery and vessel. Calculation of G_{art} and G_{ven} has been presented in chapter 3.2.5. Using G_{art} and G_{ven} the heat balance equation changes into

$$m_{bp}c_{p,bp}\frac{\partial t_{bp}}{\partial t} = G_{art}\left(t_{art,out} - t_{bp}\right) + G_{ven}\left(t_{ven,out} - t_{bp}\right) + \sum \dot{m}_{b,t}c_{p,b}t_{art,in} - \sum \dot{m}_{b,t}c_{p,b}t_{vein,in} + m_{bp}M_{bp} - h_c A_{bp}\left(t_{bp} - t_a\right) - q_{rad} - E_{sk}A_{bp} \quad (33)$$

As presented earlier in chapter 3.2.5, the microcirculation heat transfer calculation of HTM assumes a thermal equilibrium between the exiting blood and the surrounding tissue based on the very slow blood flow in the capillary bed (Fu 1995). In other words, the blood leaves the tissue at the tissue temperature. Introducing this approach the heat balance equation is converted into

$$m_{bp}c_{p,bp}\frac{\partial t_{bp}}{\partial t} = G_{art}\left(t_{art,out} - t_{bp}\right) + G_{ven}\left(t_{ven,out} - t_{bp}\right) + \sum \dot{m}_{b,t}c_{p,b}t_{art,in} - \sum \dot{m}_{b,t}c_{p,b}t_{bp} + m_{bp}M_{bp} - h_c A_{bp}\left(t_{bp} - t_a\right) - q_{rad} - E_{sk}A_{bp} \quad (34)$$

If the body part was divided into slices in horizontal direction, the conductive heat transfer between two adjacent slices n and $n+1$ would be

$$q_{cond} = Lk_{bp}\left(t_{bp,n} - t_{bp,n+1}\right), \quad (35)$$

where L is the distance between the midpoints of the adjacent slices, k_{bp} is the mean heat conductivity of the body part and $t_{bp,n}$ and $t_{bp,n+1}$ are the temperatures of the adjacent slices. The heat balance equation for a slice n is now

$$\begin{aligned} m_{bp,n} c_{p,bp,n} \frac{\partial t_{bp,n}}{\partial t} &= G_{art}\left(t_{art,out} - t_{bp}\right) + G_{ven}\left(t_{ven,out} - t_{bp}\right) \\ &+ \sum \dot{m}_{b,t} c_{p,b} t_{art,in} - \sum \dot{m}_{b,t} c_{p,b} t_{bp,n} - L k_{bp}\left(t_{bp,n} - t_{bp,n+1}\right) \\ &+ m_{bp,n} M_{bp,n} - h_c A_{bp,n}\left(t_{bp,n} - t_a\right) - q_{rad} - E_{sk} A_{bp,n} \end{aligned} \tag{36}$$

The following nodal heat balance equations describe how the heat generated by means of metabolic reactions is distributed among different tissue nodes inside of a body part. The removal of the heat is passively controlled by the thermal properties of the tissue node (e.g. heat conductivity), actively controlled by means of the blood circulation (macrocirculation and microcirculation) and externally controlled with heat transfer mechanisms consisting of the convective, radiative and evaporative heat transfer with the surroundings (Fu 1995). The green line in Figure 7 represents the passive control, red lines the active control and blue lines the external heat transfer mechanisms. Between 50% –80% of the total heat transfer in tissue is due to the blood flow (Fu 1995).

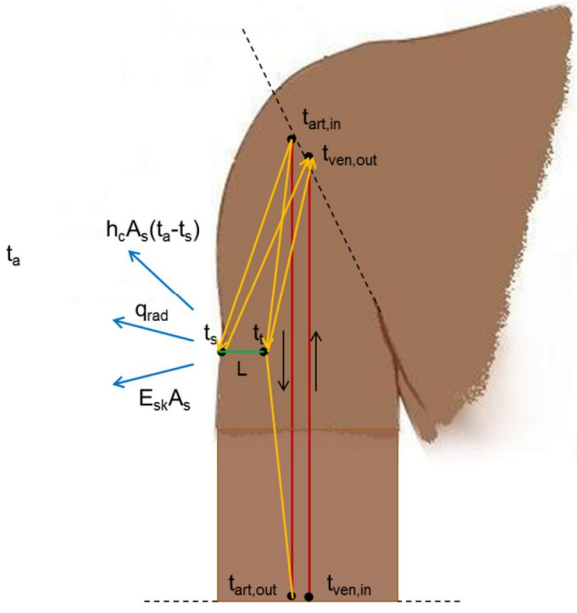

Figure 7. A simplified illustration showing parameters for the nodal energy governing equations inside of the body part. Yellow lines represent convective heat transfer with the blood circulation, green line conduction heat transfer between tissue nodes and blue lines external convective, radiative and evaporative heat transfer with the surroundings. The exemplary artery and vessel are marked with red lines.

Utilizing the final heat balance Eq. 36 the heat balance equation for a skin tissue node located on the skin surface can be written as

$$\begin{aligned} m_s c_{p,s} \frac{\partial t_s}{\partial t} &= \dot{m}_{b,s} c_{p,b} t_{art,in} - \dot{m}_{b,s} c_{p,b} t_s - L k_s (t_s - t_t) + m_s M_s \\ &- h_c A_s (t_s - t_a) - q_{rad} - E_{sk} A_s \end{aligned}, \tag{37}$$

where m_s is the mass of the skin surface node, $c_{p,s}$ is the specific heat capacity of the skin, t_s is the skin surface node temperature, $\dot{m}_{b,s}$ is the capillary blood flow in the skin tissue (basal, constricted and dilated values for skin tissue in Table 17), k_s is the heat conductivity of skin, t_t is the temperature of the adjacent tissue node, m_s is the mass of the skin surface node, M_s is the metabolic heat generation rate of the skin tissue (Table 12), and A_s is the skin surface area of the skin surface node. The thermal properties of all tissues (heat conductivity, density, specific heat capacity) are found in Table 11.

The term on the left-hand side is the rate of accumulation of thermal energy due to the changing temperature of the skin surface node. The first and second terms represent the microcirculation heat transfer rate into and out of the node by capillary blood through perfusion, the third term is the net rate of conduction heat transfer between the skin surface node and the adjacent tissue node, the fourth term is the rate of heat generation by metabolic reactions, the fifth term is the rate of convective heat transfer between the skin surface and the surrounding air, the sixth term is the radiative heat transfer between the skin surface and the surrounding surfaces and the last term is the evaporative heat transfer between the skin surface and the surrounding air. The macrocirculation heat transfer is not taken into account in the heat balance of the skin surface node because the arteries and vessels are located in the muscle tissue.

The external heat transfer mechanisms are not included in the heat balance equation for a tissue node located under the skin surface. The arteries and vessels are located in the muscle tissue, and therefore the convective heat transfer from the arteries and vessels is taken into account only in the heat balance of the muscle tissue. Inside of the muscle tissue the convective heat conductances G_{art} and G_{ven} are divided into all individual muscle tissue nodes. The convective heat transfer conductance between the macrocirculation blood flow and an individual muscle tissue node is assumed to be proportional to the mass of the muscle tissue node compared to the total mass of the muscle tissue nodes in the body part. For the exemplary case with one artery and one vessel the convective heat transfer conductance $G_{t,art}$ between the artery and the muscle tissue is calculated as

$$G_{t,art} = \frac{m_t \cdot G_{art}}{\sum m_t}, \tag{38}$$

and the convective heat transfer conductance $G_{t,ven}$ between the vessel and the muscle tissue is calculated accordingly

$$G_{t,ven} = \frac{m_t \cdot G_{ven}}{\sum m_t}, \tag{39}$$

The heat balance equation for a tissue node located under the skin surface is now

$$\begin{aligned} m_t c_{p,t} \frac{\partial t_t}{\partial t} &= G_{t,art}\left(t_{art,out} - t_t\right) + G_{t,ven}\left(t_{ven,out} - t_t\right) + \dot{m}_{b,t} c_{p,b} t_{art,in} \\ &- \dot{m}_{b,t} c_{p,b} t_t - Lk_t\left(t_t - t_s\right) + m_t M_t - q_{res} \end{aligned} \tag{40}$$

where m_t is the mass of the tissue node, $c_{p,t}$ is the specific heat capacity of the tissue, t_t is the temperature of the tissue node, $\dot{m}_{b,t}$ is the capillary blood flow in the tissue (basal values for other tissues than skin in Table 15, basal, constricted and dilated values for skin tissue in Table 17), k_t is the heat conductivity of the tissue, M_t is the metabolic heat generation rate of the tissue (Table 12), and q_{res} is the respiration heat loss for the lung tissue. The thermal properties of different tissues (heat conductivity, specific heat capacity) are found in Table 11.

The term on the left-hand side is the rate of accumulation of thermal energy due to the changing temperature of the tissue node. The first two terms on the right-hand side representing the convective heat transfer with the macrocirculation are used only for muscle tissue nodes, the third and fourth terms represent the microcirculation heat transfer rate into and out of the tissue node by capillary blood through perfusion and the fifth term is the net rate of conduction heat transfer between the tissue node and the adjacent tissue node. The sixth term is the rate of heat generation by metabolic reactions. For other tissue nodes than muscle tissue nodes, the sixth term only includes the basal metabolism from Table 12. For muscle tissue nodes, the possible effect of physical activity is obtained from Table 13 and the possible shivering power is calculated by means of Eq. 24 and Table 18. For a lung tissue node the seventh respiration term is taken into account by calculating the dry and latent heat losses with Eq. 9.

3.5 Thermal sensation and thermal comfort calculation

The new Human Thermal Model (HTM) uses Zhang's method (Zhang 2003) for the calculation of thermal sensation and thermal comfort. The method is explained in the previous chapter. The Predicted Percentage of Dissatisfied (PPD) of HTM is based on the overall thermal sensation: the PMV of Eq. 5 is substituted with the calculated overall thermal sensation.

Zhang's method defines the neutral thermal sensation level (value 0 between the scale from -4 to +4) by means of thermally neutral set point temperatures for

each body part. Utilizing Zhang's method in HTM, the thermally neutral set point temperatures for each body part had to be recalibrated for HTM by means of a simulation in a thermoneutral environment. A thermoneutral environment is not coherently defined in the literature. Thermoneutral temperature and humidity levels vary between sources, being 30 °C and 50% RH (relative humidity of air) in Ferreira & Yanagihara (2009), 30 °C and 40% RH in Fiala (1999), 28.2 °C and 30–32% RH in Smith (1991), or the values are not presented (Zhang 2003). For HTM the operative temperature of 29 °C and relative humidity of 45% were chosen as a thermoneutral environment. The set point temperatures were calculated without clothing and with the activity level of 1 Met. The thermally neutral set point temperatures of each body part by Zhang and HTM are presented in Table 19. With these set point temperatures the thermal sensation index was 0.05 (neutral) and the thermal comfort index was 1.47 (comfortable).

Table 19. Zhang's thermoneutral set point temperatures (Zhang 2003) and set point temperatures calibrated for HTM for calculation of local thermal sensation.

Body part	*Zhang set point temperature, °C*	*HTM set point temperature, °C*	*Deviation, °C*
Face	35.2	35.2	0
Head	35.8	35.3	-0.5
Neck	35.8	35.1	-0.7
Chest	35.1	34.0	-1.1
Back	35.3	34.1	-1.2
Pelvis	34.3	34.0	-0.3
Upper arm	34.2	34.1	-0.1
Forearm	34.6	33.8	-0.8
Hand	34.4	33.7	-0.7
Thigh	34.3	33.4	-0.9
Lower leg	32.9	33.1	+0.2
Foot	33.3	32.7	-0.6

In a steady state, assuming zero influence from the overall thermal state of the body the logistical thermal sensation equation by Zhang (Eq. 6) can be expressed as

$$S_{local} = 4\left(\frac{2}{1 + e^{-C1\left(t_{skin,local} - t_{skin,local,set}\right)}} - 1 \right) \tag{41}$$

or in another way

$$S_{local} = 4\left(\frac{1-e^{-C1\left(t_{skin,local}-t_{skin,local,set}\right)}}{1+e^{-C1\left(t_{skin,local}-t_{skin,local,set}\right)}}\right). \quad (42)$$

The skin temperatures representing each thermal sensation index from -3 to +3 were calculated for each body part (Table 20) using eq. 41, body part-specific set point temperatures for HTM (Table 19) and body part-specific regression coefficients C1 (Table 3). The skin temperatures representing thermal sensation values -4 and +4 would be quite extreme, because the local thermal sensation calculation is used in normal working or living conditions, where the extreme limits are not needed. The values -3 and +3 of Zhang's scale represent the maximum thermal sensations -3 and +3 of the ASHRAE thermal sensation scale (Table 1).

Table 20. Calculated body part-specific skin temperatures representing each thermal sensation index from -3 to +3.

	Thermal sensation index						
Body part	**-3**	**-2**	**-1**	**0**	**+1**	**+2**	**+3**
Face	22.2	27.9	31.8	35.2	35.9	36.8	38.0
Head	30.2	32.4	34.0	35.3	35.7	36.1	36.8
Neck	30.2	32.4	33.8	35.1	35.5	36.0	36.7
Chest	28.4	30.9	32.5	34.0	34.9	35.8	37.2
Back	27.6	30.4	32.4	34.1	34.8	35.7	36.9
Pelvis	24.3	28.5	31.4	34.0	35.3	36.7	38.9
Upper arm	27.4	30.3	32.3	34.1	35.4	36.8	39.0
Forearm	27.3	30.1	32.1	33.8	34.5	35.4	36.6
Hand	24.0	28.2	31.1	33.7	34.8	36.1	38.0
Thigh	23.7	27.9	30.8	33.4	35.2	37.2	40.1
Lower leg	26.4	29.3	31.3	33.1	34.4	35.8	38.0
Foot	24.9	28.3	30.7	32.7	34.7	36.9	40.2
Average values	**26.4**	**29.7**	**32.0**	**34.0**	**35.1**	**36.3**	**38.0**

4. Verification and validation of the Human Thermal Model

This chapter presents all tests, which were used in the development and validation process of the Human Thermal Model, HTM. Chapter 4.1 presents the various verification tests performed in the model development process. Tissue heat transfer test without blood circulation was used to test the tissue heat transfer of HTM without blood circulation and metabolism. The importance of blood circulation and moisture evaporation was studied with the qualitative head test and the body part test. The effect of different skin blood flow models on skin surface temperatures was studied with Munir's test, which was utilized in the model development for choosing the skin blood flow model from three alternative models. Chapter 4.2 presents the validation tests using the final HTM. The validation tests consisted of the clothing calculation tests presented, responses to severe temperature step changes and thermal sensation and comfort calculation tests presented.

4.1 Verification of the Human Thermal Model

4.1.1 Tissue heat transfer test without blood circulation

To test the tissue heat transfer calculation, human thermal model simulations were made in a static indoor temperature without metabolism and blood transfer. The decrease of the simulated rectal temperature in a static ambient temperature of 8 °C or 18 °C was compared to rectal temperatures calculated with the experimentally verified empirical model by Marshall and Hoare (1962) and simulated rectal temperatures of the Finite-Element model by Mall and Eisenmerger (2005). Marshall and Hoare (1962) have developed a double exponential model to describe the typical sigmoid shape of the rectal temperature time curve after death:

$$\frac{t_{re} - t_a}{t_{re,d} - t_a} = \frac{p}{p - Z} e^{-Zt} - \frac{Z}{p - Z} e^{-pt}, \tag{43}$$

where t is time, t_{re} is rectal temperature, $t_{re,d}$ is rectal temperature at the time of death and t_a is the ambient air temperature. Parameter Z takes into account the body shape. Parameter p is based on numerous experiments, and it varies from 0.275 (lower p) to 0.6 (upper p), the mean value being 0.4 (mean p).

Mall and Eisenmerger (2005) have developed a three-dimensional Finite-Element model of the human body, which can be used to estimate time since death. Mall and Eisenmerger (2005) present a test case, where the decrease in rectal temperature after death has been simulated in ambient temperatures of 8 °C and 18 °C. The weight of the test body was 80 kg. This test case was simulated with HTM, and the results were compared to simulated results by Mall and Eisenmerger (2005) and calculated mean p values by Marshall and Hoare (1962). Figure 8 shows the simulated and calculated decrease of rectal temperature in an ambient temperature of 18 °C, and Figure 9 shows the decrease of rectal temperature in an ambient temperature of 8 °C.

The mean absolute second norm of difference is the difference between the measured and simulated values to the power of two, and the relative second norm of difference is the mean absolute second norm of difference divided by the measured value. During the first 24 hours in an ambient temperature of 18 °C the mean absolute second norm was 0.32 °C and the mean relative second norm was 0.98% compared to the calculated mean p by Marshall and Hoare (1962). The corresponding values in an ambient temperature of 8 °C were 0.57 °C and 2.20%. When compared to FEM simulation results, the mean absolute second norm was 0.18 °C and the mean relative second norm was 0.55% during the first 24 hours in an ambient temperature of 18 °C. The corresponding values in an ambient temperature of 8 °C were 0.39 °C and 1.36%. The simulation results with HTM correspond well with the results of both after-death studies by Marshall and Hoare (1962), and Mall and Eisenmerger (2005).

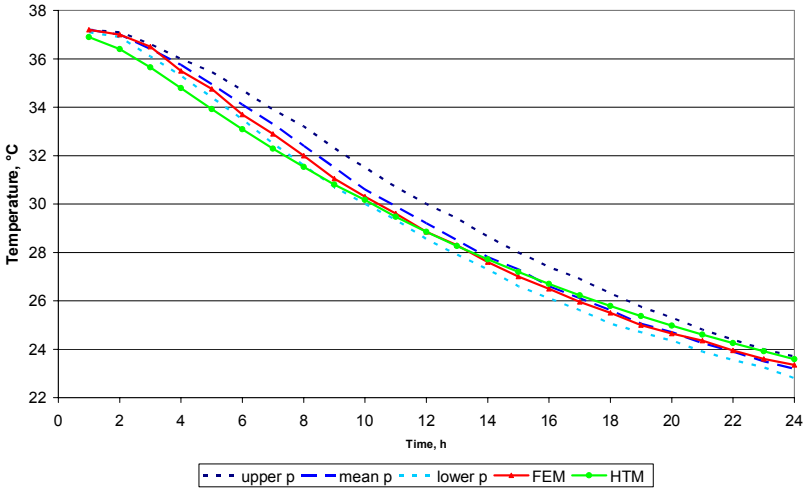

Figure 8. Calculated and simulated rectal temperatures after death in an ambient temperature of 18 °C. FEM = Finite Element Model by Mall and Eisenmerger (2005). Upper *p*, mean *p* and lower *p* present the range of parameter p by Marshall and Hoare (1962).

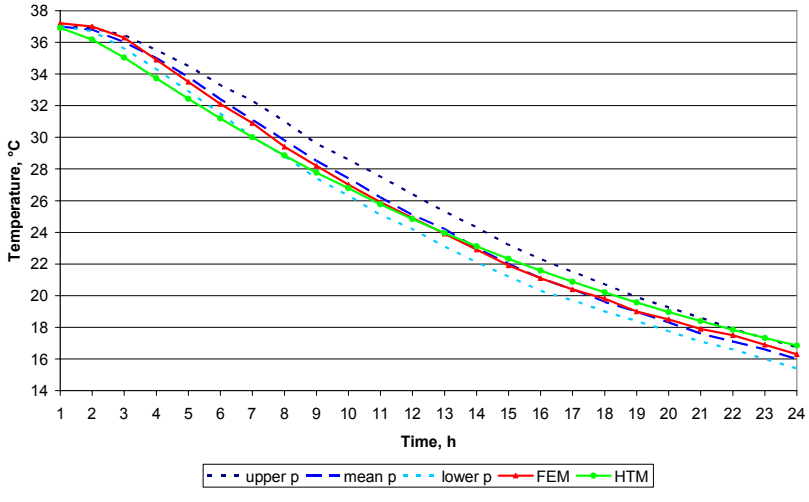

Figure 9. Calculated and simulated rectal temperatures after death in an ambient temperature of 8 °C. FEM = Finite Element Model by Mall and Eisenmerger (2005). Upper *p*, mean *p* and lower *p* present the range of parameter *p* by Marshall and Hoare (1962).

4.1.2 Importance of blood circulation and moisture evaporation

The purpose of the qualitative head test was to evaluate the relevance of the adopted thermal models on the human body part level prior to adding more complicated internal interaction mechanisms, such as the blood flow, to the model. The body part test case studied the importance of blood circulation and moisture evaporation in the head. The head was described by four concentric spheres mimicking the real head anatomy with brain, bone, fat, and skin layers. Table 21 shows the steady-state midpoint and surface temperature values of the head predicted with four different modelling approaches:

(i) thermal conduction, surface convection, no blood flow

(ii) thermal conduction, surface convection, constant basal blood flow (a constant entering blood temperature level of 37 °C)

(iii) thermal conduction, surface convection, constant basal blood flow, controlled skin layer blood flow (physiology/control model)

(iv) thermal conduction, surface convection, constant basal blood flow, controlled skin layer blood flow, moisture evaporation on skin.

Table 21. Simulated midpoint and surface temperatures of the qualitative head test.

Case definition	**Midpoint temperature, °C**	**Surface temperature, °C**
Thermal conduction and surface convection with **no blood flow**	127.9	86.70
Thermal conduction and surface convection with **constant basal blood flow**	37.34	35.72
Thermal conduction and surface convection with **constant basal blood flow** and **controlled skin layer blood flow**	37.34	36.24
Thermal conduction and surface convection with **constant basal blood flow**, **controlled skin layer blood flow**, and **moisture evaporation on skin**	37.34	34.75

The results of the qualitative head test clearly indicate the crucial importance of including a blood circulation model into realistic human thermal modelling. If the blood circulation model is excluded, both the brain and skin temperature level will rise to unrealistically high levels due to metabolic heat production in the tissues (Table 21). Adopting constant basal blood flow in all tissue layers will balance the temperature gradients very effectively. Since the brain temperature level in the basal blood flow case (ii) remains at an unwanted high level (37.34 °C), the human body control system tries to decrease the brain temperature

by increasing skin layer blood circulation – which can be seen in the skin layer blood control case (iii). However, in this test case, not even the maximum available skin layer blood circulation can reduce the brain temperature level, and therefore the skin layer will begin to sweat further removing heat from the head. Due to the limited heat transfer area of the heat, not even these ultimate actions (maximizing the local skin layer blood circulation and 100% sweating of the head) are powerful enough to reduce brain temperature level. Therefore, a whole body blood circulation and control system will be needed to achieve thermal balance in all local body parts.

The results of the qualitative head test emphasized the importance of including a blood circulation model into realistic human thermal modelling. The current version of HTM uses constant basal blood flows, because the activity levels in normal residential use and office work are quite constant and the objective was to keep the model quite simple and rapid to use. However, if the thermal sensation and comfort in e.g. a sport premises need to be simulated, the varying blood flows can be implemented in the model in the future.

4.1.3 Effect of different skin blood flow models on skin surface temperatures

Stolwijk (Munir et al. 2009), Smith (Smith 1991) and Fiala (Fiala 1999) have suggested different basal skin blood flow models, which differ noticeably from each other (Table 22). These alternative body part-specific skin blood flow rates were tested with a dynamical temperature step change test by Munir et al. (2009). The mechanisms of vasodilation and vasoconstriction that result in a higher or lower skin blood flow, respectively, were taken into account using the multiplier factors for the calculation of maximum and minimum skin blood flows from basal skin blood flow of Table 16.

Munir (Munir et al. 2009) has examined transient skin and rectal temperature variations under a series of stepwise changes in environmental conditions, including neutral (29.4ºC), low (19.1 ºC), and high (39.1 ºC) ambient temperatures (Figure 10). In the test arrangements fifteen healthy male students participated as subjects in two series of experiments under a thermal-transient condition. Their average age was 23.5 years, average weight 66.6 kg and average height 1.70 m. The metabolic rate was 60 W/m^2. The students were exposed to a series of conditions in climatic chambers: a nearly (thermally) neutral condition, followed by low air temperature, a second neutral condition, high air temperature, and finally, a third neutral condition. Munir used Stolwijk's 25-node thermal model (Stolwijk 1971) for comparing the experimental data presented above to calculated results.

Table 22. Alternative blood flow rates based on different basal skin blood flow models.

Body part	Skin blood flow rate per skin tissue mass, 10^{-9} m^3/s kg			Total basal blood flow rate in each body part, 10^{-9} m^3/s		
	Smith model	Stolwijk model	Fiala model	Smith alternative	Stolwijk alternative	Fiala alternative
Head	8 486	2 134	6 709	14 978	14 121	14 982
Neck	2 912	2 912	2 912	391	391	391
Torso	1 290	474	876	54 536	54 042	54 536
Upper arm	1 398	246	542	915	862	915
Thigh	1 185	801	503	1 488	1 590	1 488
Forearm	1 397	248	542	511	481	511
Lower leg	1 184	800	516	659	703	657
Hand	3 345	3 003	2 252	282	351	282
Foot	2 051	3 294	725	204	529	204
Total body				80 557	77 585	78 024

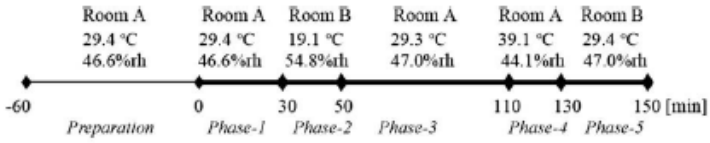

Figure 10. Munir test schedule.

Munir's test case was simulated with the HTM using the basal skin blood flow rate models suggested by Smith (Smith 1991), Stolwijk (Munir et al. 2009) and Fiala (Fiala 1999). The basal blood flow rates of other tissues were based on the Smith model. The simulation test room had a volume of 27 m^3 (3 m x 3 m x 3 m) with no windows. The surrounding structures were at the same temperature as the indoor air. The HTM was located at the middle point of the test room floor. The convective heat transfer coefficients were according to Table 8.

Simulated skin temperatures were compared to measured and calculated skin temperatures by Munir. Figure 11 – Figure 17 show the skin temperature variation during the test schedule of measured values, calculations by Munir and simulations by HTM with Fiala, Smith and Stolwijk basal skin blood flow for forehead, pelvis, lower arm, hand, thigh, lower leg and foot.

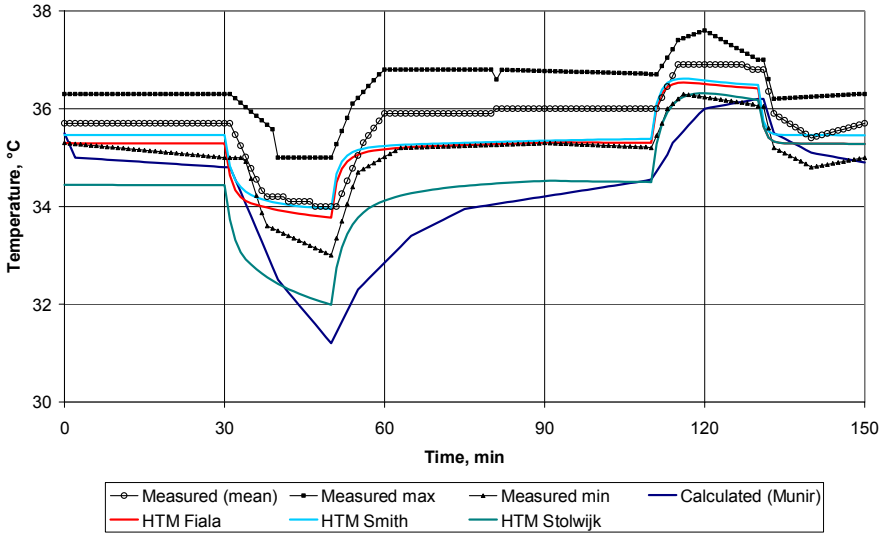

Figure 11. Simulated forehead skin temperatures with HTM using different skin blood models during the Munir test schedule compared to measured and calculated values by Munir.

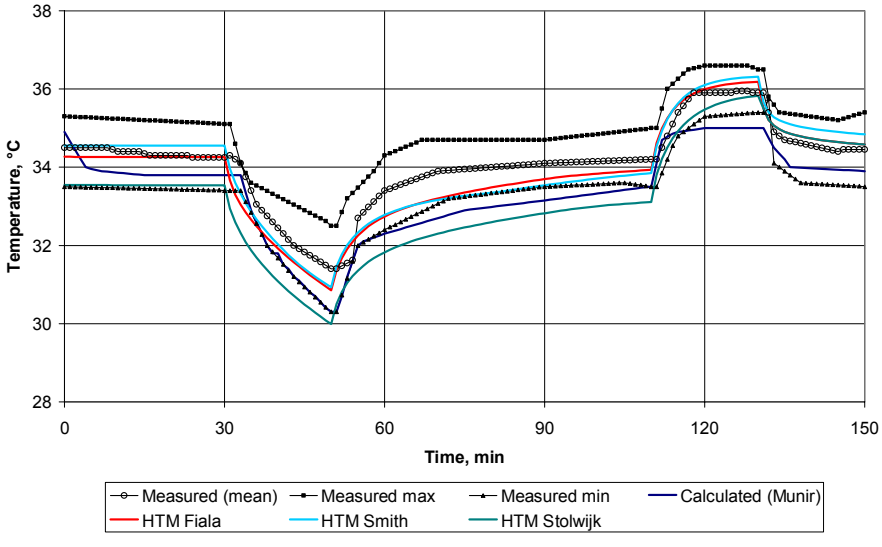

Figure 12. Simulated pelvis skin temperatures with HTM using different skin blood models during the Munir test schedule compared to measured and calculated values by Munir.

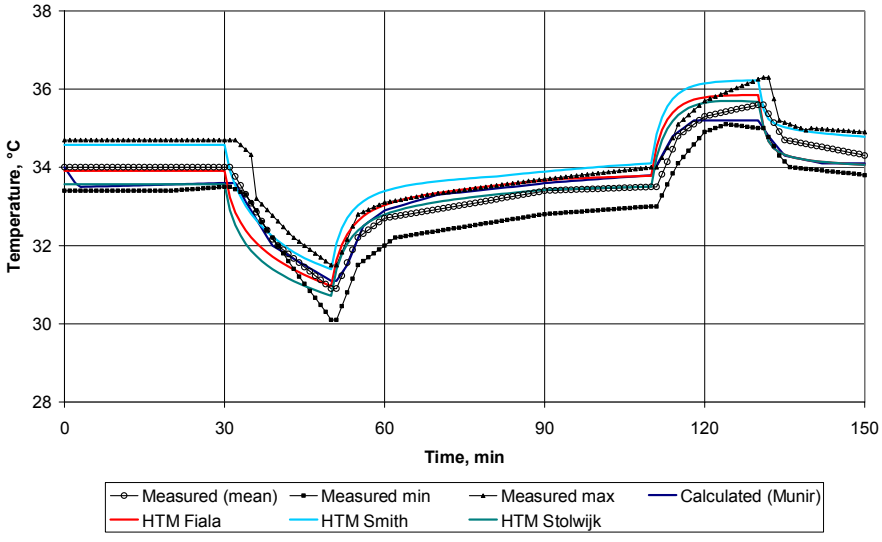

Figure 13. Simulated lower arm skin temperatures with HTM using different skin blood models during the Munir test schedule compared to measured and calculated values by Munir.

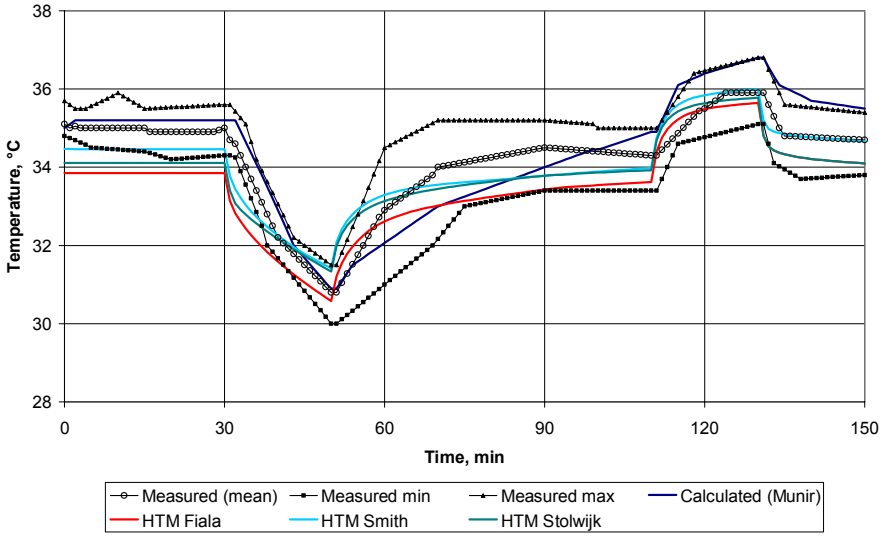

Figure 14. Simulated hand skin temperatures with HTM using different skin blood models during the Munir test schedule compared to measured and calculated values by Munir.

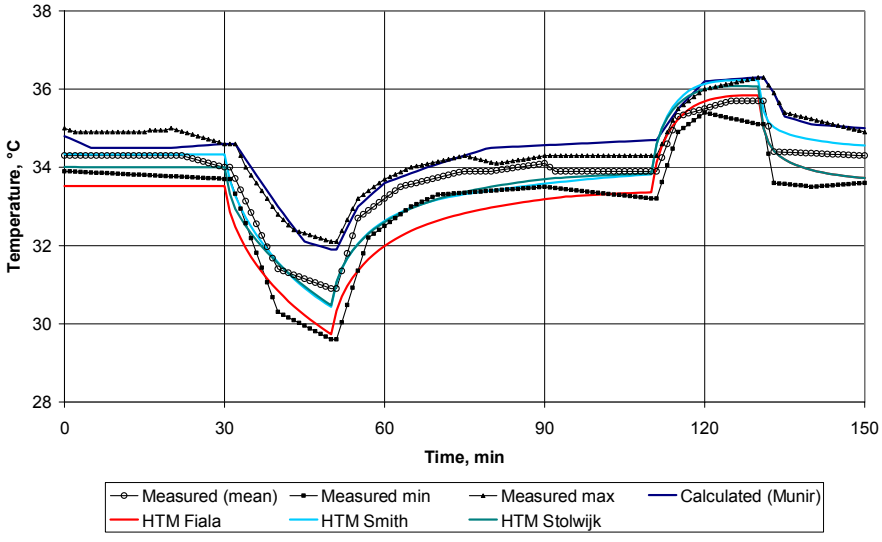

Figure 15. Simulated thigh skin temperatures with HTM using different skin blood models during the Munir test schedule compared to measured and calculated values by Munir.

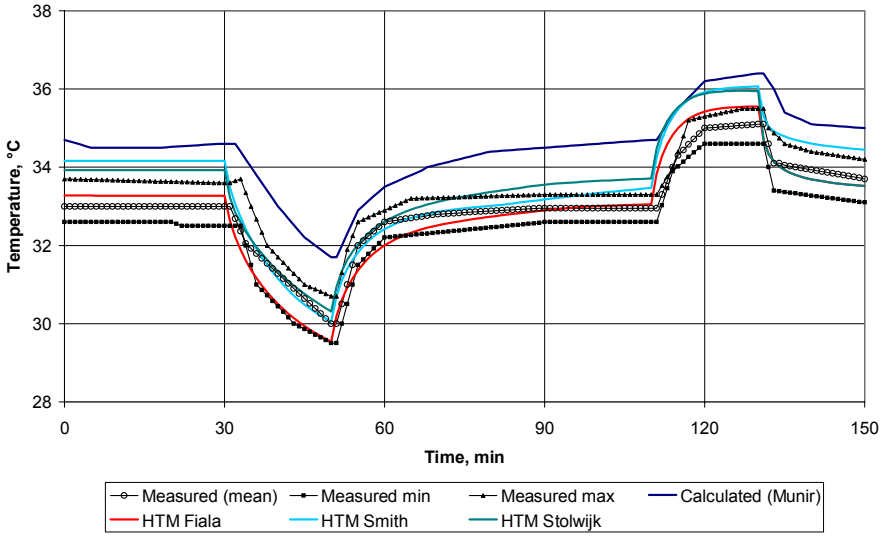

Figure 16. Simulated lower leg skin temperatures with HTM using different skin blood models during the Munir test schedule compared to measured and calculated values by Munir.

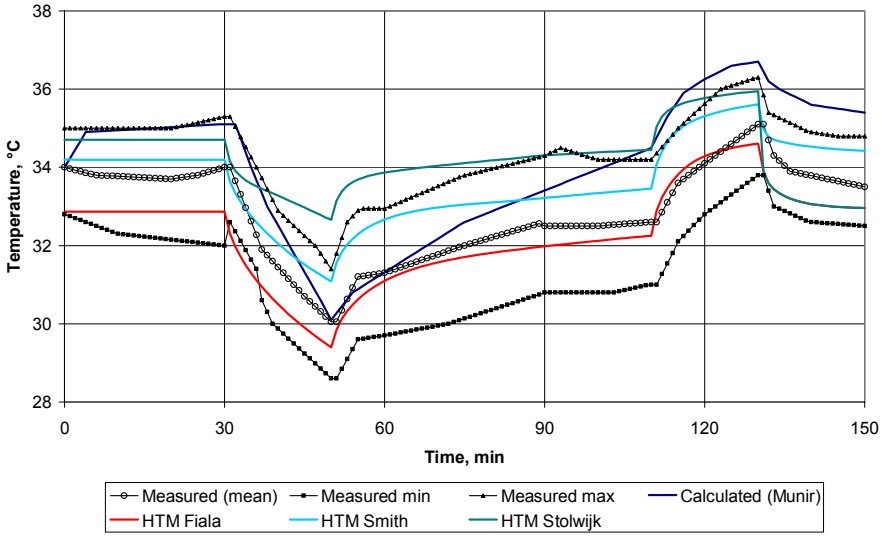

Figure 17. Simulated foot skin temperatures with HTM using different skin blood models during the Munir test schedule compared to measured and calculated values by Munir.

The mean absolute and relative second norms of difference were calculated during the test schedule with intervals of 1 minute. The mean absolute second norm of difference is the difference between the measured and simulated values to the power of two, and the relative second norm of difference is the mean absolute second norm of difference divided by the measured value. The simulation results using Fiala's skin blood flow had the best correlation with the measured values (Table 23). The maximum absolute temperature deviation was 1.78 °C (hand). The same dynamical test case has been simulated by Foda et al. (2011) with the MS-Pierce model and Fiala model. The maximum absolute temperature deviations with both models were close to 2 °C.

Table 23. HTM skin temperature simulations according to the Munir test schedule with skin blood flows of Fiala, Smith and Stolwijk: deviation from the measured values by Munir.

Body part	Mean absolute second norm of difference between measured and simulated skin temperatures [°C]				Mean relative second norm of difference between measured and simulated skin temperatures			
	HTM Fiala	HTM Smith	HTM Stolwijk	Munir Stolwijk	HTM Fiala	HTM Smith	HTM Stolwijk	Munir Stolwijk
Face	0.3	0.2	1.9	2.5	0.8%	0.6%	5.3%	7.1%
Pelvis	0.2	0.2	1.2	0.6	0.6%	0.6%	3.7%	1.8%
Arm	0.2	0.4	0.3	0.1	0.5%	1.2%	0.8%	0.3%
Hand	0.7	0.3	0.4	0.4	2.0%	1.0%	1.3%	1.2%
Thigh	0.3	0.2	0.1	0.5	0.8%	0.5%	0.4%	1.4%
Lower leg	0.1	0.5	0.5	2.2	0.3%	1.6%	1.4%	6.7%
Foot	0.4	0.9	3.0	1.8	1.2%	2.7%	9.5%	5.3%
Average error	0.3	0.4	1.1	1.2	0.9%	1.2%	3.2%	3.4%

4.2 Validation of the Human Thermal Model

4.2.1 Clothing calculation

To test the clothing calculation of HTM the simulation results of two test cases with clothing were compared to measured values. The test cases were test case 5 and test case 12 (pre-test condition) by Fu (1995). In test case 5 the dry and latent heat transfer from the body were measured in a surrounding temperature of 21.1 ºC and relative humidity of 50%. The clothing alternative was a sweat suit (clo 0.69) and the activity level 1 Met (quiet sitting). The dry heat transfer measured by Fu was 82 W, the latent heat transfer 20 W and the total heat transfer 102 W. The corresponding values from HTM were 89 W, 15 W and 104 W. In the pre-test condition of test case 12 the mean skin temperature of chest, back, forearms and thighs were calculated in a surrounding temperature of 23.9 ºC and relative humidity of 50%. The clothing alternative was a sweat suit consisting of a sweat shirt and sweat pants (clo 0.69) and the activity level was 1.0 Met (quiet sitting). The mean skin temperature measured by Fu was 34.0 ºC and the simulated value by HTM was 34.1 ºC.

4.2.2 Response to severe temperature step change

Hot exposure test case

Hardy and Stolwijk performed hot exposure tests on three male subjects (Stolwijk & Hardy 1966). The test individuals were exposed to an upward step change from 30 °C at 40% RH to 48ºC at 30% RH. The test individuals wore shorts and they were sitting quietly during the measurements. Two of the test individuals were tall and slim, and the third person was of medium height and overweight. The average weight of the test individuals was 91.6 kg.

The hot exposure test case was simulated with HTM in a similar test room as used in Munir's test case. A clothing layer representing shorts was added around the pelvis and thighs. The dry and evaporative heat transfer resistances of the clothing layer were 0.03 m^2K/W and 0.0037 m^2kPa/W, respectively. The clothing insulation was 0.19 clo. The metabolic rate of the model was 60 W/m^2 (1 MET) representing quiet sitting. The mean skin temperature of HTM was calculated as the average temperature of the same body part temperatures that were measured in the test case of Hardy and Stolwijk (face, chest, back, pelvis, 2 x thighs, upper arms, lower legs, hands and feet). The weight of HTM is 78.2 kg, noticeably less than the average weight of the test persons.

The current version of HTM uses constant convective heat transfer coefficients, which are calculated at an ambient temperature of 20 °C (Table 8). For the hot exposure test case, the convective heat transfer coefficient values were modified for the test temperature of 48 °C. To modify the convective heat transfer coefficients, the mean skin temperatures were first simulated in ambient temperatures of 20 °C and 48 °C, being 34 °C and 37 °C, respectively. Then the corresponding free convection coefficients were calculated for a vertical surface i) with the mean (skin) temperature of 34 °C in an ambient temperature of 20 °C and ii) with the mean (skin) temperature of 37 °C in an ambient temperature of 48 °C. The convective heat transfer coefficient at 48 °C was 14.9% lower than at 20 °C, thus the body part specific convective heat transfer coefficients measured by deDear at 20 °C were all decreased by 14.9% (Table 24).

Table 24. Original convective and modified convective heat transfer coefficients used in the hot and cold exposure tests.

	Original convective heat transfer coefficients by DeDear in a surrounding temperature of 20 °C, W/m^{2}K	**Modified convective heat transfer coefficients for the first and third phases of the cold exposure test in a surrounding temperature of 43 °C and skin temperature of 35 °C, W/m^{2}K**	**Modified convective heat transfer coefficients for the hot exposure test in a surrounding temperature of 48 °C and skin temperature of 37 °C, W/m^{2}K**
Head	3.7	2.85	3.15
Chest	3.0	2.31	2.55
Back	2.6	2.00	2.21
Pelvis	2.8	2.16	2.38
Upper arm	3.4	2.62	2.89
Forearm	3.8	2.92	3.23
Hand	4.5	3.46	3.83
Thigh	3.7	2.85	3.15
Lower leg	4.0	3.08	3.41
Foot	4.2	3.23	3.58

Figure 18 presents the simulated and measured skin and rectal temperatures during the hot exposure test case. In the hot phase (120 minutes in 47.8 °C) the maximum heat loss by sweating was 245 W. The average absolute second norm error between the measured and simulated mean skin temperatures was 0.18 °C and the relative second norm error was 0.5%. The average absolute second norm error between the measured and simulated core temperatures was 0.19 °C and the relative second norm error was 0.5%.

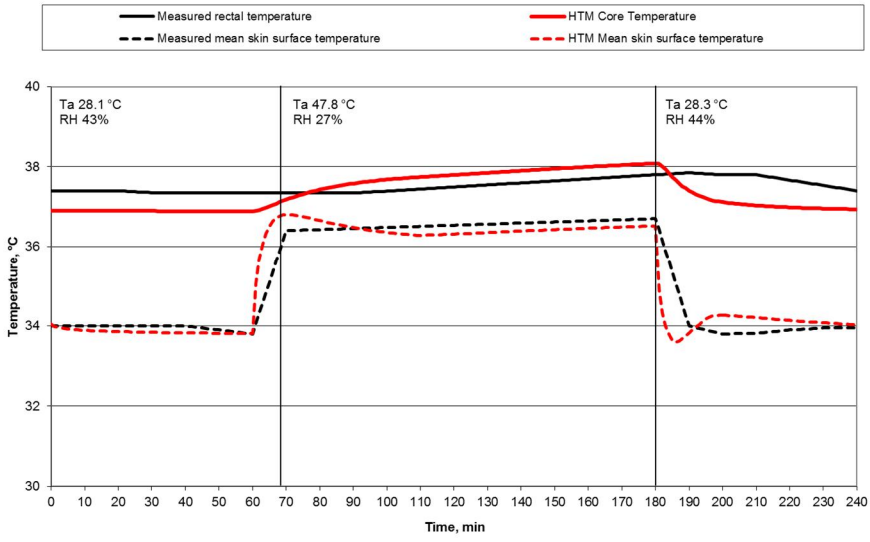

Figure 18. Measured and simulated mean skin and core temperatures during the hot exposure test.

Figure 19 presents the measured and simulated evaporative heat transfer during the test case. The simulated evaporative heat transfer from the human model to the environment was close to the measured values during the neutral and hot phases 28.1 °C and 47.8 °C (Figure 18). After the change from the hot phase to the second neutral phase the simulated evaporative heat transfer increased instantly from 141 W/m^2 to 203 W/m^2. The measured evaporative heat transfer did not increase and was only 125 W/m^2 after the change from the hot to the neutral phase. According to Eq. (21) the evaporative heat loss is linearly proportional to the difference of the saturated water vapour pressure on the skin surface and the water vapour pressure of the surrounding environment. After 120 minutes in the hot phase, the mean skin temperature is 36.5 °C. The saturated water vapour pressure at the mean skin surface is 6.1 kPa, whereas the water vapour pressure of the surrounding air (28.3 °C, relative humidity 44%) is only 1.7 kPa. The maximum evaporative heat transfer with a completely wet skin (wettedness value 1.0) calculated with Eq. (21) is 240 W/m^2. With a skin wettedness value of 0.845, the calculated evaporative heat transfer is 203 W/m^2, which equals the simulated value. As the measurement arrangement of evaporative heat loss has not been explained in the article, it could be assumed that the measured evaporative heat loss is estimated by measuring the change of the skin wettedness, which is not analogous with the actual evaporative heat loss.

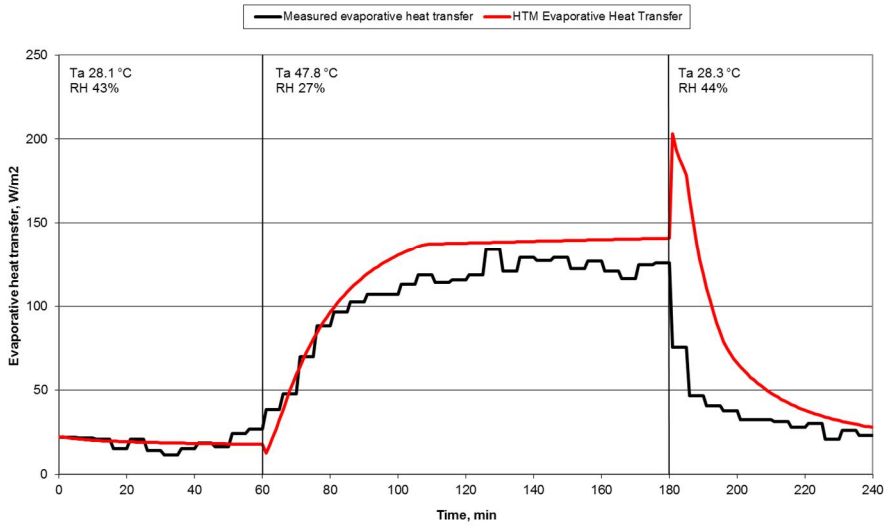

Figure 19. Measured and simulated evaporative heat transfer during the hot exposure test.

Cold exposure test case

The cold exposure test was performed by Hardy and Stoljwik 1966 with similar arrangements as the previously explained hot exposure test, except in this case the test individuals were exposed to step changes from 43 °C (30%RH) to 17 ºC (40% RH) and back to 43 °C (30% RH), and the average weight of the test individuals was 84.8 kg. For the cold exposure test case, the convective heat transfer coefficients of HTM were modified for the test temperature of 43 °C with a mean skin temperature of 35 °C (see the hot exposure test case). The convective heat transfer coefficients were 23.0% lower at 43 °C than at 20 °C (Table 24). Figure 20 presents the simulated and measured temperatures of the cold exposure test. During the cold phase at 17 °C the shivering power increased from 0 W to 51.1 W.

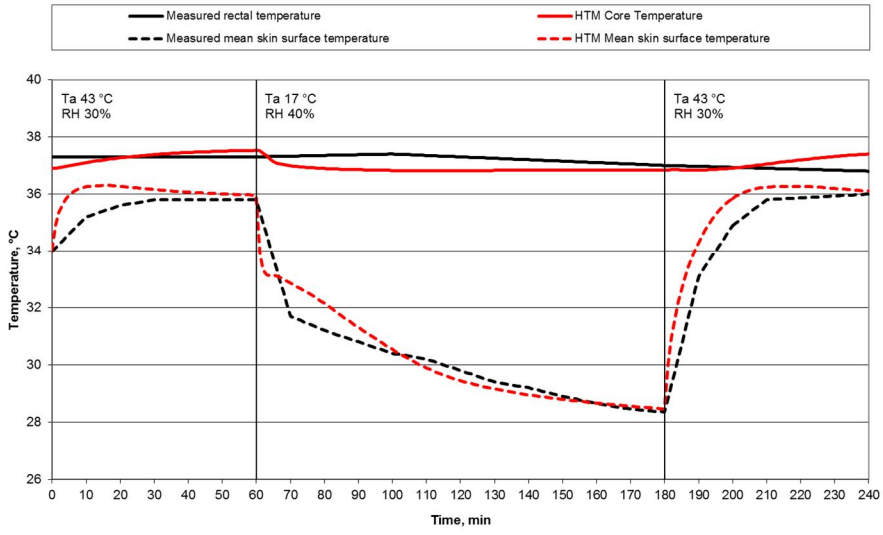

Figure 20. Measured and simulated mean skin and core temperatures during the cold exposure test.

In the cold exposure test case, the average absolute second norm error between the measured and simulated mean skin temperatures was 0.45 °C and the relative second norm error was 1.4%. The average absolute second norm error between the measured and simulated core temperatures was 0.12 °C and the relative second norm error was 0.3%.

The temperature step changes of the dynamical test cases by Munir (2009) presented in Ch. 4.1.3 and the hot and cold exposure test cases were between ± 10 °C and ± 26 °C. These kind of severe temperature changes are unrealistic in the normal living environment, but the tests served well for model validation purposes. Since the results obtained by HTM show good agreement with the test case measurement data, HTM can be regarded as a suitable approach for predicting tissue temperature levels with more moderate temperature variations in typical living conditions. The dynamical validation tests also suggest that HTM can predict the human body skin temperature changes with reasonable confidence at least between temperature levels 17 °C and 48 °C.

4.2.3 Thermal sensation and comfort calculation

Thermal sensation in a steady state temperature

Nevins et al. (1966) has measured the thermal sensation of college students, who were exposed to each thermal condition in groups of ten persons (five males and five females). The exposure period was 3 hours. The students were clothed in cotton shirts and trousers and woollen socks; the insulating value of the clothing was 0.52 clo. The students were seated during the test and their average metabolism was 1 Met. Simulated thermal sensations in nine steady state temperatures between 18.9 °C and 27.8 °C with the relative humidity of 45% were compared to the experimental series by Nevins et al. Figure 21 shows the measurement results of male test individuals and simulated values with the HTM method and the Fanger PMV method.

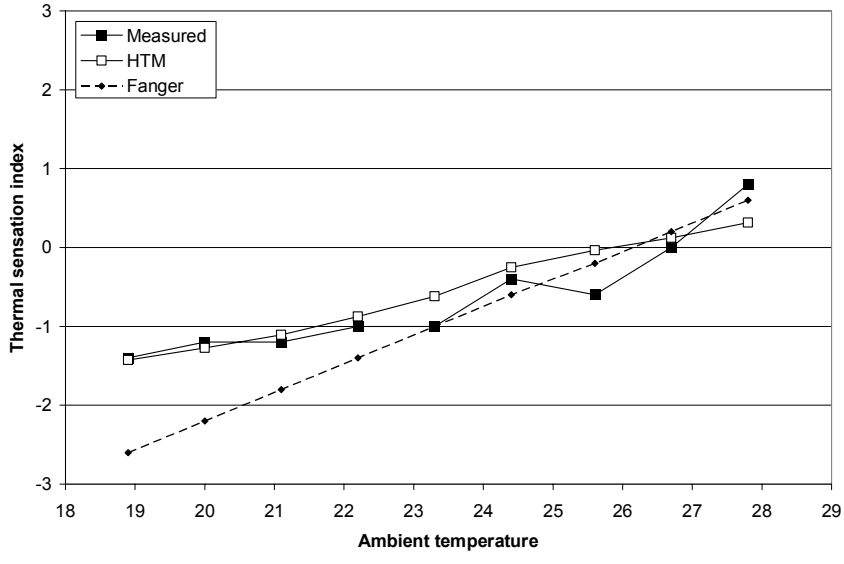

Figure 21. Measured and simulated thermal sensations of sedentary subjects (Nevins et al. 1966).

Thermal sensation and comfort response to a temperature step change

Gagge et al. (1967) have measured temperature step change responses of three male subjects. In a cold exposure test the subjects were exposed for one hour in a neutral environment of 29 °C. The subjects were then transferred to a colder room at 17.5 °C, where they stayed for 2 hours. After the cold room the subjects moved back to the neutral room for one hour. The activity level was 1 Met, and the clothing insulation was 0.1 clo (shorts). The relative humidities of the experiment

rooms were not reported; in simulations they were assumed to be 40% in both rooms. Figure 22 shows the thermal sensation measurement results and simulated thermal sensations with the HTM method and the Fanger PMV method for the cold exposure test case.

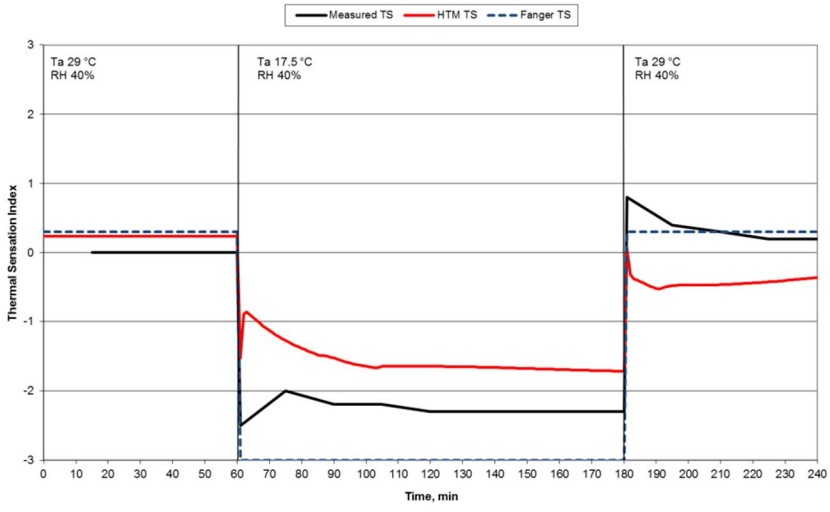

Figure 22. Thermal sensation during the cold exposure operative temperature step by Gagge (1967).

The measured thermal comfort was defined by a scale from uncomfortable to slightly uncomfortable and finally comfortable. The measured values were interpreted on the HTM thermal comfort scale (Table 7) as

- uncomfortable: -2
- slightly uncomfortable: -1
- comfortable: 2.

Figure 23 shows the thermal comfort measurement results and simulated thermal comfort with the HTM method. The thermal comfort index has a sudden drop at ca. 100 minutes. As the overall comfort is the average of the two minimum local comfort votes, it does not always develop linearly.

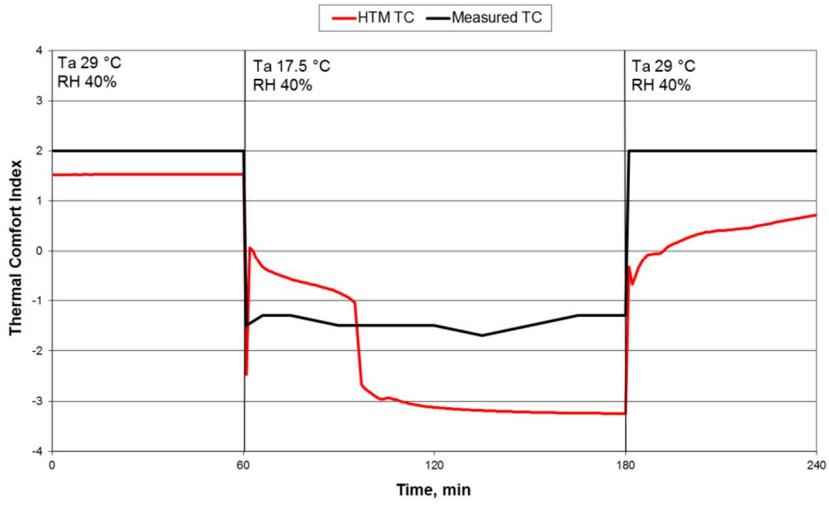

Figure 23. Thermal comfort during the cold exposure operative temperature step by Gagge (1967).

In a hot exposure test, the temperatures of the test rooms were 28 °C, 48 °C, and 28 °C. The exposure times, activity levels and clothing were similar to the cold exposure test. The relative humidities in the test rooms were not reported. In simulations the relative humidity was assumed to be 40% in the 28 °C test room and 30% in the 48 °C test room. For the simulations of the test room at 48 °C, the same modified convective heat transfer factors were used as in the Hardy and Stolwijk hot exposure case (Chapter 4.2.2).

The simulations were first made with the original thermal sensation equation by Zhang:

$$S_{local} = 4\left(\frac{2}{1+e^{-C1\left(t_{skin,local}-t_{skin,local,set}\right)-K1\left[\left(t_{skin,local}-\ddot{t}_{skin}\right)-\left(t_{skin,local,set}-\ddot{T}_{set}\right)\right]}}-1\right) + C2_i\frac{dt_{skin,local}}{dt} + C3_i\frac{dt_{core}}{dt}, \quad (44)$$

The simulated thermal sensation index showed a steep downward drop followed by a steep upward rise after changing from the 48 °C room to the 28 °C room. This effect differed from the measured thermal sensation.

According to Zhang (2003) the core temperature responds to local cooling of the most influential body parts (face, chest, back and pelvis) with an immediate increase. In the local thermal sensation equation by Zhang (Eq. 6), this phenomenon is taken into account with a core temperature change term (third term on the right-hand side). The term is based on the measurement results implying that the core temperature responds to local cooling of the most influential body parts (the

face, chest, back and pelvis) with an immediate increase. Therefore an increase in the core temperature also decreases the warm thermal sensation of the chest, back, pelvis and face regions.

To test the effect of the core temperature change term on simulated thermal sensation, the hot exposure test case was re-simulated with a modified local thermal sensation equation (Eq.6) without the core temperature change term:

$$S_{local} = 4\left(\frac{2}{1+e^{-C1\left(t_{skin,local}-t_{skin,local,set}\right)-K1\left[\left(t_{skin,local}-\bar{t}_{skin}\right)-\left(t_{skin,local,set}-\bar{t}_{set}\right)\right]}}-1\right) + C2_i\frac{dt_{skin,local}}{dt} \tag{45}$$

When the third term was left out of the thermal sensation equation, the simulated thermal sensations followed the measured values after the temperature drop. Figure 24 shows the measured thermal sensation values, the thermal sensation calculated with Fanger's PMV method and HTM thermal sensations calculated both with the original Zhang local thermal sensation equation and a modified equation without the term representing the effect of core temperature change. After the temperature rise from 28 °C to 48 °C, Zhang's original equation gave better correlation with the experimental values than the modified equation. The results suggest that using core temperature increase term in the thermal sensation simulation of a severe temperature drop should be more closely examined. Figure 25 shows the thermal comfort measurement results and simulated thermal comfort with the HTM method and modified Zhang thermal sensation calculation.

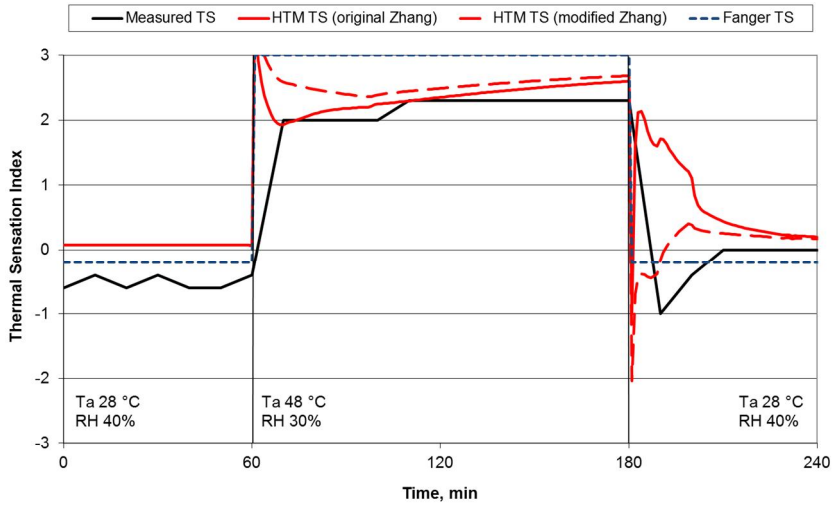

Figure 24. Thermal sensation during the hot exposure operative temperature step change by Gagge (1967).

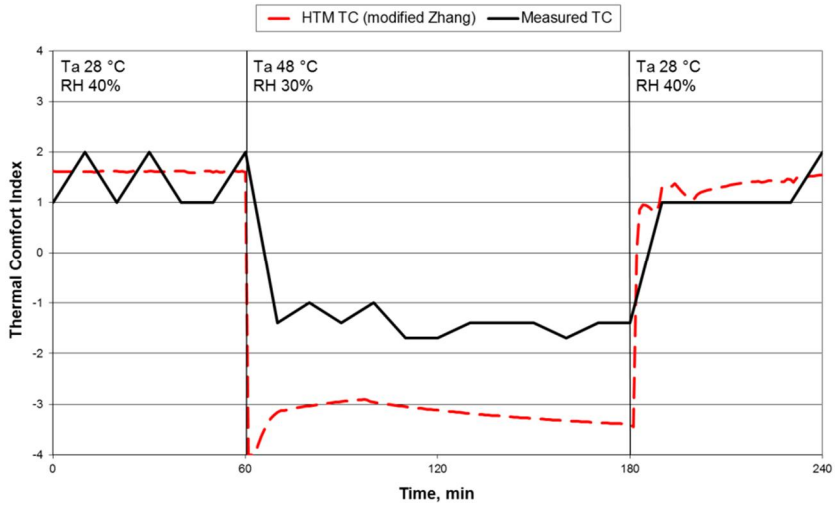

Figure 25. Thermal comfort during the hot exposure operative temperature step by Gagge (1967).

Thermal sensation response to different activity levels

McNall et al. (1967) have studied the effect of activity levels on thermal sensation and thermal comfort. The activity levels used in the experiment represented metabolic rates of 101 W/m^2 (1.7 Met), 134 W/m^2 (2.3 Met) and 168 W/m^2 (2.9 Met). The activity levels were created using a modified step test, where the test individual was walking up and down a flight of stairs. For the low activity level the walking cycle was stand for 25 minutes – walk for 5 minutes, for the medium activity level stand for 10 minutes – walk for 5 minutes, and for the high activity level stand for 5 minutes – walk for 5 minutes.

The subjects of the experiment were ten university students, five males and five females. They wore a thin cotton shirt, trousers and their own underwear. The insulation of the clothing was 0.52 clo. The surrounding temperatures were for the low activity test: 18.9 °C, 22.2 °C and 25.6 °C, for the medium activity test: 15.6 °C, 18.9 °C, 22.2 °C and 25.6 °C, and for the high activity test: 12.2 °C, 15.6 °C and 18.9 °C. The measurements were made with three different relative humidities: 25%, 45% and 65%.

The HTM simulations were made with a relative humidity of 45%. The clothing consisted of briefs (EF02), a long sleeve shirt (EF24), straight-legged slacks (EF36) and footies (EF82). The thermal and evaporative heat conductances of the garments were according to Fu (1995) and the codes in parenthesis represent the codes in Fu (1995) for different garments. The convective heat transfer coefficients were according to Table 8. The HTM simulations were made with a relative humidity of 45% and compared to the corresponding experimental values of the male subjects because the current tissue distribution of HTM represents a

male person. In the future version of HTM the gender will be taken account by means of a body builder.

Walking on a treadmill mainly increases heat generation in the lower body muscles. At least 75% of the total mechanical work needed for walking is done by the leg and hip area (Prilutsky and Gregor 2001). The lower body part muscles are used for progression, whereas the upper body muscles (mostly chest and upper arm muscles) are used for maintaining balance during walking. To test the effect of evenly and unevenly divided metabolism increases, the HTM thermal sensation was first simulated with uniformly increased heat generation in the muscle tissues of all body parts. In subsequent simulations, 80% of the increased metabolism was divided between the muscle tissues of the pelvis, thighs, lower legs and feet and the remaining 20% was divided between the chest and upper arm muscle tissues. Figure 26, Figure 27 and Figure 28 show the measured thermal sensations and the simulated values with the HTM and Fanger methods.

The simulation results demonstrate that the Zhang sensation model, originally developed for sedentary activities, is also applicable for higher activity levels. Dividing the metabolic rate increase uniformly of unevenly to the muscle tissue had a minor influence on the simulated thermal sensation with higher activity levels, but the maximum difference between the results was only 0.08 thermal sensation index units.

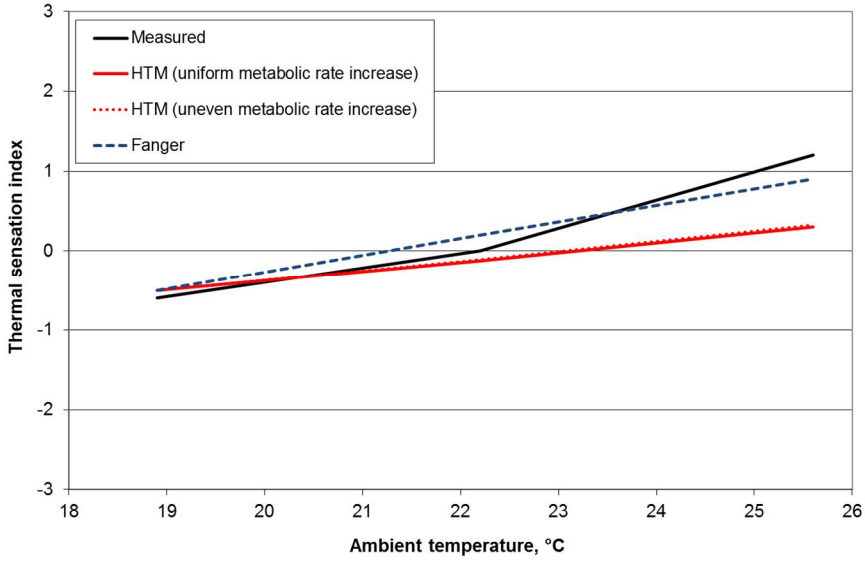

Figure 26. Measured thermal sensations during low activity levels compared to simulated values with the HTM and Fanger methods.

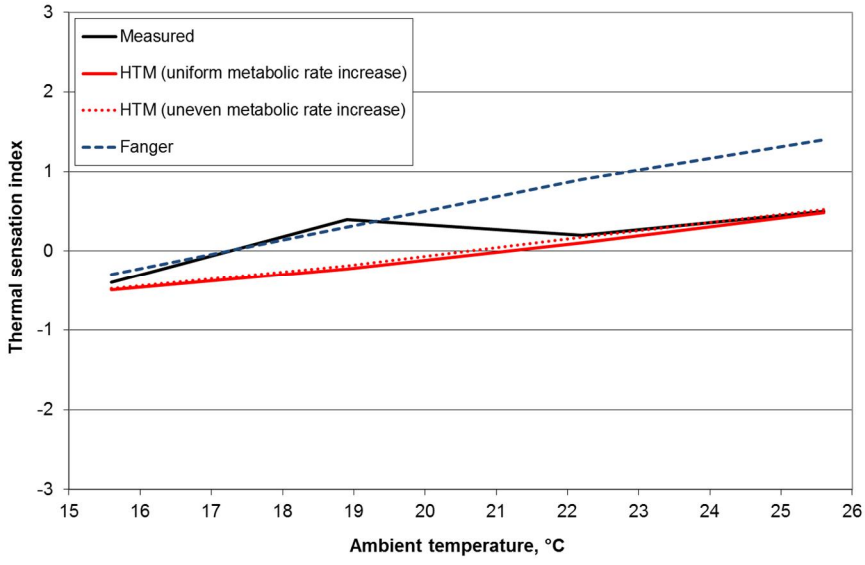

Figure 27. Measured thermal sensations during medium activity levels compared to simulated values with the HTM and Fanger methods.

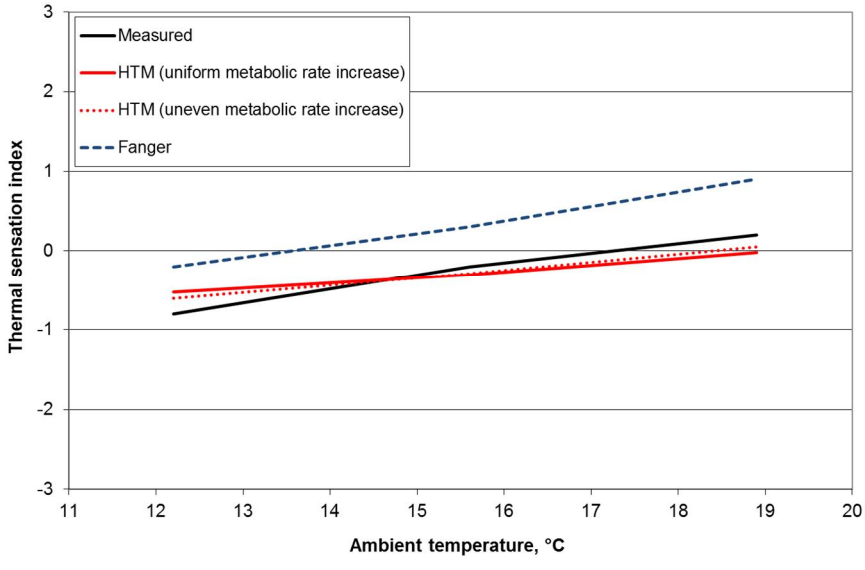

Figure 28. Measured thermal sensations during high activity levels compared to simulated values with the HTM and Fanger methods.

Summary of thermal sensation and thermal comfort test cases

As mentioned earlier in Chapter 2.2, thermal sensation is the sense of temperature, reflecting the response of thermoreceptors. Because thermal sensation is related to how people "feel", it is not possible to define it in physical or psychological terms (Hensen 1991). Measuring the effect, for example, of temperature level on thermal sensation is therefore a difficult task, because all the other boundary conditions such as relative humidity, activity level, air velocity and ventilation rate, should be kept constant during the measurement. All the experimental thermal sensation and thermal comfort test cases show at least some inconsistency in the measured thermal sensation values. Furthermore, the number of individuals tested was small.

When compared to the measurement results presented by Nevins et al. (1966), Gagge et al. (1967) and McNall et al. (1967), promising estimations of human thermal sensation and comfort were obtained with HTM. The HTM method showed a better correlation with measured values than Fanger's PMV method in four of the six separate test cases (Table 25).

Table 25. The deviations from measured thermal sensation values with the HTM and Fanger methods (thermal sensation index units).

Thermal sensation test	HTM mean absolute second norm of error	Fanger mean absolute second norm of error
Nevins static temperature test	0.09	0.36
Gagge cold exposure test	0.39	0.31
Gagge hot exposure test	0.22	0.38
McNall low activity test	0.26	0.05
McNall moderate activity test	0.28	0.33
McNall high activity test	0.03	0.37
Average error	**0.21**	**0.30**

5. Significance of internal and external boundary conditions on thermal sensation

HTM thermal sensation was simulated in a static test room to estimate the significance of different boundary conditions: internal (metabolism and clothing) and external (operational temperature level, relative humidity, air velocity) boundary conditions on thermal sensation. The simulation test room had a volume of 27 m^3 (3 m x 3 m x 3 m) with no windows. The surrounding structures were at the same temperature as the indoor air. The HTM was placed at the middle point of the test room floor. The varied internal and external boundary conditions were

- thermal insulation of the clothing
- operative temperature (indoor temperature and surface temperatures)
- relative humidity of the indoor air
- indoor air velocity
- activity level.

The clothing alternatives were shorts (0.19 clo), lighter clothing alternative (0.47 clo) and heavier clothing alternative (0.86 clo). The lighter and heavier clothing ensembles were based on Fu (1995). The garments of the lighter clothing alternative were a short-sleeve shirt, briefs, shorts, calf-length socks and soft-soled shoes. The garments of the heavier clothing alternative were a t-shirt, long-sleeve turtleneck sweater, briefs, jeans, calf-length socks and soft-soled shoes. The thermal and evaporative resistances of the garments are presented in Table 26.

Table 26. Clothing alternatives in the boundary condition test cases (Fu 1995).

Garment	Thermal resistance R, m^2K/W	Evaporative resistance Re, m^2kPa/W	Shorts	Lighter clothing	Heavier clothing
Short-sleeve shirt	0.041	0.0041		x	
T-shirt	0.030	0.0032			x
Long-sleeve turtleneck sweater	0.112	0.0105			x
Briefs	0.030	0.0032		x	x
Shorts	0.030	0.0037	x	x	
Jeans	0.037	0.0066			x
Calf-length athletic socks	0.054	0.0104		x	x
Soft-soled athletic shoes	0.108	0.0208		x	x

The skin set point temperatures for the lighter and heavier clothing alternatives were calibrated in thermoneutral environments with the relative humidity as 45%. The activity level was 1 Met. The operative temperature for the thermoneutral environment of both clothing alternative was selected using the Fanger's PMV calculation method (Fanger 1970), presented in Chapter 2.3. According to the Fanger's PMV method the thermoneutral operative temperature is for the lighter clothing alternative 26.2 °C and for the heavier clothing alternative 24.0 °C when the air speed is 0 m/s. The thermally neutral set point temperatures for a naked body presented in Table 19 of Chapter 3.5 were used for the clothing alternative "shorts". The calibrated thermoneutral set point temperatures for a naked body, a body with the lighter clothing alternative and a body with the heavier clothing alternative are presented in Table 27.

The effects of relative humidity, operative temperature, activity level and clothing on thermal sensation were simulated. The operative temperature of a space is approximately the average of the air and mean radiant temperature a person is experiencing. The base case was defined as relative humidity 40%, operative temperature 20 °C and activity level 58 W/m^2 (1 Met).

The effects were also calculated with the Fanger's PMV calculation method. This calculation was made utilizing an Excel tool made by Håkan Nilsson from the University of Gävle (Nilsson 2005). The Fanger's PMV calculation tool resulted in thermal sensation indexes below -3 in some cases. These values were converted to -3 as the Fanger's PMV scale only ranges from -3 to +3 (see Table 1).

Table 27. Skin set point temperatures for different clothing alternatives for calculation of local thermal sensation.

Body part	Naked body set point temperature, °C	Lighter clothing set point temperature, °C	Heavier clothing set point temperature, °C
Face	35.2	34.9	34.6
Head	35.3	34.9	34.6
Neck	35.1	34.7	34.4
Chest	34.0	34.4	34.9
Back	34.1	34.4	35.0
Pelvis	34.0	34.8	34.6
Upper arm	34.1	34.3	34.9
Forearm	33.8	32.9	34.2
Hand	33.7	32.9	32.9
Thigh	33.4	33.6	33.3
Lower leg	33.1	33.8	34.0
Foot	32.7	34.1	33.9

5.1 Effect of relative humidity and operative temperature

The effect of relative humidity and operative temperature on thermal sensation was simulated between relative humidities of 0% and 100% with steps of 20%, and operative temperatures between 18 °C and 28 °C with steps of 2 °C (Figure 29, Figure 31, Figure 33). Thermal sensation was also calculated with the Fanger method. (Figure 30, Figure 32, Figure 34).

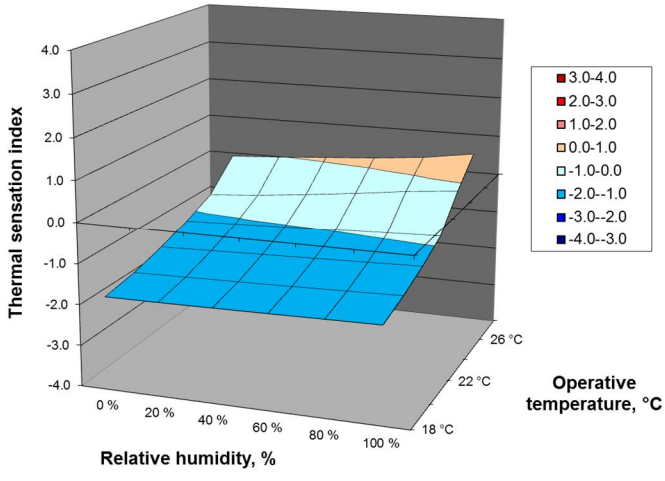

Figure 29. Effect of relative humidity and operative temperature on thermal sensation simulated with HTM, clothing 0.19 clo.

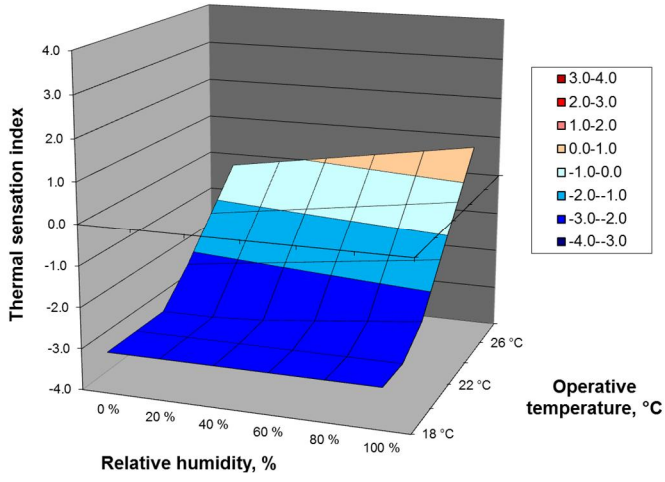

Figure 30. Effect of relative humidity and operative temperature on thermal sensation calculated with the Fanger method, clothing 0.19 clo.

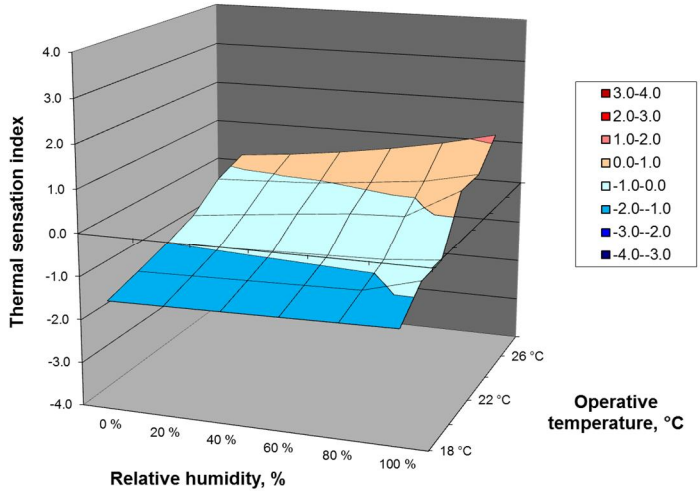

Figure 31. Effect of relative humidity and operative temperature on thermal sensation simulated with HTM, clothing 0.47 clo.

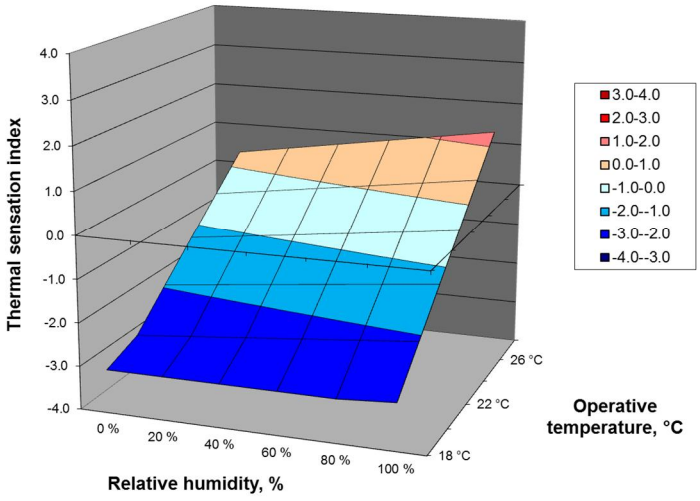

Figure 32. Effect of relative humidity and operative temperature on thermal sensation calculated with the Fanger method, clothing 0.47 clo.

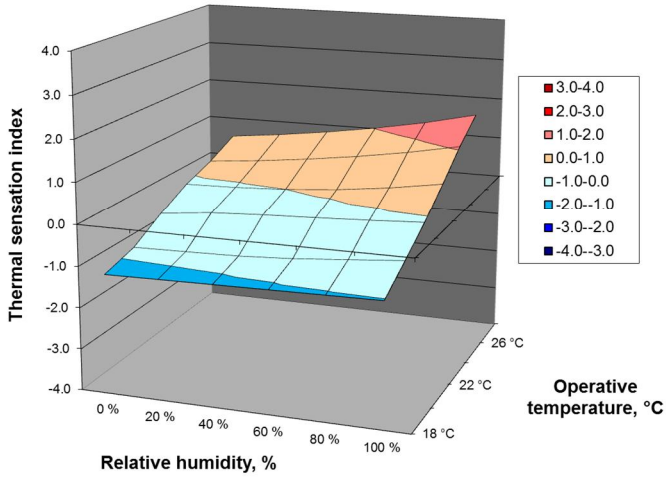

Figure 33. Effect of relative humidity and operative temperature on thermal sensation simulated with HTM, clothing 0.86 clo.

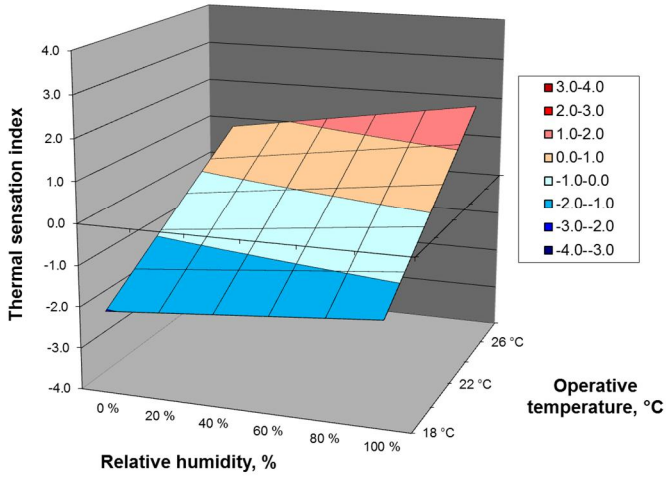

Figure 34. Effect of relative humidity and operative temperature on thermal sensation calculated with the Fanger method, clothing 0.86 clo.

5.2 Effect of activity level and operative temperature

The simulated activity levels were as defined in ISO 7730 (ISO 2005)

- 0.85 Met (46 W/m^2): resting
- 1.0 Met (58 W/m^2): relaxed sitting
- 1.2 Met (70 W/m^2): sedentary activity (office, dwelling, school, laboratory)
- 1.6 Met (93 W/m^2): standing, light activity (shopping, light industry)
- 2.0 Met (116 W/m^2): standing, medium activity (shop assistant, domestic work, machine work).

Figure 35, Figure 37 and Figure 39 show the effect of activity level and operative temperature on thermal sensation simulated with HTM. Figure 36, Figure 38 and Figure 40 show the effect of activity level and operative temperature on thermal sensation calculated with the Fanger method.

The combined effect of the metabolic rate, relative humidity and clothing on thermal sensation for a cold, neutral and hot room with operative temperatures of 18 °C, 21 °C and 25 °C, respectively, is presented in Figure 41, Figure 45 and Figure 45 with HTM simulations and in Figure 42, Figure 44 and Figure 46 with the Fanger method.

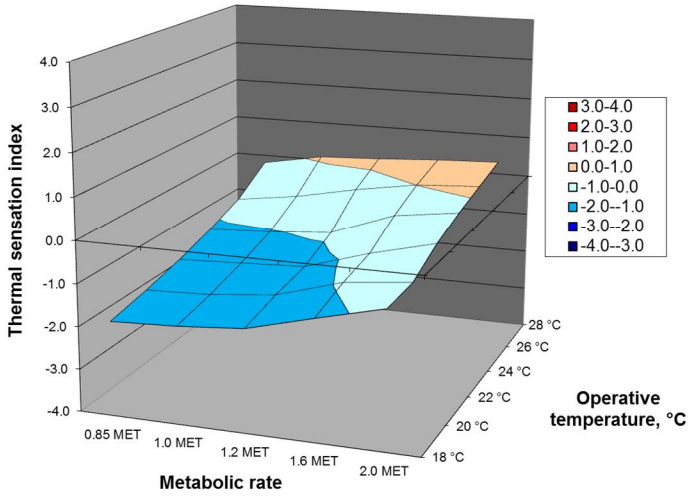

Figure 35. Effect of activity level and operative temperature on thermal sensation simulated with HTM, clothing 0.19 clo.

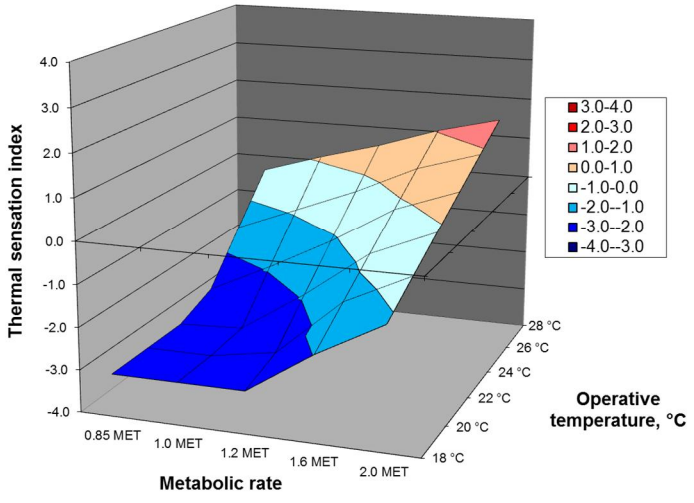

Figure 36. Effect of activity level and operative temperature on thermal sensation calculated with the Fanger method, clothing 0.19 clo.

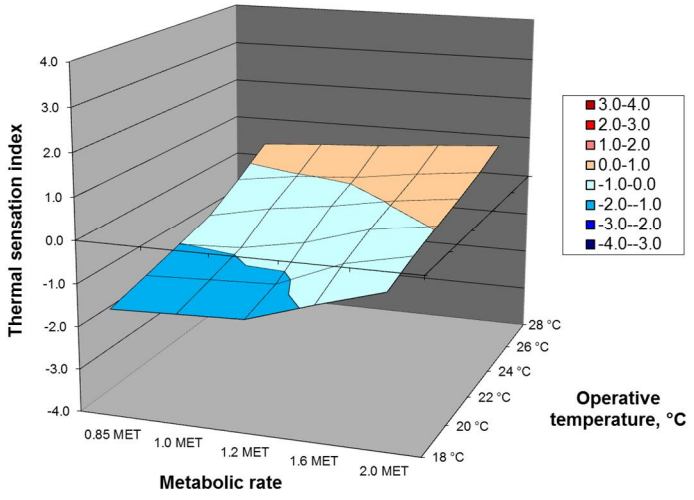

Figure 37. Effect of activity level and operative temperature on thermal sensation simulated with HTM, clothing 0.47 clo.

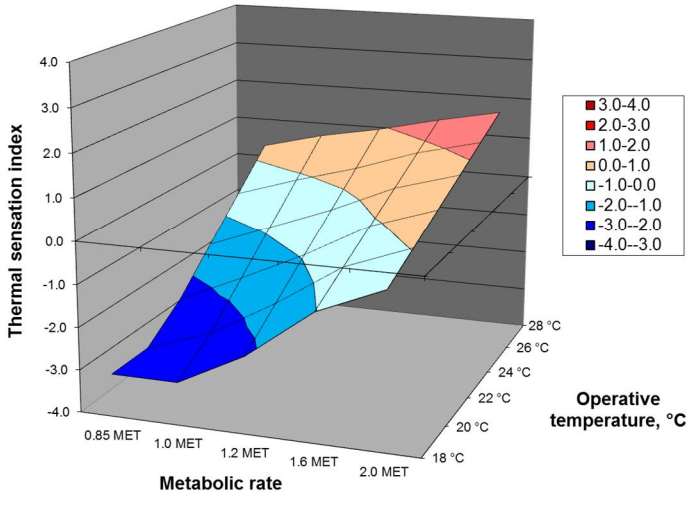

Figure 38. Effect of activity level and operative temperature on thermal sensation calculated with the Fanger method, clothing 0.47 clo.

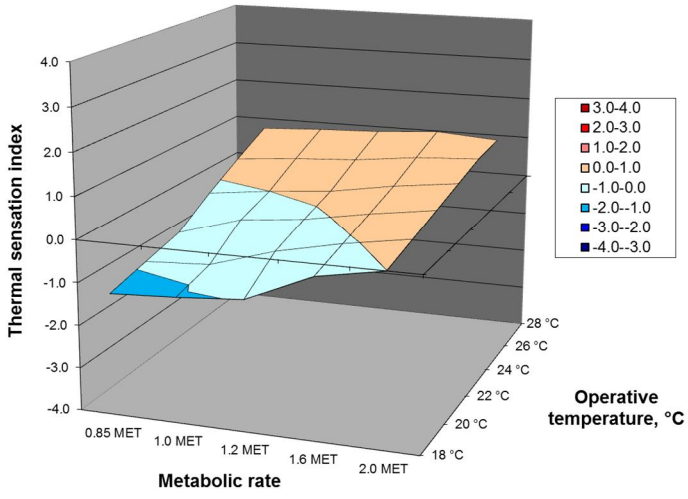

Figure 39. Effect of activity level and operative temperature on thermal sensation simulated with HTM, clothing 0.86 clo.

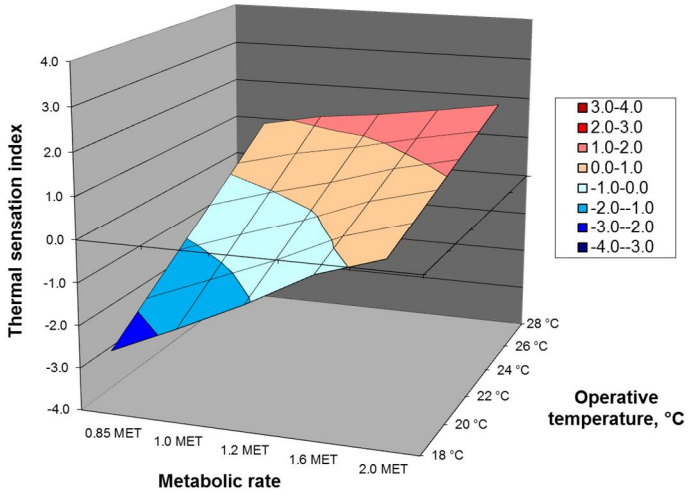

Figure 40. Effect of activity level and operative temperature on thermal calculated with the Fanger method, clothing 0.86 clo.

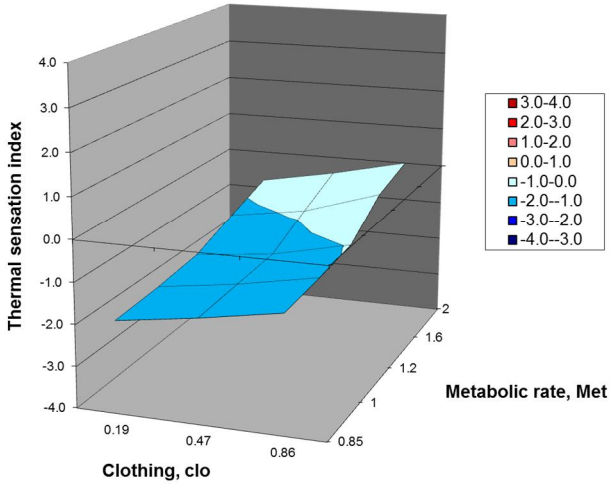

Figure 41. Effect of metabolic rate and clothing on thermal sensation in a cold room, simulated with HTM.

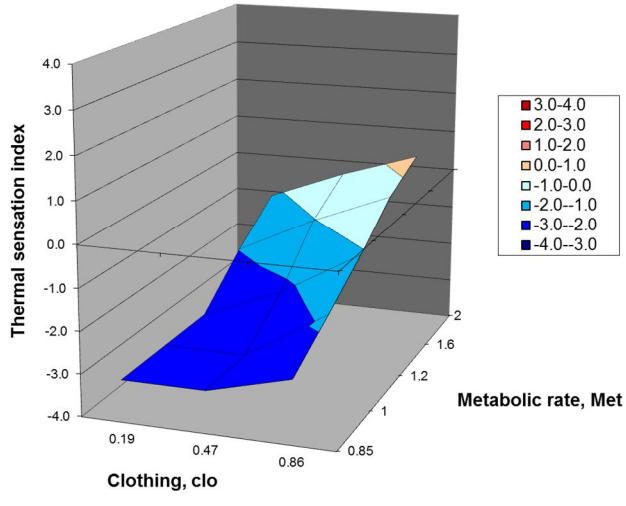

Figure 42. Effect of metabolic rate and clothing on thermal sensation in a cold room, calculated with the Fanger method.

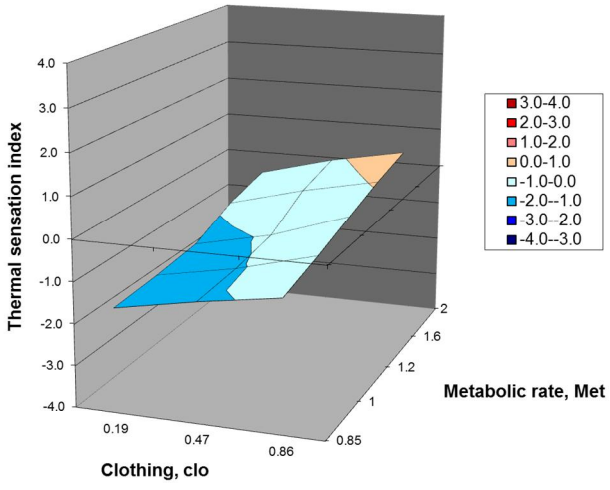

Figure 43. Effect of metabolic rate and clothing on thermal sensation in a neutral room, simulated with HTM.

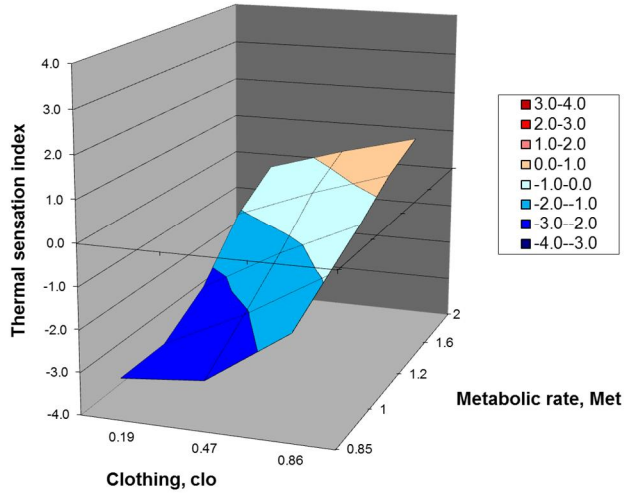

Figure 44. Effect of metabolic rate and clothing on thermal sensation in a neutral room, calculated with the Fanger method.

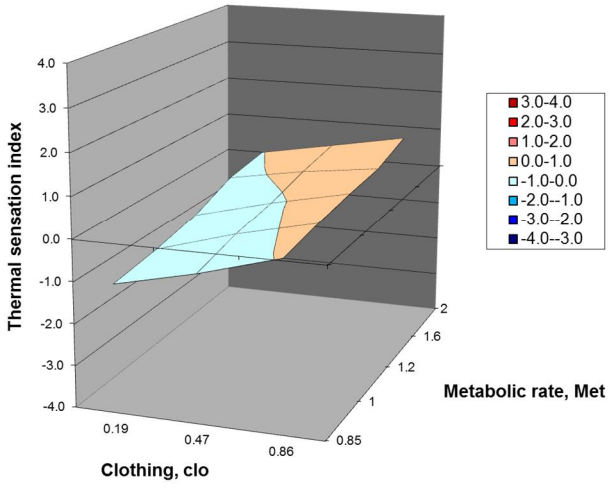

Figure 45. Effect of metabolic rate and clothing on thermal sensation in a warm room, simulated with HTM.

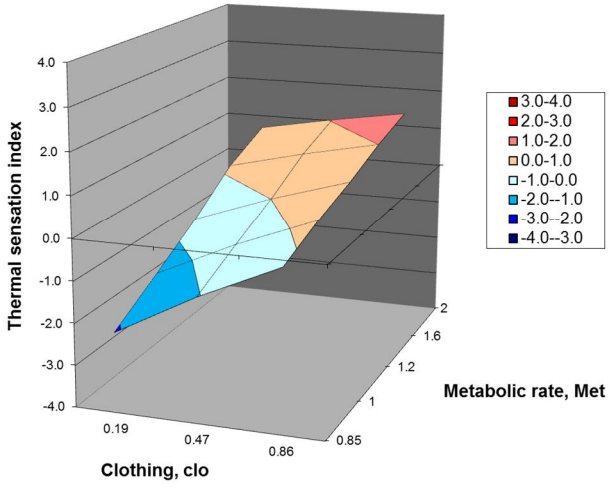

Figure 46. Effect of metabolic rate and clothing on thermal sensation in a warm room, calculated with the Fanger method.

5.3 Effect of air velocity

HTM takes into account the effect of air velocity by means of body part-specific convective heat transfer coefficients by deDear et al. (1997), which were presented in Table 8. In the following simulations the body part-specific convective heat transfer coefficients for a seated person were calculated according to deDear by taking the higher value of either the calculated forced convective heat transfer coefficient or the free convective heat transfer coefficient of each body part (Table 28).

As the convective heat transfer coefficients based on forced convection were calculated in an ambient temperature of 20 °C, the effect of air velocity on thermal sensation was simulated only at an operational temperature of 20 °C. The indoor air velocity was varied between 0 and 0.3 m/s with steps of 0.05 m/s. Figure 47 shows the simulation results with different clothing alternatives.

Table 28. Convective heat transfer coefficients (W/m^2K) (DeDear 1997).

Body part	$h_{c\_natural}$	hc (air velocity 0.10 m/s)	hc (air velocity 0.15 m/s)	hc (air velocity 0.20 m/s)	hc (air velocity 0.25 m/s)	hc (air velocity 0.30 m/s)
Head	3.7	3.7	3.7	3.7	3.7	3.7
Chest	3.0	3.0	3.0	3.5	4.0	4.5
Back	2.6	2.6	2.7	3.2	3.7	4.2
Pelvis	2.8	2.8	2.8	2.9	3.3	3.7
Upper arm	3.4	3.4	3.4	4.1	4.7	5.3
Forearm	3.8	3.8	3.8	4.4	5.0	5.6
Hand	4.5	4.5	4.5	5.1	5.8	6.5
Thigh	3.7	3.7	3.7	3.7	3.9	4.3
Lower leg	4.0	4.0	4.5	5.3	6.0	6.6
Foot	4.2	4.2	4.6	5.4	6.1	6.7

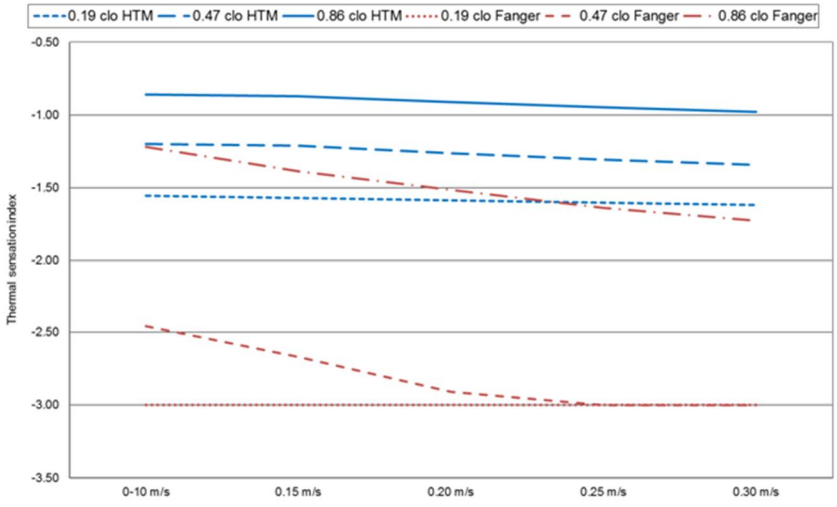

Figure 47. Effect of air velocity on thermal sensation in an operative temperature of 20 °C.

5.4 Summary

Zhang's method defines the neutral thermal sensation level by means of thermally neutral set point temperatures for each body part. Utilizing Zhang's method in HTM, the thermally neutral set point temperatures for each body part have to be recalibrated for HTM by means of a simulation in a thermoneutral environment. The neutral temperature set points were calculated for a naked person and the two clothing alternatives in their own neutral conditions.

When evaluating the significance of the effects of different internal and external boundary conditions on thermal sensation by HTM methodology, the operative temperature, metabolic rate and clothing were found to be the most dominant boundary conditions. The effect of the increased air velocity on thermal sensation with the HTM method was higher for the fully clothed person than for the person in shorts. The reason is probably that in this version of HTM the convective heat transfer coefficients used for the clothing are same that for the naked human even though the surface temperatures of the clothing are lower than the surface temperatures of the naked skin.

Table 29 shows how a change of a parameter affects the thermal sensation calculated both with HTM and Fanger methods for the lighter clothing alternative and Table 30 for the heavier clothing alternative. The changes were calculated with the base case as the reference point (relative humidity 40%, operative temperature 20 °C, activity level 1 Met, air velocity 0–0.10 m/s).

Table 29. Conclusion of the average effects of different internal and external parameters on thermal sensation for a human with the lighter clothing alternative.

Parameter	Parameter increase	Effect on thermal sensation index with HTM method	Effect on thermal sensation index with Fanger method
Operative temperature	1 ºC	+0.17	+0.37
Relative humidity	10%	+0.024	+0.062
Metabolic rate	0.1 MET	+0.07	+0.34
Air velocity	0.1 m/s	-0.03	-0.19

Table 30. Conclusion of the average effects of different internal and external parameters on thermal sensation for a human with the heavier clothing alternative.

Parameter	Parameter increase	Effect on thermal sensation index with HTM method	Effect on thermal sensation index with Fanger method
Operative temperature	1 ºC	+0.21	+0.30
Relative humidity	10%	+0.031	+0.062
Metabolic rate	0.1 MET	+0.13	+0.28
Air velocity	0.1 m/s	-0.03	-0.15

The effects of increasing or decreasing all examined internal and external parameters are larger with the Fanger method than with the HTM method. One reason for this is that the Fanger method neglects the effect of human thermoregulation on the perceived thermal sensation. As stated before, the Fanger method has been criticized to progressively overestimate the mean perceived warmth of warmer environments and the coolness of cooler environments (Humphreys and Nicol 2002). The other reason is that the current version of HTM uses the thermal sensation and comfort method by Zhang (2003). Zhang has later found that this model sometimes is insensitive to environmental conditions, especially in extreme conditions and modified the overall sensation calculation accordingly (Zhang et al. 2010). The new method by Zhang will be implemented in the following version of HTM.

6. Utilization of the Human Thermal Model

6.1 Effect of building structures on thermal sensation and comfort

The theoretical energy saving potential of the existing building stock is large. Improving the thermal properties of the existing building envelope by increasing the wall insulation level and / or replacing windows is a common strategy in building retrofit. Energy renovation of existing buildings not only reduces energy consumption, but also improves indoor thermal comfort conditions.

The effect of improving the thermal properties of the building envelope on thermal comfort was examined by utilizing HTM in a realistic case study, where the effect of energy renovation on thermal sensation and comfort during the heating season was simulated. The aim was to show quantitively how much different renovation measures affect thermal sensation and thermal comfort during an exemplary case under a cold weather period.

The effect of increasing the wall insulation level and replacing old windows with more energy-efficient new windows on thermal comfort and annual energy use was simulated for a typical 1970s-level built apartment with alternative renovation solutions. The reference apartment was based on the layout of a three-room flat in an existing apartment house in Helsinki, Finland (As Oy Helsingin Koskikartano). The living area of the flat is 65.3 m^2. The layout and room areas are presented in Figure 48.

The original wall structure was typical for Finnish apartment buildings built around 1970. The wall structure layers were from outside to inside 0.085 m concrete, 0.14 m mineral wool and 0.100 m concrete. The U-value of the structure was 0.36 W/m^2K. The original windows had double glazing. The U-value of the original window was 2.4 W/m^2K and the g-value of the glass was 0.75.

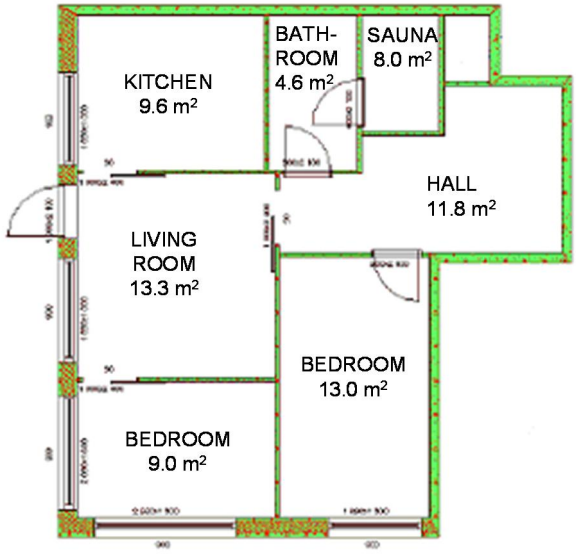

Figure 48. Reference apartment used in the renovation case study.

The air exchange system was mechanical exhaust ventilation. The total supply and exhaust air flows were both 0.037 m^3/s. The supply air flow into the living room was 0.007 m^3/s. The air velocity inside of the room was estimated to be under 0.1 m/s, therefore the body part-specific convective heat transfer coefficients from Table 8 were used. The heating distribution system was radiator heating. In the living room, the radiator was located under the window. The heating power of the radiator was controlled according to the indoor set point temperature, which was 21 °C for the living room. The indoor relative humidity was a constant 25%.

The retrofitted wall structure layers were from outside to inside 0.085 m concrete, 0.36 m polyurethane (PUR) and 0.100 m concrete. The airtightness of the structures, n_{50}-value 1.0 1/h, was held constant. The U-value of the structure was 0.10 W/m^2K. The new windows had triple glazing. The U-value of the new window was 0.67 W/m^2K (window and frame) and the g-value of the glass was 0.35. The U-values of walls and windows were of a Finnish very low-energy house level.

The structure alternatives used in the simulations were

1. original walls and windows
2. original walls and new windows
3. retrofitted walls and original windows
4. retrofitted walls and new windows.

With the dimensioning outdoor temperature of -32 °C for Central Finland and the indoor set point temperature of 21 °C, the dimensioning heating power with the original structures was 5.5 kW (85 W/m^2) for the whole flat and 1.4 kW (105 W/m^2) for the living room. The annual heating energy demand of the flat was 152 kWh/m^2. The dimensioning heating power with retrofitted walls and new windows was 3.7 kW (56 W/m^2) for the whole flat and 0.8 kW (59 W/m^2) for the living room. The annual heating energy demand of the retrofitted flat was 95 kWh/m^2.

The HTM was located in the middle of the living room floor. The activity level of the HTM was 1.2 representing light activity. The operative temperature, mean skin temperature, thermal comfort index and predicted percentage of dissatisfied were calculated during a cold and a hot weather period. The operative temperature sensor was located above the head of the human thermal model, and it took into account all surrounding surface temperatures including the window and radiator surface temperatures.The clothing insulation was 0.86 clo (heavier clothing alternative in Table 26) in the cold weather period simulation and 0.47 clo (lighter clothing alternative in Table 26) in the hot weather period simulation.

6.1.1 Cold weather period

The exemplary transient test period represented a typical cold weather period in Central Finland (3–7 February of the Jyväskylä test year 1979). The outdoor temperature and solar radiation during the test period are presented in Figure 49 and Figure 50.

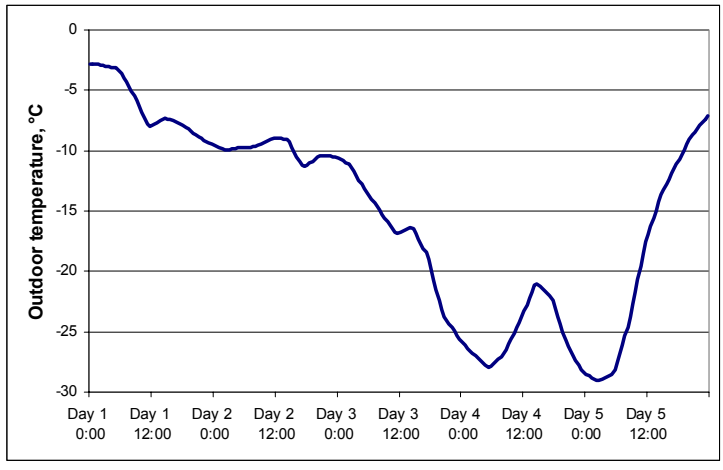

Figure 49. Outdoor temperature during the cold weather period.

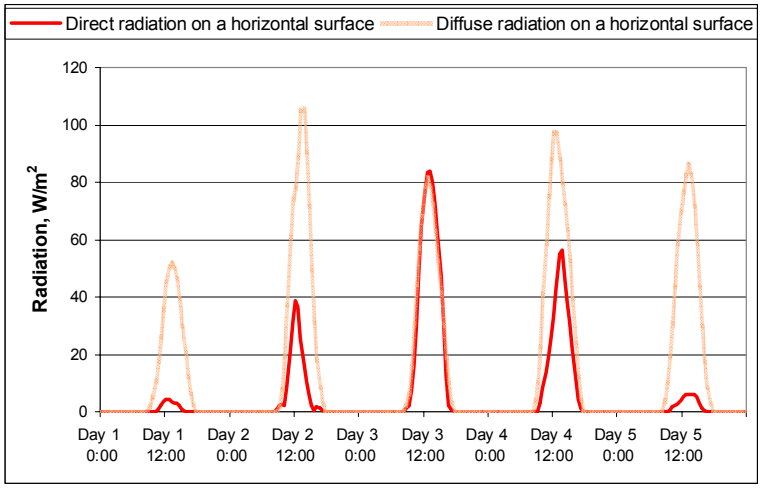

Figure 50. Direct and diffuse solar radiation during the cold weather period.

Figure 51 shows the operative temperature during the cold weather period with alternative structures. Figure 52 shows the mean skin temperatures during the test period with the alternative structures. HTM calculates the mean skin temperature as the average temperature of different body parts. Figure 53 shows the thermal sensation index and Figure 54 the thermal comfort index calculated for all the alternative structures.

Table 31 shows the average values for operative and mean skin temperatures, thermal comfort index and PPD calculated with HTM for all four structure alternatives. In Figure 55 the calculated thermal sensation index of HTM is compared to PMV calculated with Fanger's PMV method. The structure alternatives are: 1) original structures and 2) retrofitted walls with new windows. In Figure 56 the calculated Predicted Percentages of Dissatisfied (PPD) based on the thermal sensation index of HTM is compared to PPD calculated with Fanger's PMV method.

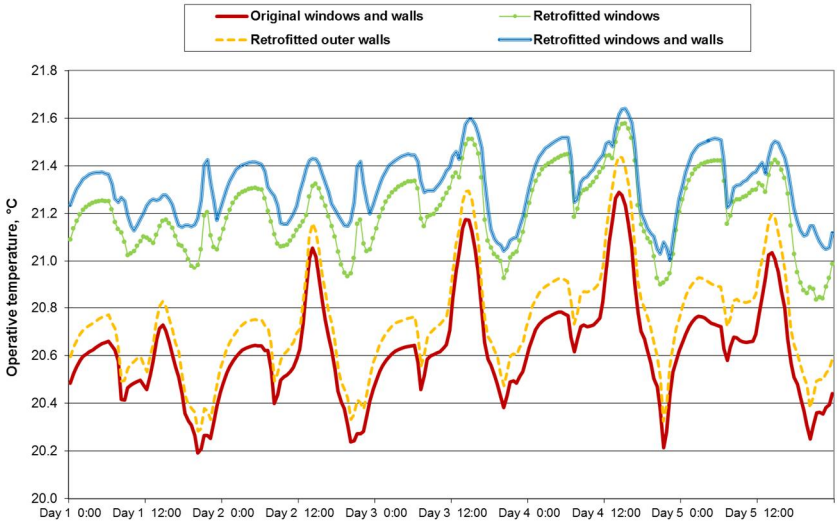

Figure 51. Operative temperature of the living room during the renovation case study, cold weather period.

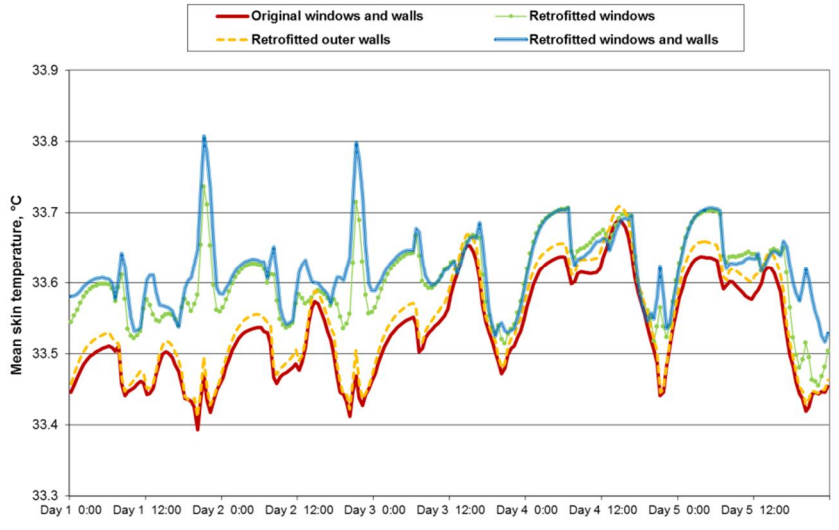

Figure 52. HTM mean skin temperature during the renovation case study, cold weather period.

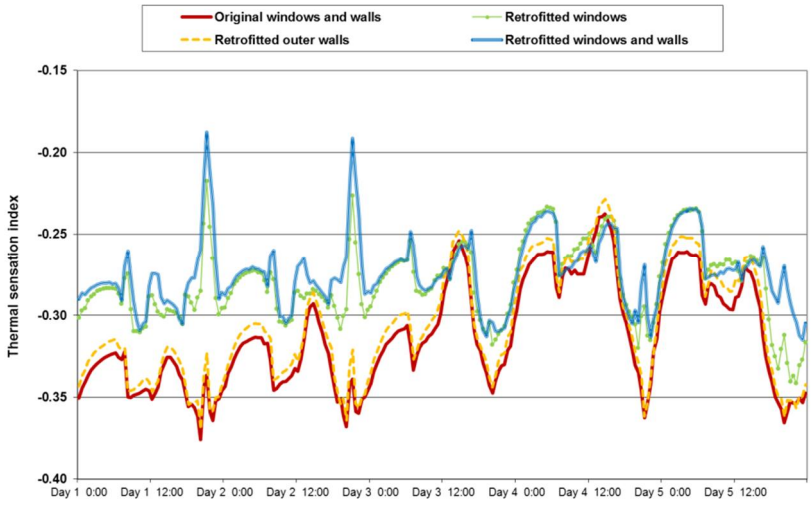

Figure 53. Thermal sensation index during the renovation case study, cold weather period.

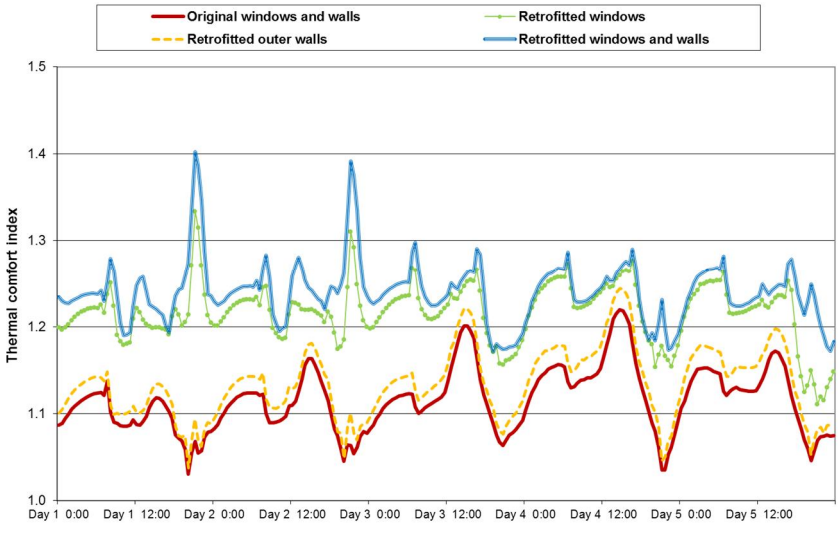

Figure 54. Thermal comfort index during the renovation case study, cold weather period.

Table 31. Average values of operative temperature, mean skin temperature, thermal comfort and predicted percentage of dissatisfied (PPD) with the HTM method during the, cold weather period.

Structure alternative	Average operative temperature, °C	Average mean skin temperature, °C	Average thermal comfort index	Average PPD
Original walls and windows	20.6	32.5	1.12	7.1%
Retrofitted walls and original windows	20.7	32.6	1.13	7.0%
Original walls and retrofitted windows	21.2	32.7	1.22	6.6%
Retrofitted walls and windows	21.3	32.8	1.24	6.6%

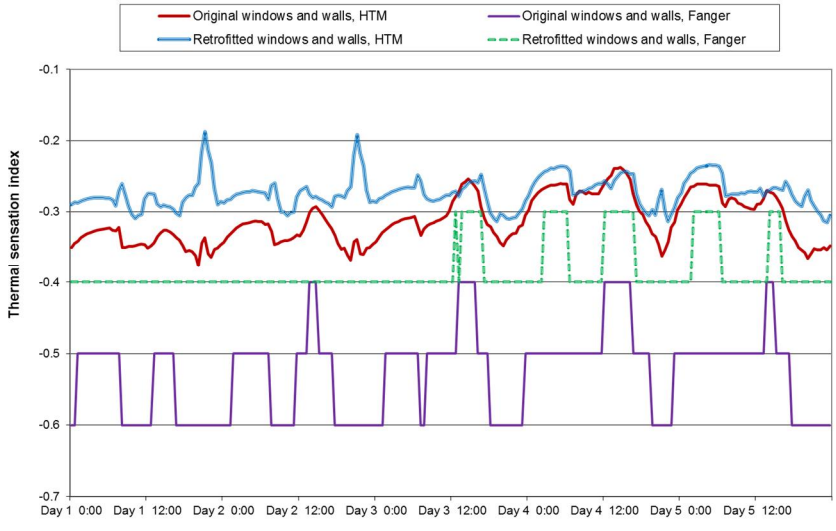

Figure 55. Thermal sensation with original and retrofitted structures calculated with the HTM and Fanger methods, cold weather period.

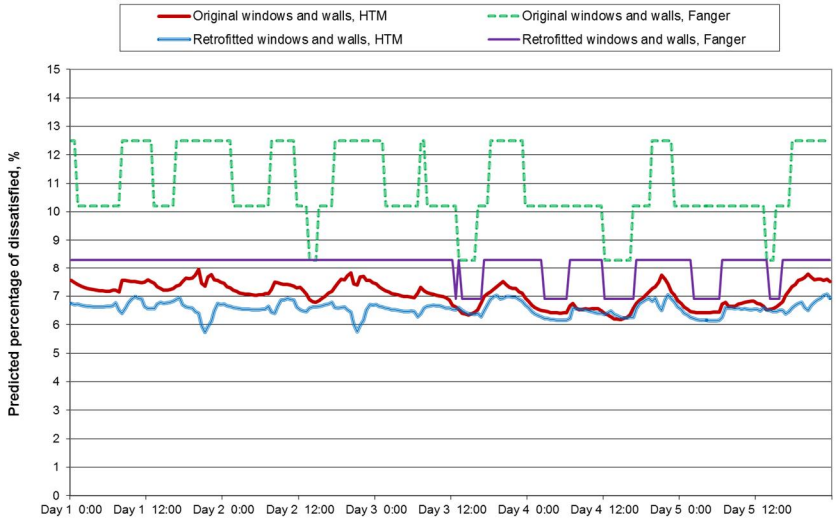

Figure 56. Predicted percentage of dissatisfied with original and retrofitted structures calculated with the HTM and Fanger methods, cold weather period.

The cold weather period results show that improving the thermal resistance of the building structure increases thermal comfort during the heating season. The higher inner surface temperatures of retrofitted walls and new windows increased the operative indoor temperature and mean skin temperatures resulting in a lower variation of the temperature levels inside a living space and a higher thermal comfort index. The effect of retrofitted windows was higher than the effect of retrofitted walls. The combined effect of retrofitted windows and walls was only slightly higher than the effect of just retrofitted windows.

Besides improving indoor conditions, energy renovation decreases the annual heating energy use. Retrofitting walls and installing new windows lowers the annual heating energy demand of the test flat by 38%. Increased indoor surface temperature levels of retrofitted envelope components decrease the draught experienced by the radiation of cold surfaces and increase the operative temperature. Therefore the indoor set point temperature demand with retrofitted structures is lower than with the original structures, which will further decrease the heating energy demand of a retrofitted building.

The effect of increasing the wall insulation level and replacing old windows with more energy-efficient new windows on thermal comfort and annual energy use was simulated for a typical 1970s-level built apartment with alternative renovation solutions. The operative temperature, mean skin temperature, thermal comfort index and predicted percentage of dissatisfied were calculated during a cold and a hot weather period.

6.1.2 Hot weather period

The exemplary transient test period represented a typical hot weather period in Central Finland (22–26 June of the Jyväskylä test year 1979). The outdoor temperature and solar radiation during the test period are presented in Figure 57 and Figure 58.

Figure 59 shows the operative temperature during the hot weather period with alternative structures. Figure 60 shows the mean skin temperatures during the test period, Figure 61 shows the thermal sensation index and Figure 62 shows the thermal comfort index calculated for all the alternative structures.

Table 32 shows the average values for operative and mean skin temperatures, thermal comfort index and PPD calculated with HTM for all four structure alternatives. In Figure 63 the calculated thermal sensation index of HTM is compared to PMV calculated with Fanger's PMV method. The structure alternatives are: 1) original structures and 2) retrofitted walls with new windows. In Figure 64 the calculated Predicted Percentages of Dissatisfied (PPD) based on the thermal sensation index of HTM is compared to PPD calculated with Fanger's PMV method.

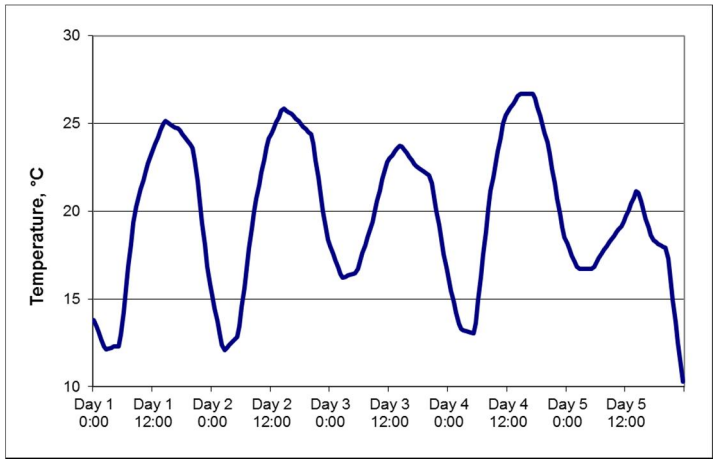

Figure 57. Outdoor temperature during the hot weather period.

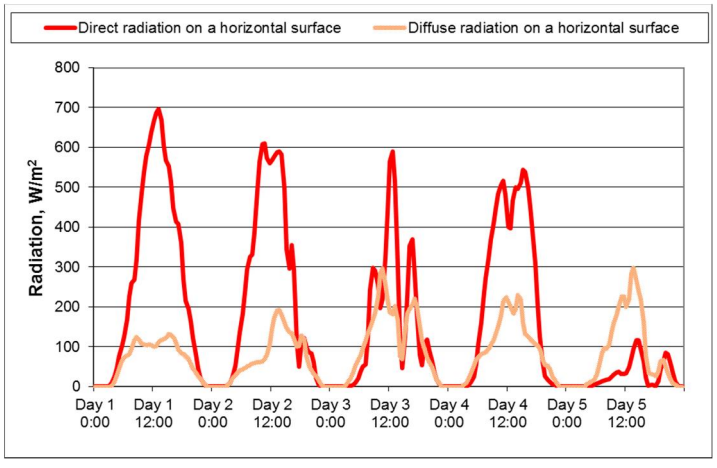

Figure 58. Direct and diffuse solar radiation during the hot weather period.

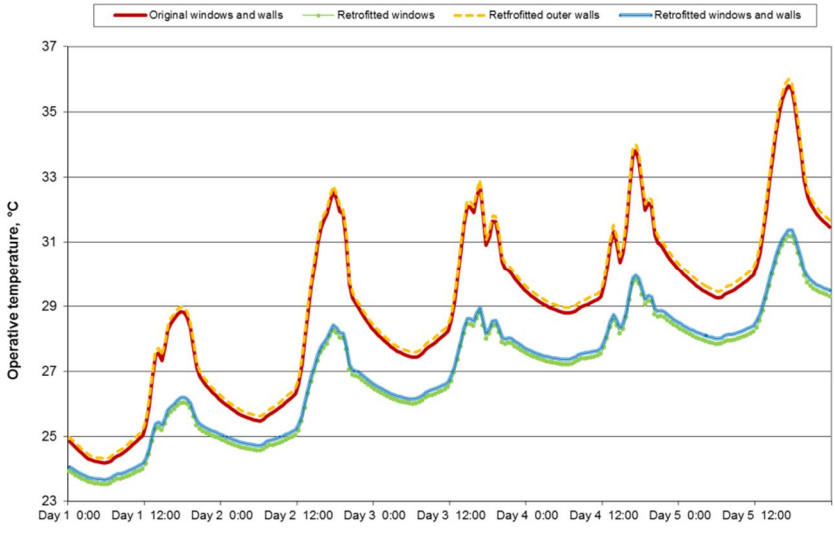

Figure 59. Operative temperature of the living room during the renovation case study, hot weather period.

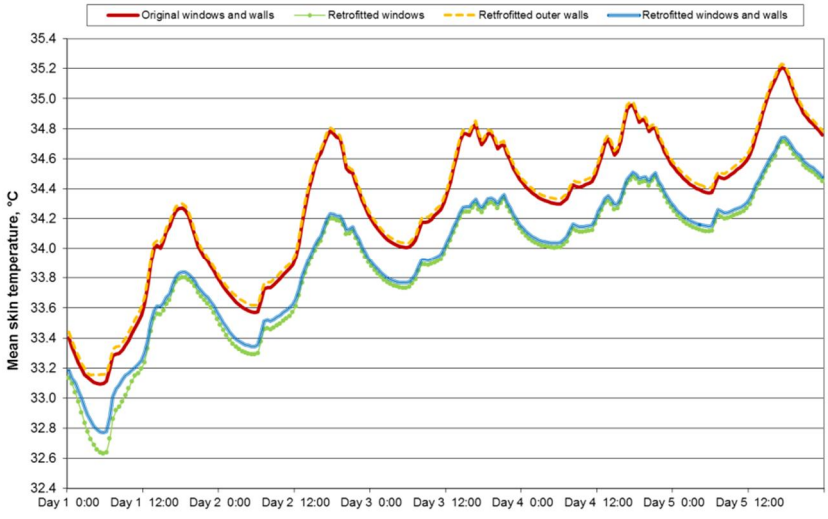

Figure 60. HTM mean skin temperature during the renovation case study, hot weather period.

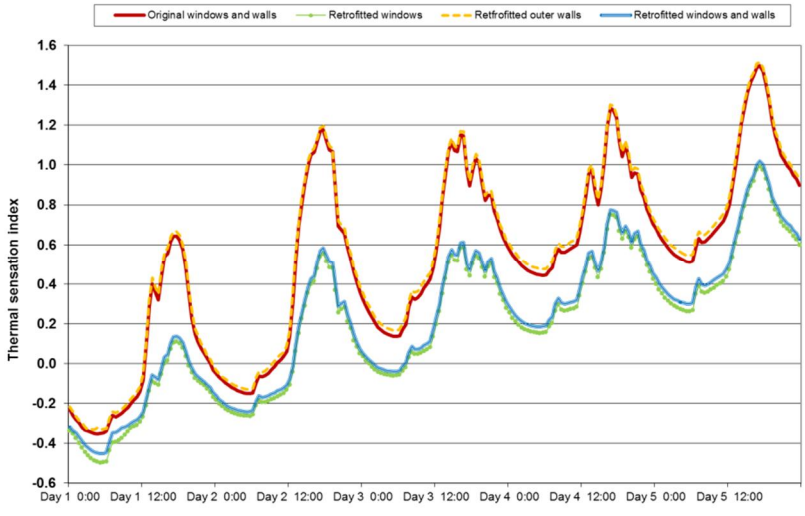

Figure 61. Thermal sensation index during the renovation case study, hot weather period.

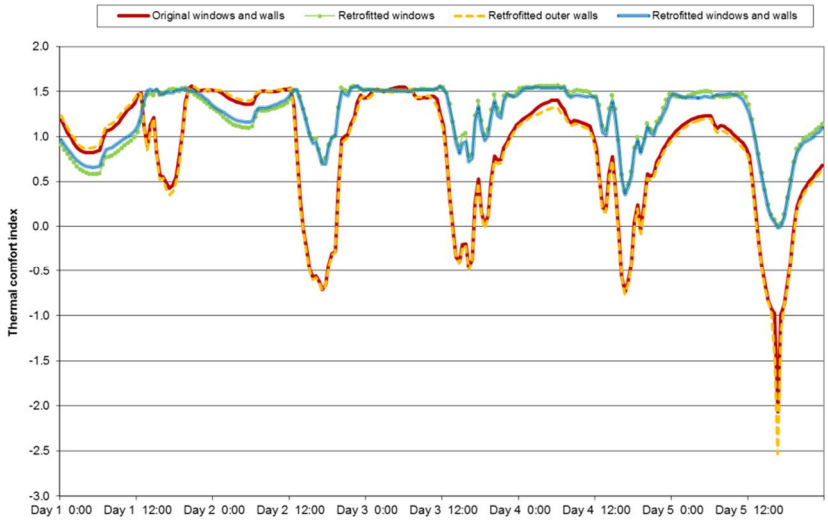

Figure 62. Thermal comfort index during the renovation case study, hot weather period.

Table 32. Average values of operative temperature, mean skin temperature, thermal comfort and predicted percentage of dissatisfied (PPD) with the HTM method during the hot weather period.

Structure alternative	**Average operative temperature, °C**	**Average mean skin temperature, °C**	**Average thermal comfort index**	**Average PPD**
Original walls and windows	28.9	34.3	0.84	15.2%
Retrofitted walls and original windows	29.1	34.3	0.81	15.7%
Original walls and retrofitted windows	26.9	33.9	1.22	8.5%
Retrofitted walls and windows	27.1	34.0	1.21	8.7%

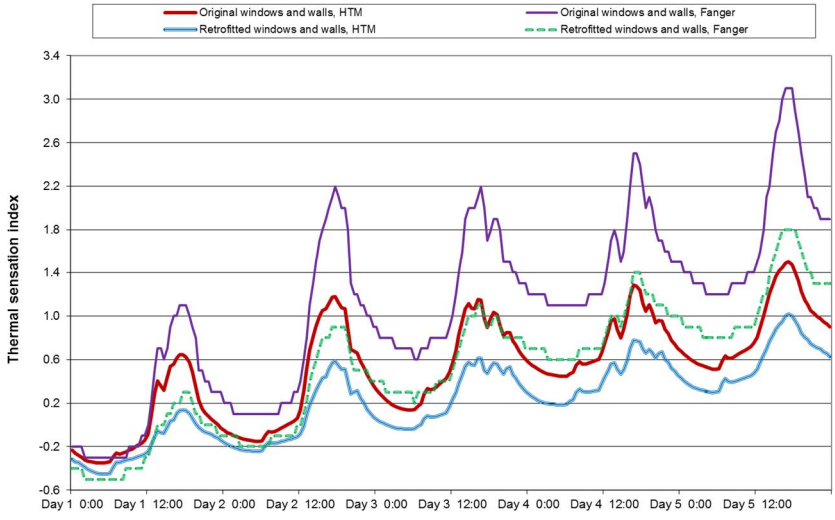

Figure 63. Thermal sensation with original and retrofitted structures calculated with the HTM and Fanger methods, hot weather period.

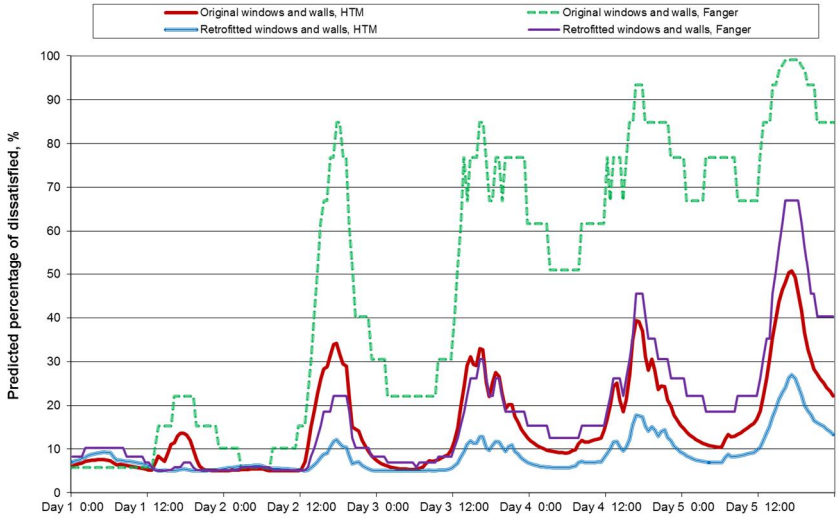

Figure 64. Predicted percentage of dissatisfied with original and retrofitted structures calculated with the HTM and Fanger methods, hot weather period.

The hot weather period results also emphasize the larger effect of window properties on thermal comfort. The highest thermal comfort levels were obtained with

the retrofitted windows whereas the retrofitted walls combined with retrofitted windows slightly lower the thermal comfort by diminishing heat loss through the walls and thus increasing the indoor temperature.

The Predicted Percentages of Dissatisfied (PPD) calculated with Fanger's PMV method were clearly higher than the PPD values with HTM with both weather periods. The results support the findings of Humphreys and Nicol (2002) that Fanger's PMV method progressively over-estimates the mean perceived coolness of a cool environment and hotness of a hot environment.

6.2 Effect of the heating distribution system on thermal sensation and comfort

HTM was utilized in a case study where the effect of different heating distribution systems on thermal sensation and comfort was examined. The reference apartment was the same three-room flat as in the renovation case study (Figure 48). The air exchange system was mechanical supply and exhaust ventilation with heat recovery. The ventilation air flow was 0.037 m^3/s. The supply air flow into the living room was 0.007 m^3/s.

The heating distribution alternatives were

1. ventilation heating
2. radiator heating
3. window heating
4. floor heating.

The HTM was placed in the middle of the living room floor. The indoor set point temperature was 21 °C for the living room. The operative temperature in the living room was calculated during the test periods. The sensor was located above the head of the human thermal model, and it took into account all surface temperatures. The radiator was located under the window. The heating powers of all the heating distribution systems were controlled according to the indoor set point temperature. The simulation was first conducted for a defined base case, then the effects of different boundary conditions on the results were studied.

6.2.1 Base case

In the simulation base case, the wall and window U-values were according to existing Finnish building regulations. The wall U-value was 0.17 W/m^2K, the window U-value was 1.0 W/m^2K and the window g-value was 0.55. The exemplary transient test period represented the same typical cold weather period as in the renovation case study (3–7 February of the Jyväskylä test year 1979). The outdoor temperature and solar radiation during the test period were presented in Figure 49 and Figure 50. The indoor relative humidity was a constant 25%. The clothing insulation level was 0.86 clo (the heavier clothing alternative in Table 26.). The activity level was 1.2 Met representing light activity. The dimensioning

heating power demand of the base case was 480 W for the living room and 1.7 kW for the whole flat (Jyväskylä dimensioning outdoor temperature -32 °C). Operative temperature, mean skin temperature, thermal sensation, thermal comfort and the predicted percentage of dissatisfied (PPD) were simulated with all the heating distribution systems for the base case and four other cases with different boundary conditions:

1. very low-energy structures
2. intermediate test period
3. lighter clothing alternative
4. higher activity level.

Figure 65 shows the operative temperature with alternative heat distribution systems. Figure 66 shows the mean skin temperatures during the test period, Figure 67 shows the thermal sensation index, Figure 68 shows the thermal comfort index and Figure 69 shows the Predicted Percentage of Dissatisfied (PPD) calculated with HTM. Table 36 shows the average values for operative and mean skin temperatures and thermal comfort index calculated with HTM for all heating distribution systems, and Table 34 compares the average values of thermal sensation and predicted percentage of dissatisfied (PPD) simulated with HTM and calculated with Fanger's PMV method.

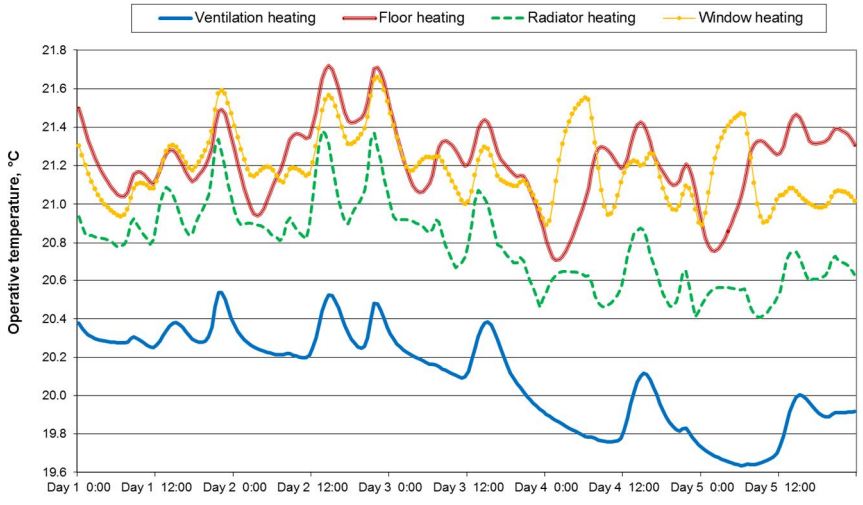

Figure 65. Operative temperature during the test period, base case.

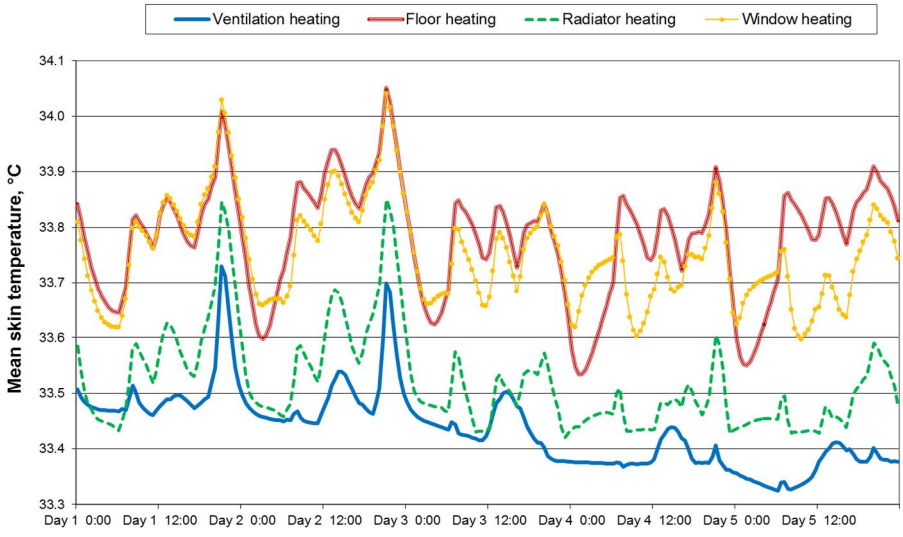

Figure 66. Mean skin temperature during the test period, base case.

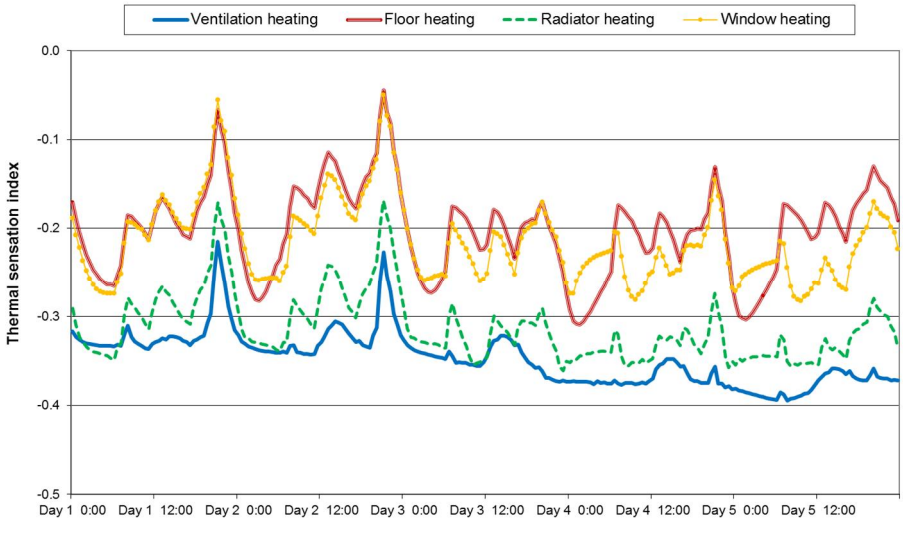

Figure 67. Thermal sensation during the test period, base case.

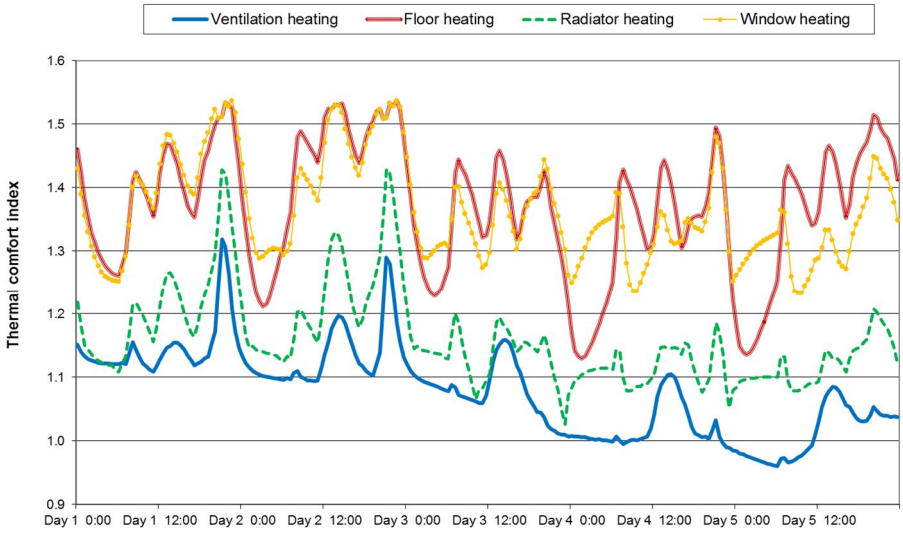

Figure 68. Thermal comfort index during the test period, base case.

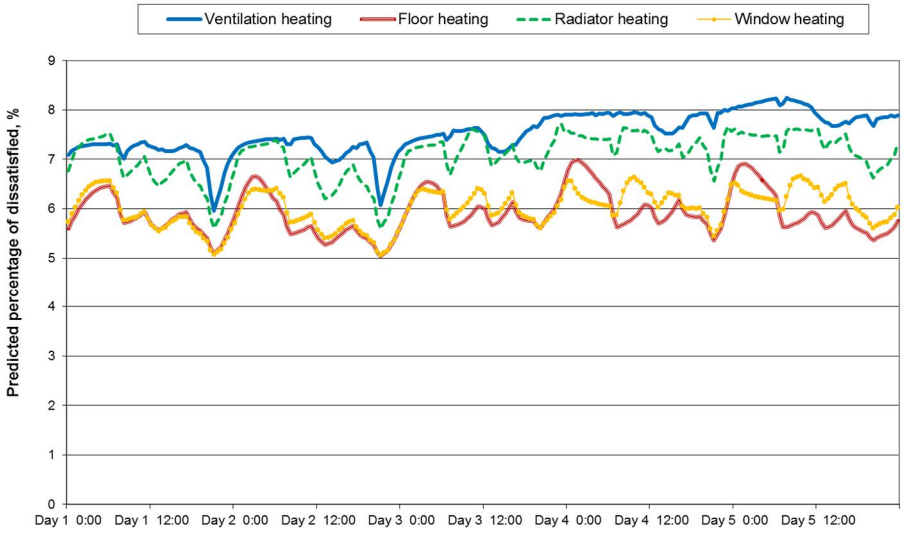

Figure 69. PPD with the HTM method during the test period, base case.

Table 33. Average values of operative temperature, mean skin temperature and thermal comfort, base case.

Heating distribution system	Average operative temperature, °C	Average mean skin temperature, °C	Average thermal comfort index
Ventilation heating	20.1	32.3	1.08
Radiator heating	20.8	32.5	1.16
Window heating	20.9	32.9	1.36
Floor heating	21.2	33.2	1.37

Table 34. Average values of thermal sensation and predicted percentage of dissatisfied (PPD) with HTM and Fanger's PMV method.

Heating distribution system	Average thermal sensation index, HTM	Average thermal sensation index, Fanger	Average PPD with HTM.%	Average PPD with Fanger,%
Ventilation heating	-0.35	-0.66	7.5	12.5
Radiator heating	-0.31	-0.50	7.1	10.2
Window heating	-0.21	-0.45	6.0	9.3
Floor heating	-0.20	-0.41	5.9	6.9

6.2.2 Very low-energy house structures

The effect of the building insulation level on the simulation results was studied by decreasing the U-values of outer walls and windows to very low-energy house levels. The new U-value of the walls was 0.10 W/m^{2}K. The new U-value of the windows was 0.67 W/m^{2}K and glass g-value 0.3. Figure 70 shows the operative temperature with alternative heat distribution systems. Figure 71 shows the mean skin temperatures during the test period, Figure 72 shows the thermal sensation index, Figure 73 shows the thermal comfort index and Figure 74 shows the Predicted Percentage of Dissatisfied (PPD) calculated with HTM. The average values of the results are presented in Table 35.

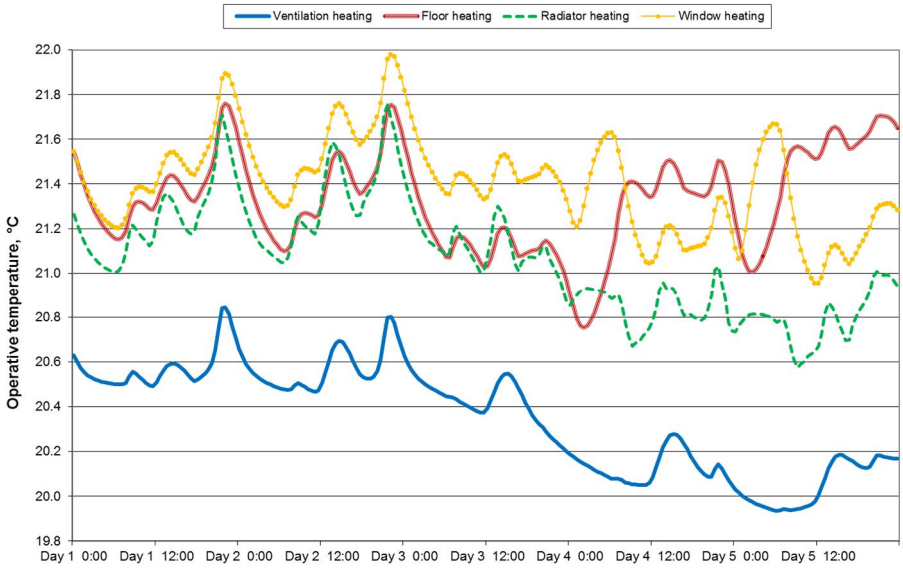

Figure 70. Operative temperature during the test period, very low-energy structures.

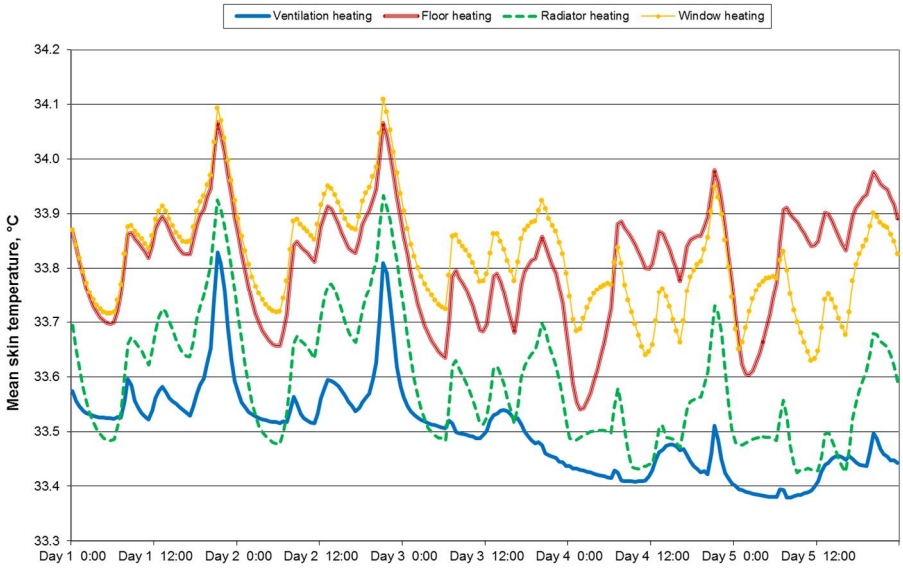

Figure 71. Mean skin temperature during the test period, very low-energy structures.

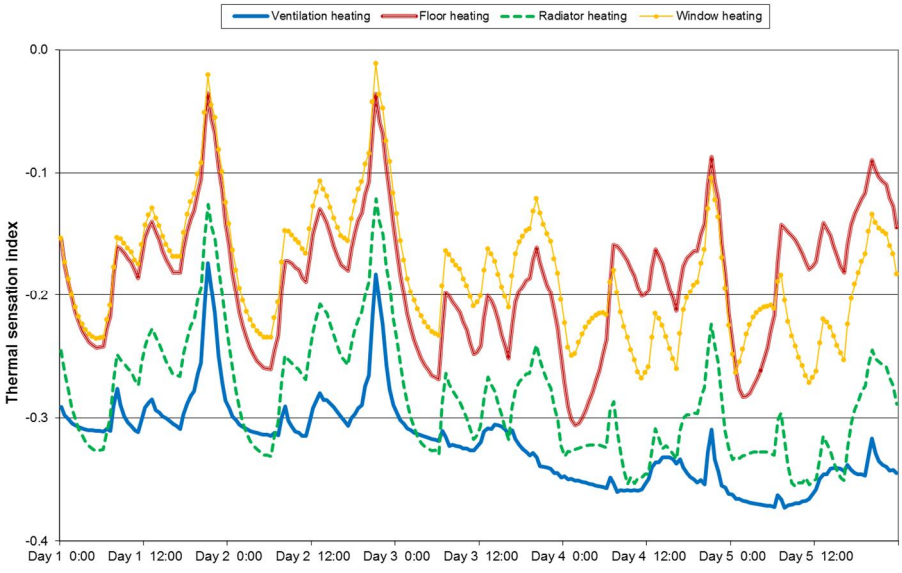

Figure 72. Thermal sensation during the test period, very low-energy structures.

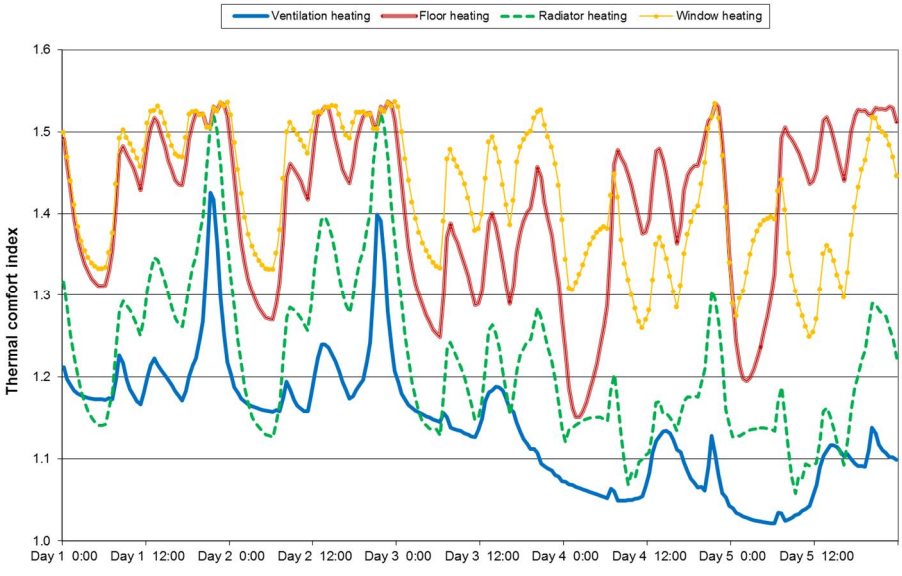

Figure 73. Thermal comfort index during the test period, very low-energy structures.

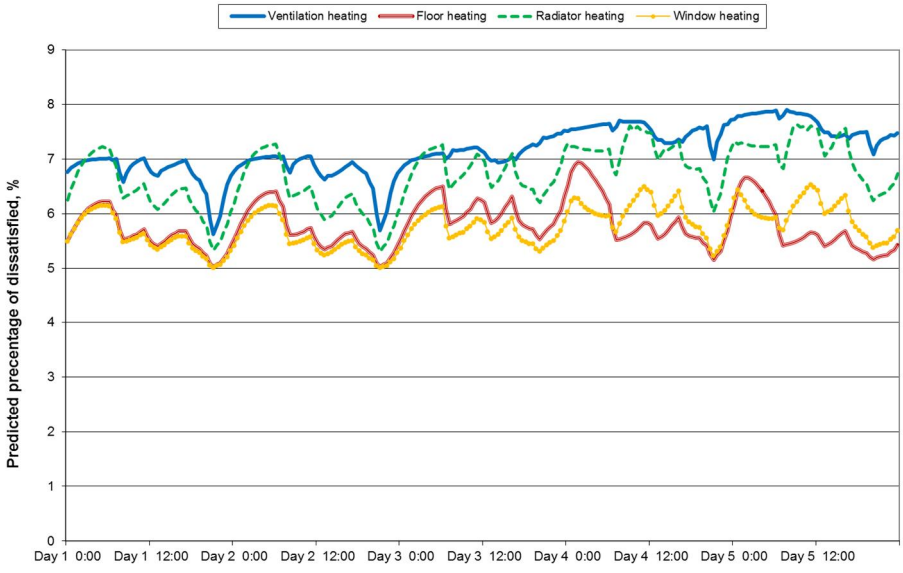

Figure 74. PPD with the HTM method during the test period, very low-energy structures.

Table 35. Average values of operative temperature, mean skin temperature, thermal comfort and predicted percentage of dissatisfied (PPD) with very low-energy structures.

Heating distribution alternative	Average operative temperature, °C	Average mean skin temperature, °C	Average thermal sensation index	Average thermal comfort index	Average PPD,%
Ventilation heating	20.4	33.5	-0.32	1.14	7.2
Radiator heating	21.1	33.6	-0.28	1.22	6.7
Window heating	21.4	33.8	-0.18	1.42	5.7
Floor heating	21.3	33.8	-0.19	1.41	5.8

6.2.3 Intermediate weather period

The effect of the weather conditions on the simulation results was studied by replacing the cold weather period with an intermediate weather period (Figure 75, Figure 76). Figure 77 shows the operative temperature with alternative heat distribution systems. Figure 78 shows the mean skin temperatures during the test

period, Figure 79 shows the thermal sensation index, Figure 80 shows the thermal comfort index and Figure 81 shows the Predicted Percentage of Dissatisfied (PPD) calculated with HTM. The average values of the results are presented in Table 36.

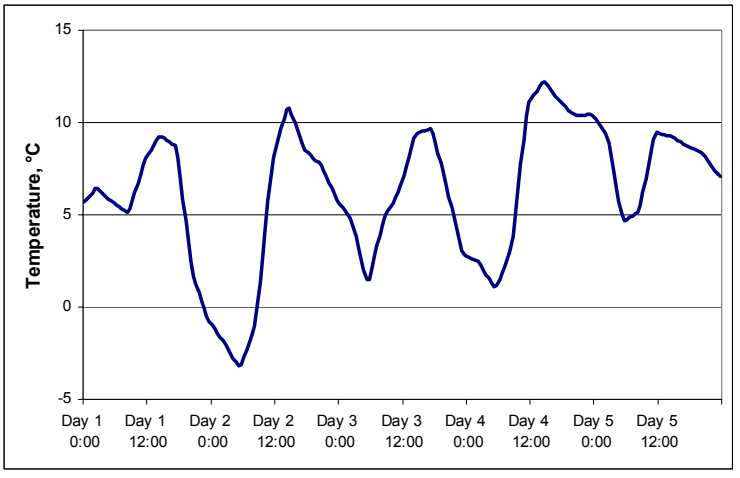

Figure 75. Outdoor temperature during the intermediate test weather period.

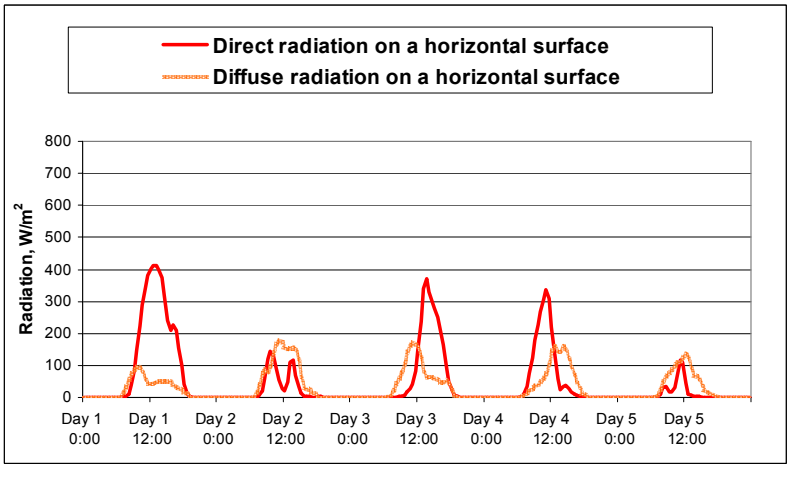

Figure 76. Direct and diffuse solar radiation during the intermediate test weather period.

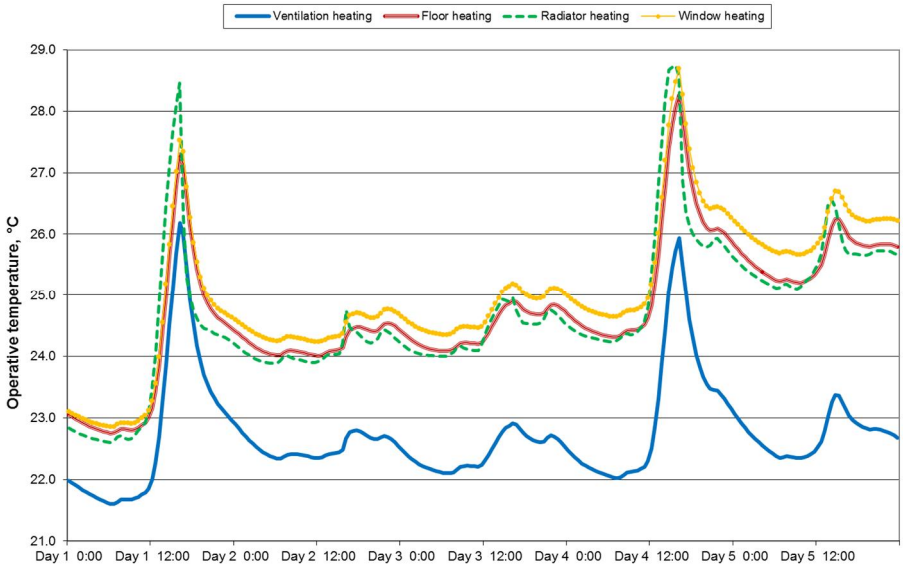

Figure 77. Operative temperature during the test period, intermediate weather period.

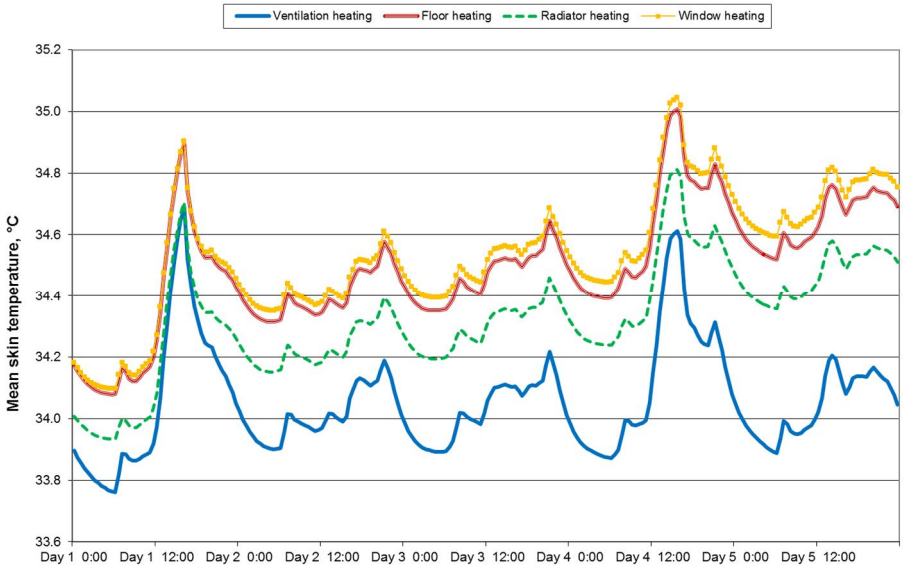

Figure 78. Mean skin temperature during the test period, intermediate weather period.

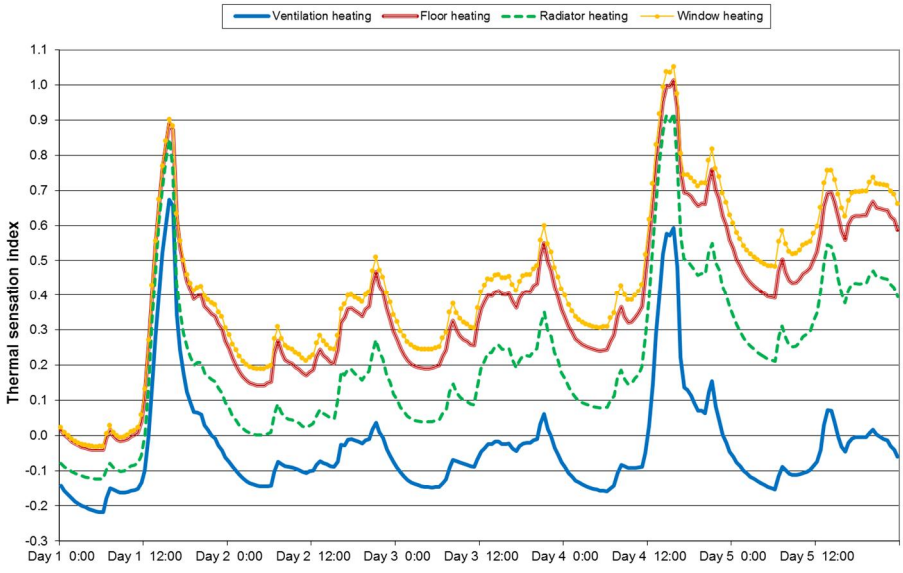

Figure 79. Thermal sensation during the test period, intermediate weather period.

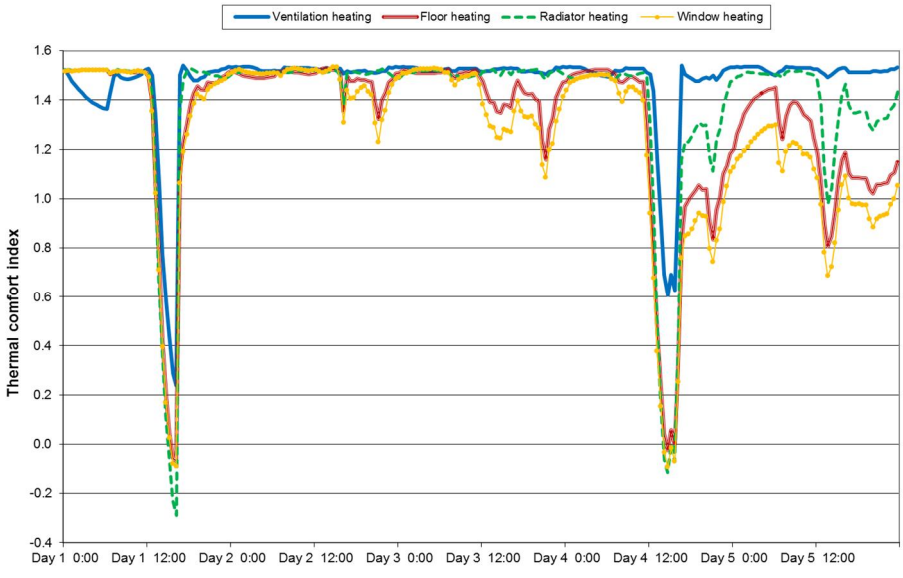

Figure 80. Thermal comfort index during the test period, intermediate weather period.

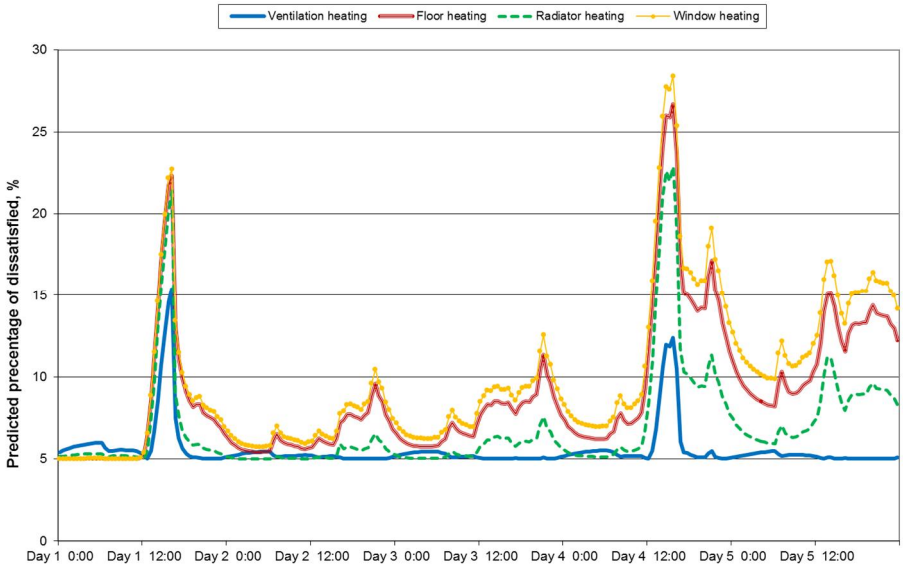

Figure 81. PPD with the HTM method during the test period, intermediate weather period.

Table 36. Average values of operative temperature, mean skin temperature, thermal comfort and PPD with the intermediate test weather period.

Heating distribution alternative	Average operative temperature, °C	Average mean skin temperature, °C	Average thermal sensation index	Average thermal comfort index	Average PPD
Ventilation heating	22.7	34.1	-0.03	1.47	6%
Radiator heating	24.7	34.3	0.21	1.39	7%
Window heating	25.0	34.5	0.42	1.26	7%
Floor heating	24.8	34.5	0.37	1.32	9%

6.2.4 Lighter clothing alternative

The effect of the clothing on the simulation results was studied by decreasing the insulation of the clothing from 0.86 clo to 0.47 clo. The lighter clothing alternative was presented in Table 26. Figure 82 shows the mean skin temperatures during the test period, Figure 83 the thermal sensation index, Figure 84 the thermal comfort index and Figure 85 the PPD. The average values of the simulation results are presented in Table 37.

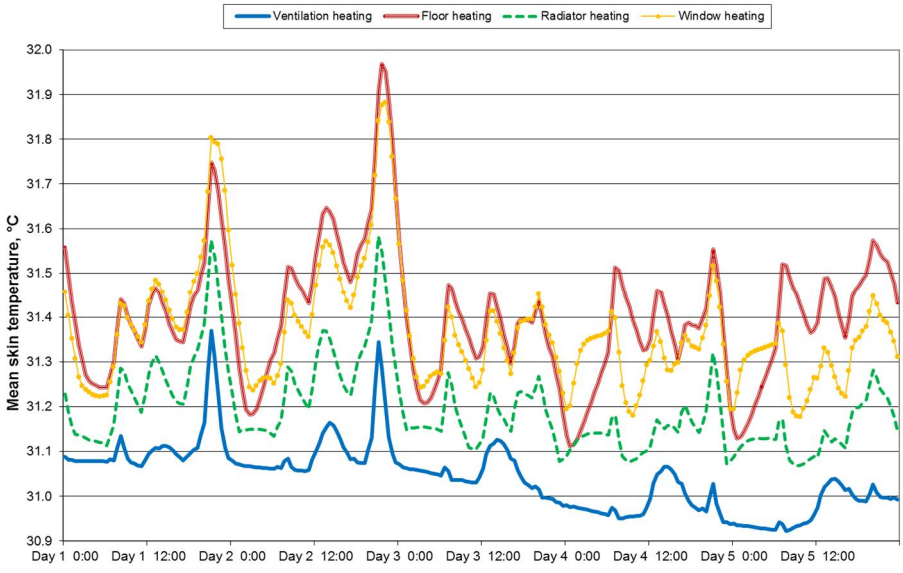

Figure 82. Mean skin temperature during the test period, lighter clothing alternative.

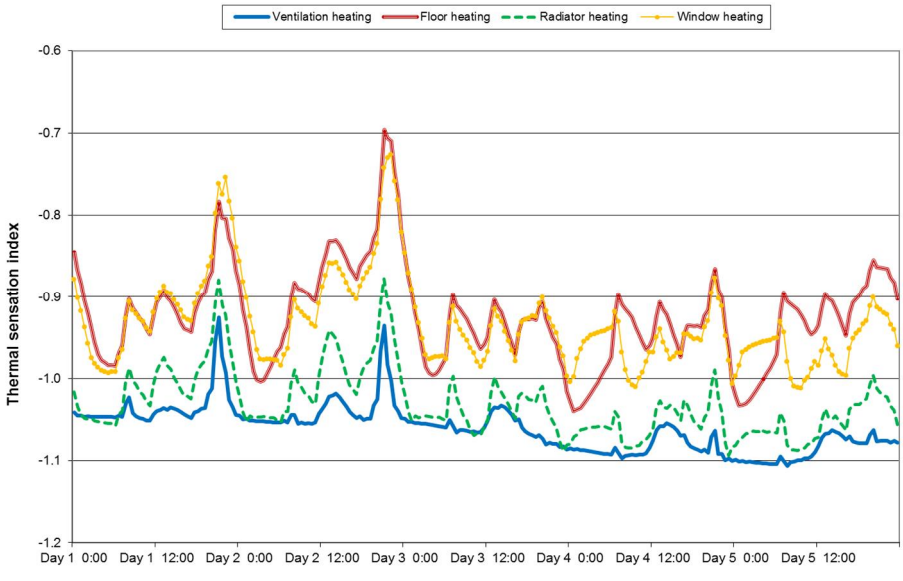

Figure 83. Thermal sensation during the test period, lighter clothing alternative.

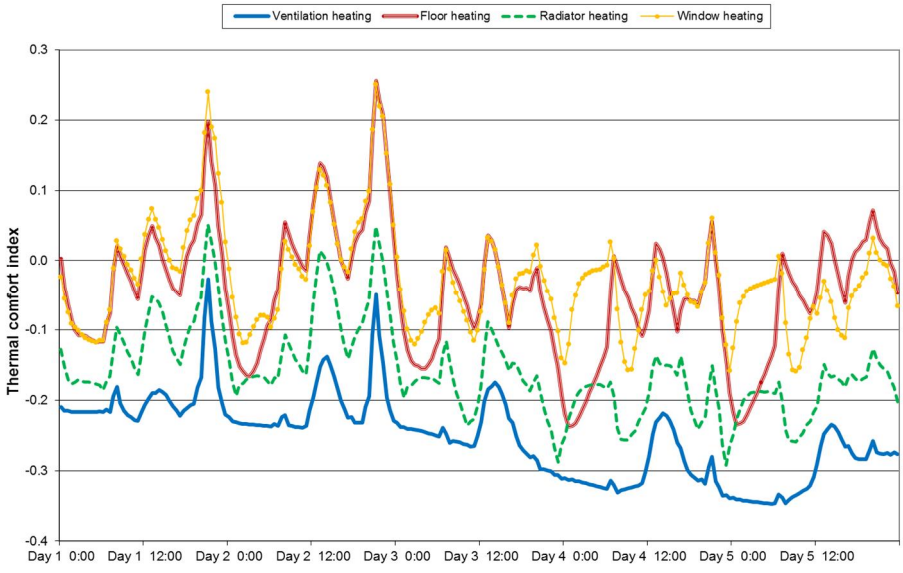

Figure 84. Thermal comfort index during the test period, lighter clothing alternative.

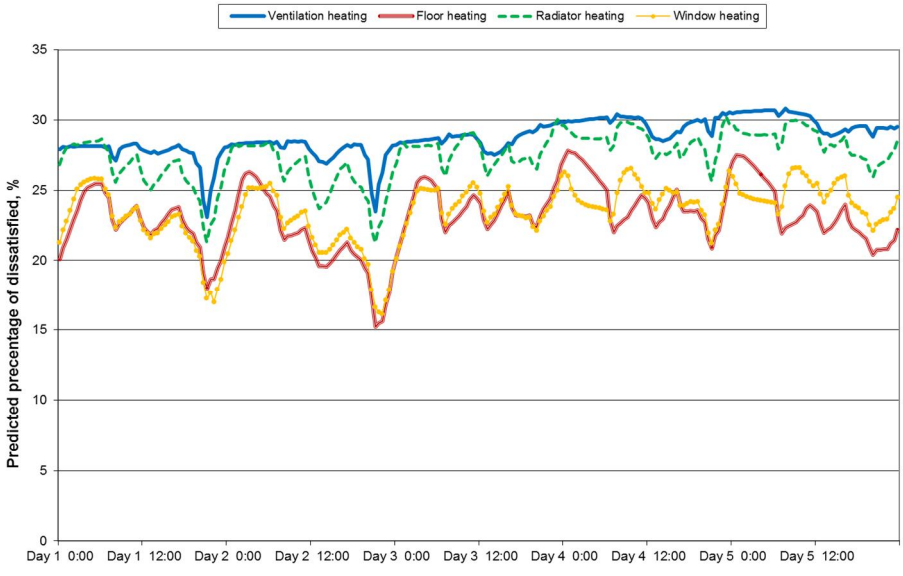

Figure 85. PPD with the HTM method during the test period, lighter clothing alternative.

Table 37. Average values of mean skin temperature, thermal comfort and predicted percentage of dissatisfied (PPD) with a lighter clothing alternative.

Heating distribution alternative	Average mean skin temperature, °C	Average thermal sensation index	Average thermal comfort index	Average PPD,%
Ventilation heating	31.0	-1.06	-0.25	28.8
Radiator heating	31.2	-1.03	-0.16	27.5
Window heating	31.4	-0.93	-0.03	23.4
Floor heating	31.4	-0.92	-0.04	23.1

6.2.5 Lower metabolic rate

The effect of the activity level on the simulation results was studied by decreasing the metabolic rate from 1.2 Met (light activity, e.g. active sitting) to 1.0 Met (sedantary activity, e.g. quiet sitting). Figure 86 shows the mean skin temperatures during the test period, Figure 87 the thermal sensation index, Figure 88 the thermal comfort index and Figure 89 the PPD. The average values of the results are presented in Table 38.

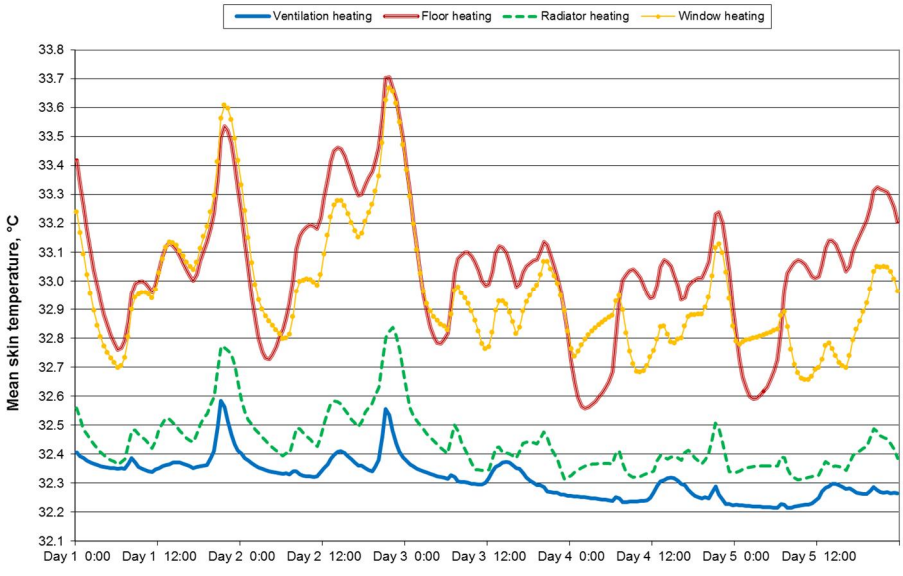

Figure 86. Mean skin temperature during the test period, lower metabolic rate.

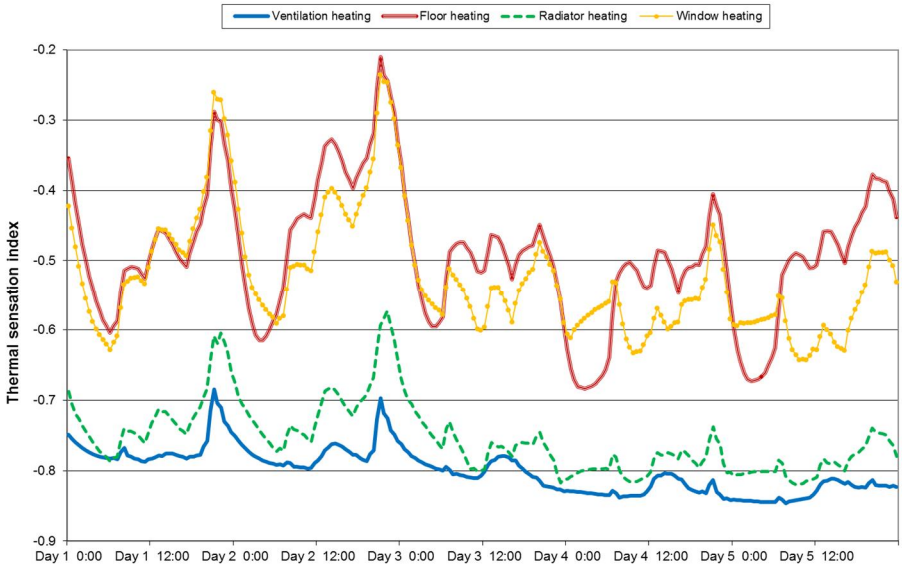

Figure 87. Thermal sensation during the test period, lower metabolic rate.

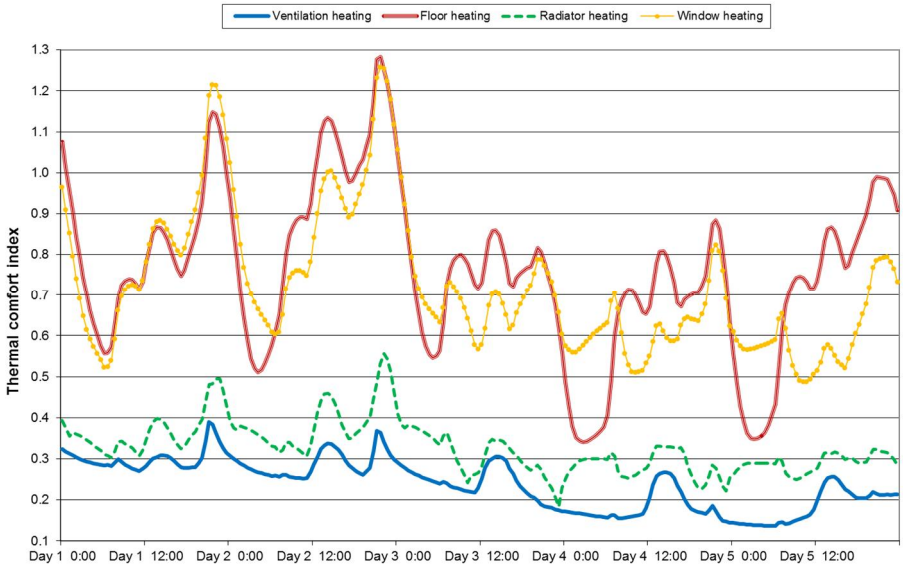

Figure 88. Thermal comfort index during the test period, lower metabolic rate.

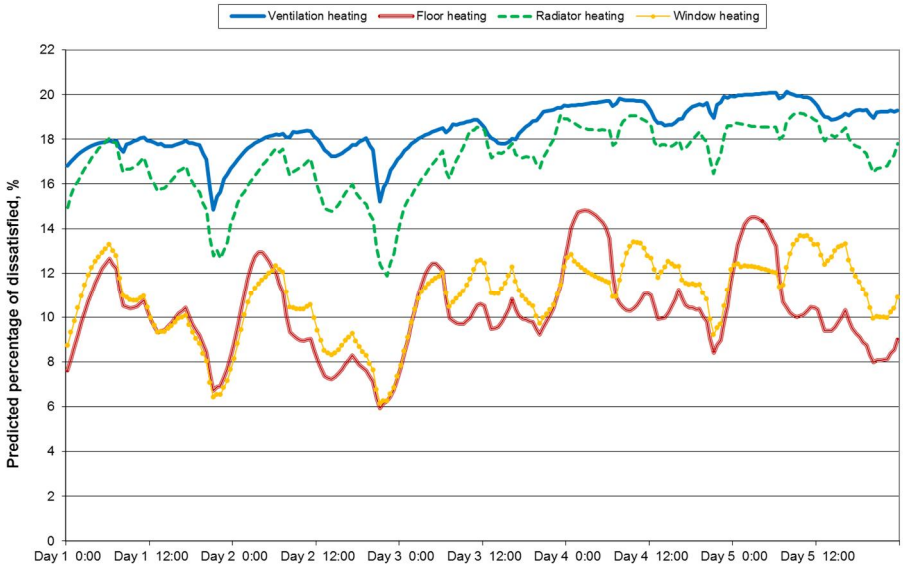

Figure 89. PPD with the HTM method during the test period, lower metabolic rate.

Table 38. Average values of operative temperature, mean skin temperature, thermal comfort and predicted percentage of dissatisfied (PPD) with a decreased activity level.

Heating distribution alternative	Average mean skin temperature, °C	Average thermal sensation index	Average thermal comfort index	Average PPD,%
Ventilation heating	32.3	-0.80	0.24	18.5
Radiator heating	32.4	-0.75	0.33	17.0
Window heating	33.0	-0.52	0.72	10.9
Floor heating	33.0	-0.49	0.76	10.3

6.2.6 Summary

According to the calculation results the variation of alternative heating distribution systems on the thermal comfort index (scale -4 … +4) is between 0.01–0.29 units in the base case. The variation in the Predicted Percentage of Dissatisfied (PPD) is between 0.1–1.6%.

With very low-energy structures, the variance of average thermal comfort between heat distribution systems is between 0.01–0.28 units, with milder outdoor temperatures 0.04–0.21 units, with a lighter clothing alternative 0.01–0.22 units and with a decreased metabolic rate: 0.04–0.52 units.

The overall effect of increasing the insulation level of the building envelope from a level fulfilling the building regulations to a very low-energy building level increases the thermal comfort index only between 0.04–0.06 units. Changing the weather file from a cold weather period to an intermediate weather period increases the thermal comfort index between 0.05–0.39 units. Lowering the clothing insulation level from 0.86 clo to 0.47 clo decreases the thermal comfort index between 1.32–1.41 units. Decreasing the activity level from 1.2 MET to 1.0 MET decreases the thermal comfort index between 0.61–0.84 units.

Clothing level and activity level have the greatest influence on thermal sensation and comfort. The differences between different heating distribution systems are relatively small in all cases. The highest thermal comfort is achieved with the floor heating system, which has the largest heating area. The second highest thermal comfort is with window heating, which prevents the cold radiation through the window. Radiator heating is in third place and the lowest thermal comfort is achieved by ventilation heating, which has no heating area.

7. Discussion

7.1 Main results

In spite of the high number of different developed human thermal models, there are few approaches where a human thermal model has been integrated with a CFD tool and presumably no previous approaches, where the model has been integrated with a building simulation environment. Therefore the major new scientific knowledge of this thesis is combining the human thermal modelling with a thermal sensation and comfort model inside of a building simulation program. This approach enables i) calculating more realistically the interaction and non-uniform transient heat transfer between the skin surface and the surrounding air and building structures and ii) taking into account the effect of human thermoregulation and individual human parameters on thermal sensation and comfort.

The commonly used Fanger's PMV method for thermal sensation and thermal comfort calculation takes into account the average operative temperature as a function of the indoor and average surface temperatures. It does not pay attention to the fact that the surface temperatures vary inside of a room, e.g. during the winter the heating devices are warmer and window surfaces colder than other surfaces. This uneven surface temperature distribution can cause thermal discomfort even though the average surface temperature might be acceptable.

Fanger's PMV method is a heat balance model, which views the human being as a passive recipient of thermal stimuli, assuming that the effects of the surrounding environment are explained only by the physics of heat and mass exchanges between the body and the environment, and neglecting the human thermoregulation system. The HTM method takes into account the human tissue distribution and thermoregulation system in calculation of the skin and core temperatures, their change in time and the resulting local and overall thermal sensation and thermal comfort. Previous research has shown that Fanger's PMV method is valid for everyday prediction of the comfort vote only under severely restricted conditions, because it progressively overestimates the mean perceived warmth of warmer environments and the coolness of cooler environments.

In Chapter 5 the significances of different internal and external boundary conditions on thermal sensation were evaluated with HTM and Fanger's PMV method. The effects of increasing or decreasing all examined internal and external

parameters were larger with the Fanger's PMV method than with the HTM method. The major reason for these results is that the Fanger's PMV method neglects the effect of human thermoregulation on the perceived thermal sensation. Neglecting the effect of human thermoregulation leads to the overestimation of the mean perceived warmth of warmer environments and the coolness of cooler environments. The other reason is that the thermal sensation and comfort method by Zhang (2003), used in the current version of HTM, has been found to sometimes be insensitive to environmental conditions, but mainly in extreme conditions.
Current indoor environment classifications are based on the Fanger's PMV method, which means that they are defined for stationary conditions. The highest indoor environment class is hard to achieve if simultaneously aiming on cost efficiency and highest energy class. The indoor conditions inside of a real building change constantly due to varying heat loads, in example the solar heat load entering the building through window openings. Using Fanger's PMV method at the design stage might therefore, for example, misleadingly indicate that a building would need a cooling system to maintain comfortable indoor conditions in summer. HTM can e.g. be used to simulate more realistically if the cooling system could be replaced by passive cooling methods, such as solar glass, solar shading and phase-change-accumulators.

It would be useful to revise the current indoor environment classification based on a more realistic thermal sensation simulation method, which takes into account also the occupant's ability to adapt in the surrounding environment. HTM could thus be utilized not only for design of specific renovated or new-erected buildings, but also for updating the current indoor quality level classes affecting the whole building mass.

In fulfilling the ambitious energy saving targets for the building sector caused by the EU 20-20-20 targets, the true and realistic occupant thermal comfort must be taken into account in order to ensure the thermal comfort in energy-efficient buildings. The HTM method implemented in a building simulation program minimises sub-optimisation by giving the overall picture of the different parameters affecting the thermal comfort and enables the design of new and refurbished houses with the occupant comfort as a design parameter.

7.2 Future work

This chapter introduces some important features which will be added to the model in the future.

The current version of HTM uses constant body part-specific heat transfer coefficient values, defined by a set of laboratory measurements. The heat transfer coefficients are calculated for a naked skin surface temperature and not for the surface clothing temperature. This overestimates the heat loss through convection. Further development needs will be the addition of a real time calculation of convective heat transfer coefficients by means of a CFD (Computational Fluid Dynamics) calculation.

The current version uses constant basal blood flows in other tissues than the skin tissue, because the activity levels in normal residential use and office work are quite constant and the objective was to keep the model quite simple and rapid to use. The varying blood flows of the muscle tissue will be implemented in the model in the future.

The current version "floats" above the floor. In the following version the interaction between the model and e.g. a chair or floor surface will be added to the model. The effect of the accumulation of moisture in the clothing layer will be studied to estimate its importance in thermal sensation calculation.

The current version uses the thermal sensation and comfort method by Zhang (2003). Zhang has later found that this model sometimes is insensitive to environmental conditions, especially in extreme conditions and modified the overall sensation calculation accordingly (Zhang et al. 2010). The new method by Zhang will be implemented in the following version of HTM.

The pleasant indoor conditions of e.g. kindergartens or schools compared to an elderly home differ significantly from each other. Age, gender, weight, and the amount of muscle and fat tissue have a clear effect on a human being's experiences of thermal sensation and comfort. These phenomena will be taken into account by adding a "body builder" to HTM. The body builder will enable the modification of the model according to age, gender, weight and tissue distribution (fat and muscle).

This thesis presents validation test cases performed in climate chambers. The model validation will be extended to local perceptual responses and responses of building occupants. Also the effect of thermal sensation and comfort on the health and productivity of the building user will be studied in the future.

Even though the current version of the Human Thermal Model, HTM has some restrictions and the planned improvements will further develop the model, the current version has been shown in this thesis to estimate accurately enough the thermal sensation and thermal comfort of the human and the HTM method is a major improvement to the currently used Fanger's PMV model.

8. Conclusions

The aim of this thesis was developing a new multi-node Human Thermal Model (HTM) implemented in a dynamic building simulation environment. The objectives of this thesis were to present the main features of the developed new human thermal model, show its accuracy in calculation of both tissue temperatures, thermal sensation and comfort, estimate the significance of internal and external parameters on thermal sensation and finally show with two realistic case studies how the model can be effectively utilized in estimating more accurately than before the effects of different structures and building service systems on the thermal sensation and comfort of the building user.

This thesis has developed a new method for estimating human thermal sensation and comfort: a Human Thermal Model (HTM) implemented as a module of a dynamical building simulation environment. The validated heat transfer methods of VTT House building simulation environment, reliable estimates of thermal interaction between building structures, building service systems, and occupants have been utilized, which is extremely important when evaluating thermal comfort aspects under different boundary conditions. The thermal sensation and thermal comfort estimation methodology by Zhang is integrated in HTM allowing more detailed thermal sensation and thermal comfort index estimations than the traditional Fanger's PMV methodology.

The main features of HTM consisting of the passive system, the control system and the thermal sensation and thermal comfort calculation have been explained and justified, and the supporting evidence and references have been provided. The accuracy of HTM in calculation of tissue temperatures, thermal sensation and comfort has been proven by means of various steady-state and dynamical test cases also used by other human thermal model developers.

A dynamical test case by Munir (2009) with temperature step changes of ±10 °C was used to compare three different skin blood flow models suggested by Stolwijk (Munir et al. 2009), Smith (Smith 1991) and Fiala (Fiala 1999). The best correlation with measured values was achieved with the Fiala basal skin blood flow model, which was selected to be used within the Human Thermal Model.

Two other dynamical test cases were used to validate the tissue temperature calculation of the whole human thermal model with connected body parts, metabolism and blood circulation:

(i) a severe hot exposure test with the maximum temperature step change of +18 °C by Hardy & Stolwijk (1966) and

(ii) a severe cold exposure test with the maximum temperature step change of -26 °C by Hardy & Stolwijk (1966).

To validate the thermal sensation and comfort simulation of HTM, three different test cases were used: steady state thermal sensation in different ambient temperatures by Nevins (1966), thermal sensation and comfort responses to a sudden temperature change by Gagge (1967) and thermal sensation response to different metabolism levels by McNall (1967). The test results show a good correlation between measurements and simulated values by HTM. The overall conclusion of the validation tests is that HTM is a reliable and suitable tool for the estimation of thermal sensation and comfort.

The boundary conditions for a good thermal comfort were estimated by studying the effects of different internal and external parameters on thermal sensation. According to simulation results the operative temperature, metabolic rate and clothing are most dominant boundary conditions for the thermal sensation. The operative temperature sets clear boundaries for combinations of clothing and metabolic rate when aiming for thermal neutrality of a human.

The ability of the HTM method to estimate the interaction of alternative building structures, building service systems and individual human parameters (e.g., metabolic rate and clothing) on occupants was highlighted by means of two realistic case studies: effect of different structure alternatives and effect of different heat distribution methods on thermal sensation and comfort. The case studies presented how the HTM method can show the quantitative differences on thermal sensation and comfort with different structural and building service system alternatives, and the various utilization possibilities of HTM in designing buildings with a high thermal comfort level.

The calculation results of the renovation case showed how improving the thermal resistance of the building structure to a very low-energy level increases thermal comfort. During the heating season the higher inner surface temperatures of retrofitted walls and new windows increased the operative indoor temperature and mean skin temperatures resulting in a lower variation of the temperature levels inside a living space and a higher thermal comfort index. During a hot season the highest thermal comfort levels were obtained with the retrofitted windows whereas the retrofitted walls combined with retrofitted windows slightly lowered the thermal comfort level by diminishing heat loss through the walls and thus increasing the indoor temperature. With both weather periods the Predicted Percentages of Dissatisfied (PPD) calculated with Fanger's PMV method were clearly higher than the PPD values calculated with HTM method.

The effect of different heating distribution systems on thermal sensation and comfort and the impact of varying different boundary conditions were examined with HTM. The overall conclusions of the test case were that the clothing and activity levels have the greatest influence on thermal sensation and comfort. Very low-energy structures increased the thermal comfort only slightly when compared to

2010 level structures. The differences between different heating distribution systems were relatively small in all cases. The highest thermal comfort was achieved with the floor heating system, which has the largest heating area. The second highest thermal comfort was with window heating, which prevents the cold radiation through the window. Radiator heating was in third place and the lowest thermal comfort was achieved by ventilation heating, which has no heating area.

References

Alahmer et al. 2011. Vehicular thermal comfort models; a comprehensive review. *Applied Thermal Engineering,* Vol. 31, pp. 995–1002.

ASHRAE 1993. American Society of Heating, Refrigerating and Air-Conditioning Engineers, Physiological principles and thermal comfort, ASHRAE Handbook Fundamentals, ASHRAE, Atlanta, USA, pp. 8.1–8.32.

ASHRAE 2004. American Society of Heating, Refrigerating and Air-Conditioning Engineers, Standard 55P Thermal Environmental Conditions for Human Occupancy, ASHRAE, Atlanta, USA.

Avolio, A.P. 1980. Multi-branched model of the human model arterial system. Med. & Biol. Eng. & Comput., Vol. 18, pp. 709–718.

COM 2008. Summary of the Impact Assessment. Communication Staff Working Document, Accompanying Document to the Proposal for a Recast of the Energy Performance of Buildings Directive (2002/91/EC); COM(2008) 755/SEC(2008) 2821. Commission of the European Communities. Brussels, Belgium.

Crosbie, R.J., Hardy, J.D. and Fessenden, E. 1963. Electrical analog simulation of temperature regulation in man. Temperature – its Measurement and Control in Science and Industry, Vol. 3 (3), pp. 627–635.

deDear, R.J., Arens, E., Hui, Z., and Oguro, M. 1997. Convective and radiative heat transfer coefficients for individual human body segments, *International Journal of Biometeorology,* Vol. 40, pp. 141–156.

deDear, R.J. 1998. A global database of thermal comfort field experiments. Field studies of thermal comfort and adaptation. ASHRAE Technical Data Bulletin 14 (1) pp. 15–26.; *ASHRAE Transactions*, Vol. 104 (1). ASHRAE, Atlanta, USA.

European Communities 2008. EU Energy and Transport in Figures 2008. Statistical Pocket Book 2007/2008. Brussels, Belgium.

Fanger, P. O. 1970. Thermal Comfort. McGraw-Hill, New York, USA.

Ferreira, M. S. and Yanagihara, J. I. 2009. A transient three-dimensional heat transfer model of the human body, *International Communications in Heat and Mass Transfer*, Vol. 36, pp. 718–724.

Fiala, D. 1999. A computer model of Human Thermoregulation for a Wide Range of Environmental Conditions, The American Physiological Society, 8750–7587, p. 1957.

Fiala, D. et al. 2001. Computer prediction of human thermoregulatory and temperature response to a wide range of environmental conditions, *International Journal of Biometeorology,* Vol. 45, pp. 143–159.

Fiala, D., Lomas, K. and Stohrer, M. 2003. First Principles Modeling of Thermal Sensation Responses in Steady-State and Transient Conditions. *ASHRAE Transactions*, Vol. 109, pp. 179–186.

Foda, E. and Sirén, K. 2011. A new approach using the Pierce two-node model for different body parts. *International Journal of Biometeorology*, Vol. 55, pp. 519-532.

Foda, E., Almesri, I., Hazim, B. and Sirén, K. 2011. Models of human thermoregulation and the prediction of local and overall thermal sensations. *Building and environment*, Vol. 46, pp. 2023–2032.

Fu, G. 1995. A Transient, 3-D Mathematical Thermal Model for the Clothed Human, Doctoral Dissertation, Kansas State University, USA.

Gagge, A.P., Stolwijk, J.A.J. and Hardy, J.D. 1967. Comfort and thermal sensation and associated physiological responses at various ambient temperatures. *Environmental Research*, Vol. 1, pp. 1–20.

Gagge, A.P., Stolwijk, J.A.J. et al. 1971. An effective temperature scale based on a simple model of human physiological regulator response. *ASHRAE Transactions*, Vol. 77 (1), pp. 247–262.

Gagge, A.P., Fobelets, A.P. and Berglund, L.G. 1986. A Standard Predictive Index of Human Response to the Thermal Environment. *ASHRAE Transactions*, Vol. 92, pp. 709–731.

Hardy, J. D. and Stolwijk, J. A. J. 1966. Partitional calorimetric studies of man during exposures to thermal transients, *Journal of Applied Physiology,* Vol. 21, pp. 1799–1806.

Hensel, H. 1981. Thermoreception and temperature regulation. Academic Press Inc. London, UK.

Hensen, J. 1991. On the thermal interaction of building structure and heating and ventilation system. Doctoral Dissertation, Technische Universiteit Eindhoven, The Netherlands.

Huang, J. 2006. Thermal parameters for assessing thermal properties of clothing. *Journal of Thermal Biology*, Vol. 31, pp. 461–466.

Huizenga, C., Hui, Z. and Arens, E. 2001. A model of human physiology and comfort for assessing complex thermal environments. *Building and Environment,* Vol. 36, pp. 691–699.

Humphreys, M.A. 2000. In Proceedings of the World Renewable Energy Congress on the Recent Progress in the Adaptive Approach to Thermal Comfort, Brighton, UK, pp. 438–443.

Humphreys, M.A. and Nicol, J.F. 2000. Effects of measurement and formulation error on thermal comfort indices in the ASHRAE database of field studies. *ASHRAE Transactions*, Vol. 106 (2), pp. 493–502.

Humphreys, M.A. and Nicol, J.F. 2002. The validity of ISO-PMV for predicting comfort votes in every-day thermal environments. *Energy and Buildings,* Vol. 34, pp. 667–684.

IPCC 2001. Climate Change 2001: Mitigation; Third Assessment Report, Working Group III. Intergovernmental Panel on Climate Change (IPCC). New York, NY, USA.

ISO 2005. ‘‘Ergonomics of the thermal environment – Analytical determination and interpretation of thermal comfort using calculation of the PMV and PPD indices and local thermal comfort criteria’’ International Standard ISO 7730, International Organisation for Standardization.

Itard, L. and Meijer, F. 2009. Towards a Sustainable Northern European Housing Stock: Figures, Facts and Future. IOS Press. Amsterdam, The Netherlands.

Jones, B.W. and Ogawa, Y. 1992. Transient interaction between the human and the thermal environment. *ASHRAE Transactions*, Vol. 98 (1), pp. 189–195.

Lotens, W.A. 1993. Heat transfer from humans wearing clothing, Doctoral Dissertation, Technische Universiteit Delft, the Netherlands.

Mall, G. and Eisenmerger, W. 2005. Estimation of time since death by heat-flow Finite-Element model. Part I: method, model, calibration and validation. *Legal Medicine*, Vol. 7, pp. 1–14.

Marken Lichtenbelt, W.D.v., Frijns, A.J.H., Fiala, D., Janssen, F.E.M., Ooijen, A.M.J.v. and Steenhoven, A.A.v. 2004. Effect of individual characteristics on a mathematical model of human thermoregulation. *Journal of Thermal Biology*, Vol. 29, pp. 577–581.

Marshall, T.K. and Hoare, F.E. 1962. Estimating the time of death – Parts 1, 2 and 3. *Journal of Forensic Sciences*, Vol. 7, pp. 56–81, 189–210 and 211–217.

McGullough, E.A. and Jones, B.W. 1984. A comprehensive data base for estimating clothing insulation. IER Technical Report 84–01, ASHRAE 411-RP. Kansas, USA.

McNall, P.E. et al. 1967. Thermal comfort (thermally neutral) conditions for three levels of activity. *ASHRAE Transactions*, Vol. 73 (1), pp. I.3.1–I.3.14.

Munir, A., Takada, S. and Matsushita, T. 2009. Re-evaluation of Stolwijk's 25-node human thermal model under thermal-transient conditions: Prediction of skin temperature in low-activity conditions. *Building and Environment*, Vol. 44, pp. 1777–1787.

Nevins, R.G. et al. 1966. Temperature-humidity chart for thermal comfort of seated persons. *ASHRAE Transactions*, Vol. 72, pp. 283–291.

Nilsson, H. 2005. PMV calculation tool. University of Gävle. Internet page: www.dftunipd.org/assets/files/PMVcalc_v2_English.xls (23.5.2012)

Prilutsky, B.I. and Gregor, R.J. 2001. Swing- and support-related muscle actions differentially trigger human walk–run and run–walk transitions. *The Journal of Experimental Biology* 204, pp. 2277–2287.

Rugh, J.P., Farrington, R.B., Bharathan, D., Vhalinos, A., Burke, R., Huizenga, C. and Zhang, H. 2004. Predicting human thermal comfort in a transient nonuniform thermal environment. *European Journal of Applied Physiology*, Vol. 92, pp. 721–727.

Salloum, M., Ghaddar N. and Ghali, K. 2007. A new transient bioheat model of the human body and its integration to clothing model. *International Journal of Thermal Sciences,* Vol. 46, pp. 371–384.

Salloum, M., Ghaddar N. and Ghali, K. 2007. A new transient bioheat model of the human body and its integration to clothing model. *International Journal of Thermal Sciences,* Vol. 46, pp. 371–384.

Seppänen, O., Fisk, W. and Mendell, M. 1999. Association of ventilation rates and CO2-concentrations with health and other human responses in commercial and institutional buildings. *Indoor Air*, Vol. 9, pp. 226–252.

Seppänen, O., Fisk, W.J. and Lei, Q.H. 2006. Effect of temperature on task performance in office environment. Lawrence Berkeley National Laboratory.

Shitzer, A. and Eberhart, R.C. 1985 (Eds.). Heat transfer in medicine and biology–analysis and applications. Plenum Press, New York, USA. pp. 261–324.

Smith, C. 1991. A Transient, Three-Dimensional Model of the Human Thermal System. Doctoral Dissertation, Kansas State University, USA.

Stolwijk, J. A. J. and Hardy, J. D. 1966. Partitional calorimetric studies of responses of man to thermal transients. *Journal of Applied Physiology* Vol. 21, pp. 967–977.

Stolwijk, J.A.J. 1971. A mathematical model of physiological temperature regulation in man. NASA-Langley, CR-1855.

Stolwijk, J.A.J. 1977. Control of body temperature. Handbook of Physiology-Reaction to Environmental Agents, pp. 45–67.

Tuomaala, P. and Piira, K. 2000. Thermal radiation in a room: an improved progressive refinement method. *Building Service Engineering and Technology*, Vol. 21, pp. 9–17.

Tuomaala, P. 2002. Implementation and evaluation of air flow and heat transfer routines for building simulation tools, Doctoral Dissertation, VTT Publications 471, Espoo, Finland. 45 p. + app. 52 p. http://www.vtt.fi/inf/pdf/publications/2002/P471.pdf

Tuomaala, P., Simonson, C. and Piira, K. 2002. Validation of Coupled Airflow and Heat Transfer Routines in a Building Simulation Tool. *ASHRAE Transactions*, Vol. 108, pp. 435–449.

Wargocki, P., Wyon, D.P., Sundell, J., Clausen, G. and Fanger, P.O. 2000. The effects of outdoor air supply rate in an office on perceived air quality, Sick Building Syndrome (SBS) symptoms and productivity. *Indoor Air*, Vol. 10, pp. 222–236.

Wissler, E.H. 1964. A Mathematical Model of the Human Thermal System, *Bulletin of Mathematical Biophysics*, Vol. 62, pp. 66–78.

Wissler, E.H. 1985. Mathematical simulation of human thermal behaviour using whole-body models, Plenum Press, New York.

Wissler, E.H. 1988. A review of human thermal models. Environmental Ergonomics. Taylor & Franics, London. pp. 267–285.

Zhang, H. 2003. Human Thermal Sensation and Comfort in Transient and Non-Uniform Thermal Environments Hensen 1991, University of California, Berkeley, USA.

Zhang, H., Arens, E., Huizenga, C and Han, T. 2010. Thermal sensation and comfort models for non–uniform and transient environments, part III: Whole-body sensation and comfort. *Building and Environment*, Vol. 45, pp. 399–410.

Series title and number
VTT Science 23

Title	**A human thermal model for improved thermal comfort**
Author(s)	Riikka Holopainen
Abstract	Energy efficient very low-energy houses, passive houses and nearly zero-energy houses have a significantly lower heating power demand than traditional buildings. Therefore, the typical design and dimensioning criteria of conventional structural and building service system concepts need to be verified to avoid problems concerning the thermal sensation and comfort of the building users. Fanger's PMV-method is traditionally used for estimating thermal sensation and comfort. The PMV method does not take into account the human thermoregulatory system, therefore it progressively over-estimates the mean perceived warmth of warmer environments and the coolness of cooler environments. Human thermal models represent the human body from a thermokinetic point of view and they have been used for modelling the thermoregulation system. This thesis presents the first approach, where a human thermal model is implemented in a building simulation environment: the Human Thermal Model (HTM). HTM can be used for predicting thermal behaviour of the human body under both steady-state and transient indoor environment conditions. It is based on true anatomy and physiology of the human body. The connection with the building simulation environment enables defining the external boundary conditions such as surface temperatures and radiation heat transfer more accurately than with the previous human thermal models. HTM tissue heat transfer, thermal sensation and thermal comfort calculation has been successfully validated under various steady-state and transient indoor environment boundary conditions comparing the simulation results to measurements made with real human beings. The simulated thermal sensations with the HTM method showed a better correlation with measured values than the Fanger's PMV method. According to the simulation results, the operative temperature, metabolic rate and clothing are the most dominant boundary conditions for the human thermal sensation and comfort. HTM can be used for estimating the effects of alternative building structures, as well as building service systems, on occupants under different conditions more accurately and easily than before. The realistic thermal comfort of the user can be used as a design parameter for designing better thermal environments in new and renovated buildings.
ISBN, ISSN	ISBN 978-951-38-7948-8 (soft back ed.) ISSN 2242-119X (soft back ed.) ISBN 978-951-38-7949-5 (URL: http://www.vtt.fi/publications/index.jsp) ISSN 2242-1203 (URL: http://www.vtt.fi/publications/index.jsp)
Date	December 2012
Language	English, Finnish abstract
Pages	141 p.
Keywords	Human thermoregulation, building simulation
Publisher	VTT Technical Research Centre of Finland P.O. Box 1000, FI-02044 VTT, Finland, Tel. 020 722 111

Julkaisun sarja ja numero
VTT Science 23

Nimeke	**Termisellä ihmismallilla parempaan lämpöviihtyvyyteen**
Tekijä(t)	Riikka Holopainen
Tiivistelmä	Energiatehokkaissa passiivi- ja nollaenergiataloissa on merkittävästi pienempi lämmitystarve kuin perinteisissä rakennuksissa. Tämän vuoksi perinteisiä rakenne- ja talotekniikkaratkaisuiden suunnittelukriteerejä on tarkistettava lämpöviihtyvyyden varmistamiseksi. Lämpöviihtyvyyden laskentamenetelmänä perinteisesti käytetty Fangerin PMV-menetelmä ei huomioi ihmisen lämmönsäätelyjärjestelmää, joten menetelmä yliarvioi koettua lämpötilaa lämpimissä olosuhteissa ja aliarvioi sitä viileissä olosuhteissa. Termisten ihmismallien avulla voidaan mallintaa ihmisen lämpöfysiologista ja -fysikaalista toimintaa ja lämmönsäätelyjärjestelmää. Tässä väitöskirjassa esitetään ensimmäinen sovellus, jossa kehitetty terminen ihmismalli Human Thermal Model (HTM) on liitetty dynaamiseen rakennuksen energialaskentaohjelmaan. HTM-mallia voidaan käyttää lämpöviihtyvyyden laskentaan sekä pysyvissä että muuttuvissa olosuhteissa. Malli perustuu ihmisvartalon todelliseen anatomiaan ja fysiologiaan. Koska malli on osa dynaamista rakennuksen energialaskentaohjelmaa, ulkoiset reunaehdot kuten ympäröivien pintojen lämpötilat ja säteilylämmönsiirto eri pintojen välillä voidaan kuvata tarkemmin kuin aiemmissa ihmismalleissa. Kudosten lämmönsiirron, lämpöaistimuksen ja lämpöviihtyvyyden laskenta on validoitu vertaamalla simulointituloksia oikeilla ihmisillä tehtyihin mittauksiin. HTM-mallilla simuloidut lämpöaistimukset vastasivat mittaustuloksia paremmin kuin Fangerin PMV-menetelmällä lasketut. Tulosten mukaan operatiivinen lämpötila, aktiivisuustaso ja vaatetus ovat tärkeimpiä reunaehtoja lämpöaistimukselle ja -viihtyvyydelle. HTM-mallilla on mahdollista vertailla aiempaa tarkemmin eri rakennevaihtoehtojen ja talotekniikkajärjestelmien vaikutusta rakennuksen käyttäjän todelliseen lämpöviihtyvyyteen, joten lämpöviihtyvyyttä voidaan pitää lähtökohtana suunniteltaessa laadukkaampia sisäolosuhteita sekä uudisrakennuksiin että korjauskohteisiin.
ISBN, ISSN	ISBN 978-951-38-7948-8 (nid.) ISSN 2242-119X (nid.) ISBN 978-951-38-7949-5 (URL: http://www.vtt.fi/publications/index.jsp) ISSN 2242-1203 (URL: http://www.vtt.fi/publications/index.jsp)
Julkaisuaika	Joulukuu 2012
Kieli	Englanti, suomenkielinen tiivistelmä
Sivumäärä	141 s.
Avainsanat	Human thermoregulation, building simulation
Julkaisija	VTT PL 1000, 02044 VTT, Puh. 020 722 111

VTT Technical Research Centre of Finland is a globally networked multitechnological contract research organization. VTT provides high-end technology solutions, research and innovation services. We enhance our customers' competitiveness, thereby creating prerequisites for society's sustainable development, employment, and wellbeing.

Turnover: EUR 300 million
Personnel: 3,200

VTT publications

VTT employees publish their research results in Finnish and foreign scientific journals, trade periodicals and publication series, in books, in conference papers, in patents and in VTT's own publication series. The VTT publication series are VTT Visions, VTT Science, VTT Technology and VTT Research Highlights. About 100 high-quality scientific and professional publications are released in these series each year. All the publications are released in electronic format and most of them also in print.

VTT Visions

This series contains future visions and foresights on technological, societal and business topics that VTT considers important. It is aimed primarily at decision-makers and experts in companies and in public administration.

VTT Science

This series showcases VTT's scientific expertise and features doctoral dissertations and other peer-reviewed publications. It is aimed primarily at researchers and the scientific community.

VTT Technology

This series features the outcomes of public research projects, technology and market reviews, literature reviews, manuals and papers from conferences organised by VTT. It is aimed at professionals, developers and practical users.

VTT Research Highlights

This series presents summaries of recent research results, solutions and impacts in selected VTT research areas. Its target group consists of customers, decision-makers and collaborators.

A human thermal model for improved thermal comfort

Energy efficient very low-energy houses, passive houses and nearly zero-energy houses have a significantly lower heating power demand than traditional buildings. Therefore, the typical design and dimensioning criteria of conventional structural and building service system concepts need to be verified to avoid problems concerning the thermal sensation and comfort of the building users. Fanger's PMV-method is traditionally used for estimating thermal sensation and comfort. The PMV method does not take into account the human thermoregulatory system, therefore it progressively over-estimates the mean perceived warmth of warmer environments and the coolness of cooler environments.

Human thermal models represent the human body from a thermokinetic point of view and they have been used for modelling the thermoregulation system. This thesis presents the first approach, where a human thermal model is implemented in a building simulation environment: the Human Thermal Model (HTM). HTM can be used for predicting thermal behaviour of the human body under both steady-state and transient indoor environment conditions. It is based on true anatomy and physiology of the human body. The connection with the building simulation environment enables defining the external boundary conditions such as surface temperatures and radiation heat transfer more accurately than with the previous human thermal models.

HTM tissue heat transfer, thermal sensation and thermal comfort calculation has been successfully validated under various steady-state and transient indoor environment boundary conditions comparing the simulation results to measurements made with real human beings. The simulated thermal sensations with the HTM method showed a better correlation with measured values than the Fanger's PMV method. According to the simulation results, the operative temperature, metabolic rate and clothing are the most dominant boundary conditions for the human thermal sensation and comfort.

HTM can be used for estimating the effects of alternative building structures, as well as building service systems, on occupants under different conditions more accurately and easily than before. The realistic thermal comfort of the user can be used as a design parameter for designing better thermal environments in new and renovated buildings.

ISBN 978-951-38-7948-8 (soft back ed.)
ISBN 978-951-38-7949-5 (URL: http://www.vtt.fi/publications/index.jsp)
ISSN 2242-119X (soft back ed.)
ISSN 2242-1203 (URL: http://www.vtt.fi/publications/index.jsp)